D. ÖZKÖK

MODELLING, SIMULATION AND DESIGN OF A GREEN HYDROGEN-BASED HYBRID ENERGY SYSTEM

THE GRADUATE SCHOOL OF NATURAL AND APPLIED SCIENCES
OF
ATILIM UNIVERSITY

DUYGU ÖZKÖK

A MASTER OF SCIENCE
THESIS
IN
THE DEPARTMENT OF MECHANICAL ENGINEERING

JANUARY 2022

ATILIM UNIVERSITY 2022

MODELLING, SIMULATION AND DESIGN OF A GREEN HYDROGEN-BASED HYBRID ENERGY SYSTEM

A THESIS SUBMITTED TO
THE GRADUATE SCHOOL OF MECHANICAL ENGINEERING
OF
ATILIM UNIVERSITY

BY

DUYGU ÖZKÖK

IN PARTIAL FULFILLMENT OF THE REQUIREMENTS
FOR
THE DEGREE OF MASTER OF SCIENCE
IN
THE DEPARTMENT OF MECHANICAL ENGINEERING

JANUARY 2022

Approval of the Graduate School of Natural and Applied Science, Atilim University

_____

Prof. Dr. Ender Keskinkılıç
Director

I certify that this thesis satisfies all the requirements as a thesis for the degree of **Master of Science in Mechanical Engineering Department, Atilim University.**

_____

Prof. Dr. Sadık Engin Kılıç
Head of Department

This is to certify that we have read the thesis MODELLING, SIMULATION AND DESIGN OF A GREEN HYDROGEN-BASED HYBRID ENERGY SYSTEM submitted by DUYGU KEMERİZ ÖZKÖK and that in our opinion it is fully adequate, in scope and quality, as a thesis for the degree of Master of Science.

_____

Prof. Dr. Yılser Devrim
Supervisor

Examining Committee Members :

Prof. Dr. Can Özgür Çolpan
Mechanical Engineering, Dokuz Eylul University _____

Prof. Dr. Yılser Devrim
Energy Systems Engineering, Atilim University _____

Prof. Dr. Ayhan Albostan
Energy Systems Engineering, Atilim University _____

Date: JANUARY 20, 2022

I hereby declare that all information in this document has been obtained and presented in accordance with academic rules and ethical conduct. I also declare that, as required by these rules and conduct, I have fully cited and referenced all material and results that are not original to this work.

Name, Last Name : Duygu ÖZKÖK

Signature :

ABSTRACT

MODELLING, SIMULATION AND DESIGN OF A GREEN HYDROGEN-BASED HYBRID ENERGY SYSTEM

Özkök, Duygu

M.S., Department of Mechanical Engineering

Supervisor: Prof. Dr. Yılser DEVRİM

January 2022, 98 pages

As global warming increases and fossil fuel sources are depleted, renewable energy sources gain importance. Clean energy sources such as sunlight, wind, geothermal energies, and hydro energies constitute renewable energy sources. The fact that the sun and wind are endless sources makes renewable energy more important day by day. In addition, reducing foreign dependency increases the importance of renewable energy sources even more. Turkey has a very productive position in terms of both solar radiation and wind potential. This makes electricity generation from solar and wind energy even more important. However, the current high initial costs and low energy conversion efficiencies of renewable energy sources reduce the availability of renewable energy. Failure to produce electricity from solar energy in the evening also leads to blackouts. Therefore, the integration of solar and wind energy systems is used as complementary systems. The use of two or more renewable energy sources together is called hybrid systems. Rather than using a single renewable energy source, the use of a hybrid system is more advantageous in terms of both cost and efficiency. The system established in solar-wind energy integration can solve the problem of intermittent electricity that may occur from the sources installed as a single system.

The fact that the sun produces electricity during the daytime and the wind produces

electricity in the evening provides complementary features. Another problem that can be encountered in renewable energy sources is storage. As is known, batteries used in solar energy do not store seasonally. This shows that the electricity produced in excess cannot be used. Therefore, hydrogen energy comes into play as an alternative energy source. Storage of energy in the form of hydrogen (H_2) provides solutions for both daily and seasonal storage. With the help of the electrolyzer, water molecules are decomposed into hydrogen (H_2) and oxygen (O_2) and stored as H_2 and O_2 in high-pressure tanks. Fuel cells are also a source that converts the chemical energy created by hydrogen into electrical energy in this system. Fuel cells integrated into the solar-wind system are also an alternative solution in terms of increasing energy conversion. There are six types of fuel cells. Among them, the proton exchange membrane fuel cell (PEMFC) is the most attractive due to its quiet operation and lower corrosion, high power density, low local emissions, low operating temperatures. Therefore, they can be powered by a PEMFC for hybrid systems with photovoltaic panels and wind turbines. The most important process in the studies of renewable energy sources is the simulation steps.

This thesis study was carried out to meet the 25 kW electricity needs of Ankara Atilim University from hybrid systems without being connected to the grid. To solve the system storage problem, hydrogen energy and, accordingly, the fuel cell were designed. The Proton Exchange Membrane Fuel cell design, which will operate for 5 hours a day, was designed through the MATLAB program and integrated into the TRNSYS software program. System simulation was done using the TRNSYS program. The optimum number of panels was determined according to a fixed number of selected wind turbines for the operation of the electrolyzer. Finally, the leveled cost calculations were calculated, and the optimum system was selected.

Keywords: Photovoltaic, Wind turbine, PEM Fuel cell, Hybrid energy systems, Techno-economic analysis

ÖZ

YEŞİL HİDROJEN TEMELLİ HİBRİT ENERJİ SİSTEMİNİN MODELLENMESİ, SİMÜLASYONU VE TASARIMI

Özkök, Duygu
Yüksek Lisans, Makine Mühendisliği Bölümü
Tez Yöneticisi : Prof. Dr. Yılser DEVRİM

Ocak 2022, 98 sayfa

Küresel ısınma arttıkça ve fosil yakıt kaynakları tükendikçe yenilenebilir enerji kaynakları önem kazanmaktadır. Güneş ışığı, rüzgar, jeotermal enerjiler ve hidro enerji gibi temiz enerji kaynakları yenilenebilir enerji kaynaklarını oluşturur. Güneşin ve rüzgarın sonsuz kaynak olması yenilenebilir enerjiyi gün geçtikçe daha önemli hale getirmektedir. Ayrıca, dışa bağımlılığı azaltması da yenilenebilir enerji kaynaklarının önemini daha da arttırmaktadır. Ülkemiz gerek güneş ışınımı gerekse rüzgar potansiyeli yönünden oldukça verimli bir konuma sahiptir. Bu da güneş enerjisi ve rüzgar enerjisinden elektrik üretimini daha da önemli hale getirmektedir. Ancak ,yenilenebilir enerji kaynaklarının mevcut yüksek başlangıç maliyetleri ve düşük enerji dönüşüm verimlilikleri yenilenebilir enerjinin kullanılabilirlik durumunu azaltmaktadır. Güneş enerjisinden elektrik üretiminin akşam saatlerinde yapılmaması da kesintilere yol açmaktadır. Bu yüzden birbirini tamamlayıcı sistemler olarak güneş ve rüzgar enerji sistemleri entegrasyonu kullanılmaktadır. İki ya da daha fazla yenilenebilir enerji kaynağının bir arada kullanılmasına hibrit sistemleri denir. Tek bir yenilenebilir enerji kaynağının kullanılmasından ziyade hibrit sisteminin kullanımı hem maliyet açısından daha avantajlı hem de verimlilik açısından daha avantajlıdır. Tek sistem olarak kurulu kaynaklardan oluşabilecek kesintili elektrik sorunu, güneş-rüzgar enerjisi entegrasyonunda kurulan sistem çözebilir. Güneşin gündüz saatlerinde elektrik üretmesi ve rüzgarın akşam saatlerinde elektrik üretmesi birbirini tamamlayıcı

özellik sağlar. Yenilenebilir enerji kaynaklarında karşılaşabilinecek diğer bir sorun ise depolamadır. Bilindiği gibi güneş enerjisinde kullanılan bataryalar mevsimsel depolama yapmamaktadır. Bu da fazla üretilen elektriğin kullanılamayacağını gösterir. Bu yüzden alternatif enerji kaynağı olarak hidrojen enerjisi devreye girer. Enerjinin hidrojen şeklinde depolanması hem günlük hem de mevsimsel depolama için çözüm oluşturur. Elektrölizör yardımıyla su molekülleri hidrojen (H_2) ve oksijene (O_2) ayrıştırılır ve yüksek basınçlı tanklarda H_2 ve O_2 olarak depolanır. Yakıt hücreleri de bu sistemde hidrojenin oluşturduğu kimyasal enerjiyi elektrik enerjisine dönüştüren bir kaynaktır. Güneş-rüzgar sistemine entegre edilen yakıt hücreleri de enerji dönüşümünü yükseltmek açısından alternatif bir çözümdür. Yakıt hücresi türleri içinde proton değişim membranlı yakıt hücresi (PEMYH) sessiz çalışma ve daha düşük korozyon, yüksek güç yoğunluğu, düşük yerel emisyonlar, düşük çalışma sıcaklıkları gibi özelliklerinden dolayı en çekici olanıdır. Bu nedenle fotovoltaik paneller ve rüzgar türbinleri bulunan hibrit sistemler için PEMYH ile çalıştırılabilirler. Yenilenebilir enerji kaynaklarının çalışmalarındaki en önemli süreci simülasyon adımları oluşturmaktadır.

Bu tez çalışması, Ankara Atılım Üniversitesinin 25 kW'lık elektrik ihtiyacını şebekeye bağlı olmadan, hibrit sistemlerden karşılamak için yapılmıştır. Sistem depolama sorunun çözmek için hidrojen enerjisi ve buna bağlı olarak yakıt hücresi tasarlanmıştır. Günde 5 saat çalışacak PEMYH tasarımı MATLAB program aracılığıyla tasarlanmış ve TRNSYS programına entegre edilmiştir. Sistem simülasyonu TRNSYS programı kullanılarak yapılmıştır. Elektrölizörün çalışması için sabit sayıda seçilen rüzgar türbinlerine göre optimum panel sayısı belirlenmiştir. Son olarak Seviyelendirilmiş maliyet hesaplamaları hesaplanarak ve optimum sistem belirlenmiştir.

Anahtar Kelimeler: Hibrit Sistemler, Fotovoltaik, PEM Yakıt Hücresi, MATLAB/Simulink

To my family

ACKNOWLEDGMENTS

I would like to thank my advisor Prof. Dr. Yılser Devrim for advice, criticism, encouragement, insight throughout the research, for guiding me in data acquisition, interpretation, and analysis, and for his support in completing my study.

I would like to thank the TRNSYS internet network and Alastair McDowell, whose training I purchased from Udemy, for answering my questions about the TRNSYS Software.

I would like to thank my husband for helping me get help from the industry and for supporting me. I am grateful to my mother and my family for their patience and efforts and moral supports.

This study is supported by the Scientific and Technological Research Council of Turkey (TUBITAK) 1001 Project (Grant number: 119F182).

TABLE OF CONTENTS

ABSTRACT iii

ÖZ v

ACKNOWLEDGMENTS viii

LIST OF TABLES xii

LIST OF FIGURES xiii

CHAPTER 1 1

1. INTRODUCTION 1

1.1. Energy Systems 1

1.2. Renewables Energy Systems 2

1.3. Literature Survey 3

CHAPTER 2 6

2. OVERVIEW OF HYBRID POWER SYSTEM 6

2.1. Hybrid Power System 6

2.1.2. Hydrogen Energy System Based Hybrid System 6

2.2.1.Solar Radiation Model 7

2.2.1.1. Extraterrestrial Radiation and Solar Radiation Geometry 7

2.2.1.2. Terrestrial Solar Radiation 8

2.2.1.3. Solar Radiation on the Tilted Surface 8

2.2.2. Photovoltaic Model 10

2.2.2.1. Electrical Model 10

2.2.2.2. Maximum Power Tracking System Model 14

2.2.3. Wind Turbine Model 14

2.2.4. Controller 16

2.2.6. Proton Exchange Membrane (PEM) Electrolyzer 16
2.2.7. Proton Exchange Membrane Fuel Cell (PEMFC) 19
2.3. Levelized Cost of Energy Analysis (LCOE) 21
2.4. Motivation of Study 22
CHAPTER 3 24
3. METHODOLOGY 24
3.1. Data Collection 24
3.1.1. Data Obtained from Meteonorm Program 25
3.1.2. Data Obtained through Atilim University Meteorology Station Data . 25
3.2.Design of Proposed Hybrid Energy System 26
3.2.1. Hybrid Energy System with H_2/O_2 PEMFC 30
3.2.2. Hybrid Energy System with H_2/Air PEMFC 30
3.3. Modeling of the Hybrid System with TRNSYS 30
3.4.Optimal Design Strategy of Proposed System 31
3.5.Design Calculations 34
3.5.1. Solar Calculation 35
3.5.2. Wind Calculation 41
3.5.3. PEM Electrolyzer Calculation 44
3.5.4. PEMFC Calculation 46
3.5.5. H_2 Storage Calculation 53
3.5.6. Economic Optimization and Levelized Cost of Energy (LCOE) 53
CHAPTER 4 56
4. RESULTS AND DISCUSSION 56
4.1. Hybrid System Design Results 56
4.2. Hybrid System Optimization Studies 59

4.3. Comparison of Hybrid System with H_2/O_2 and H_2/Air supplied PEMFC Systems 66
CHAPTER 5 72
5. CONCLUSION 72
REFERENCES 74
APPENDIX A 82
APPENDIX B 83
APPENDIX C 90
APPENDIX D 96
APPENDIX E 97
APPENDIX F 98

LIST OF TABLES

TABLES

Table 3. 1. Properties of PV Panel 35
Table 3. 2. Monthly angle values of the selected location 39
Table 3. 3. Properties of WT 41
Table 3. 4. Properties of Electrolyzer 45
Table 3. 5. Properties of PEMFC 47
Table 3. 6. Parameters to LCOE calculation 55
Table 4.1. Design results of the hybrid system with H_2/O_2 PEMFC for different operating scenarios 57
Table 4.2. Design results of the hybrid system with Meteonorm program data according to different initial H_2 tank volume 58
Table 4.3. Satisfying the condition in Equation 4.1. (n_1, n_2) (when A_0=250 m^2) 60
Table 4.4. Comparison of the results obtained with Atilim University meteorology station data and Meteonorm program data in hybrid energy system simulation 61
Table 4.5. Comparison of the LCOE values of the hybrid system design for the meteorology station (PV=95, WT=1) and Meteonorm program data (WT=1 PV=72) 66
Table 4.6. Design results of the hybrid system with H_2/O_2 PEMFC for Atilim University meteorology station data 67
Table 4.7. Design results of the hybrid system with H_2/air PEMFC for Atilim University meteorology station data 68

LIST OF FIGURES

FIGURES

Figure 2. 1. Wind Turbine Equipment [37]..... 15
Figure 2. 2. Working principle of PEM electrolyzer [45]..... 18
Figure 2. 3. Schematic Operation Diagram of PEMFC 20
Figure 2. 4 Schematic diagram of the proposed hybrid energy system 23
Figure 3. 1. Location of Atilim University Incek Campus (Ankara, Turkey) 24
Figure 3. 2. Atilim University Meteorology Data Station 26
Figure 3.3. TRNSYS Model O_2 inlet hybrid system..... 28
Figure 3.4. TRNSYS Model Air inlet hybrid system 29
Figure 3.5. Power and gas management strategy of the hybrid power system with H_2/O_2 PEMFC 32
Figure 3.6. Power and gas management strategy of the hybrid power system with H_2/Air PEMFC 33
Figure 3. 7. Hourly Global Solar Radiation data received from a) Meteonorm program, b) Atilim University meteorology station..... 36
Figure 3. 8. Side view of PV arrays 40
Figure 3. 9. Wind data obtained from the Meteonorm program 42
Figure 3. 10. Wind speed data obtained from Atilim University meteorology station 42
Figure 3. 11. Power & Wind Speed curve of WT..... 43
Figure 3. 12. Wind farm layout..... 44
Figure 4.1. Time-dependent power generation of the hybrid system (PV=95 and WT=1) with Meteonorm program data……...62
Figure 4.2. Time-dependent power generation of the hybrid system design (PV=95 and WT=1) using weather station data 62
Figure 4.3. Comparison of the one-year H_2 gas storage of the hybrid system (PV=95 and WT=1) for meteorology station and Meteonorm program data..... 63
Figure 4.4. Comparison of the electrolyzer operating time of the hybrid system (PV=95 and WT=1) for meteorology station and Meteonorm program data..... 64
Figure 4.5. Comparison of the stored H_2 gas during one-year simulation for the hybrid system design for the meteorology station (PV=95, WT=1) and Meteonorm program (WT=1 PV=72) data..... 65

Figure 4.6. Time-dependent power generation of the hybrid system with H_2/O_2 PEMFC (PV= 72 and WT= 1) using meteorology station data 69
Figure 4.7. Time-dependent power generation of the hybrid system with H_2/air PEMFC (PV= 69 and WT= 1) using meteorology station data 69
Figure 4.8. Comparison of the stored H_2 gas during one-year simulation for the hybrid system with H_2/O_2 PEMFC (PV= 72 and WT=1) and H_2/air PEMFC (PV= 69 and WT= 1) for the data of meteorology station 70
Figure 4.9. Comparison of electrolyzer operating times of hybrid system with H_2/O_2 PEMFC (PV= 72 and WT= 1) and H_2/air PEMFC (PV= 69 and WT=1) for the data of meteorology station 71

LIST OF SYMBOL/ABBREVIATIONS

DS	Daylight-saving time application
ET	Time correction
FF	Fill factor
H_2	Hydrogen
LCOE	Levelized Cost Analysis
LT	Local standard time
LL	Local meridian
MPPT	Maximum Peak Power
NOCT	Nominal Operating Cell Temperature
O_2	Oxygen
PV	Photovoltaic Panel
PEMFC	Proton Exchange Membrane Fuel Cell
STC	Standard Test Condition
SL	Standard meridian
ST	Solar time
TC	Absolute temperature
TC_i	Total tax credits in the year i
WT	Wind Turbine
A_r	Rotor swept area
A	Electrolyzer active area
D_s	Shadow length
D_r	Spacing between the two rows in the south direction
E_i	Generated energy in the year I
F	Faraday constant
F_i	Fuel cost in the year I
G_{th}	Total radiation on horizontal surface
G_{Bh}	Beam radiation on a horizontal surface

G_{Dh}	Diffuse radiation on a horizontal surface
G_{Rh}	Ground reflected on a horizontal surface
G_{Tt}	Total radiation on an inclined surface
G_{Bt}	Beam radiation on inclined surface
G_{Dt}	Diffuse radiation on an inclined surface
G_{Rt}	Ground reflected on an inclined surface
G_I	Solar irradiance
$G_{I_{ref}}$	Solar irradiance on reference condition
G_{0h}	Total radiation falling on the atmosphere on a horizontal surface
G_{sc}	Solar constant
h_{H_2O}	Enthalpies of water
h_{H_2}	Enthalpies of hydrogen
h_{O_2}	Enthalpies of oxygen
I	Interest rate
I_{ph}	Photo-generated current
I_{sc}	Short-circuited current
I_{MPPT}	Maximum power point current
I_L	Light current
I	Output current
I_0	Dark saturation current
I_{stack}	Current of the electrolyzer
I_i	Capital cost in year i
i_{cell}	Electrolyzer current density
k	Boltzmann's gas constant
L_m	Module length
L_t	Total length
L_r	Row length of the turbine
m_{H_2}	Mass flow rate
mw_{H_2}	Molecular weight of hydrogen
mw_{O_2}	Molecular weight of oxygen

N	Time period
N_d	Day of year
N_{PV}	Number of PV array
N_{TR}	Number of turbines in a row
$N_{H_{2\_out}}$	Molar flow of hydrogen leaving the cell
$N_{H_{2\_con}}$	Number of moles of hydrogen consumed
n_m	Number of PV modules connected in series
n_r	Number of PV modules connected in parallel
$n_{H_{2\_produced}}$	Number of moles produced by the electrolyzer
n_{cell}	Number of fuel cell
n	Number of electrons
O_i	Operation and maintenance costs in the year I
P_{max}	Maximum power
P	Pressure
R	Ideal gas constant
R_s	Series Resistance
R_h	Shunt Resistance
r_s	Solar radius
r_b	Ratio of beam radiation on the tilted surface to a horizontal surface
r_d	Ratio of diffuse radiation on the tilted surface to a horizontal surface
r_d	Net drag coefficient
r_r	Ratio of ground reflected incident on the tilted surface
S_R	Row spacing
s_{H_2O}	Entropies of water

s_{H_2}	Entropies of hydrogen
s_{O_2}	Entropies of oxygen
T_{cell}	PV Temperature
$T_{cell,ref}$	PV Temperature on reference condition
T	Temperature
T_a	Ambient temperature
V	Voltage
V_{oc}	Open-circuit Voltage
V_{MPPT}	Maximum power point voltage
V_t	Thermoneutral Voltage
V^0	Minimum potential difference
V_{cell}	Cell Voltage
V_{act}	Activation voltage
V_{ohm}	Ohmic voltage
Vconc	Concentration voltage
V_{stack}	Stack voltage
V_{H_2}	Volumetric flow rate of hydrogen
V_{O_2}	Volumetric flow rate of oxygen
V_{ST}	Volume of the compressed gas storage tank
W_t	Total width
W_m	Width of a PV module
W_{ele}	Power of the electrolyzer
α	Altitude angle
ϕ	Latitude of the location
$\boldsymbol{\delta}$	Declination angle of the sun
$\boldsymbol{\omega}$	Solar hour angle
μ_P	Power thermal coefficient
ρ_{air}	Air density
v	Wind speed
η_{ele}	Electrolyzer efficiency

c_p	Wind shear exponent
δ_{H2}	Stoichiometric rate of hydrogen
δ_{O2}	Stoichiometric rate of oxygen
h_c	Current hour
γ_s	Solar azimuth angle
γ	Surface azimuth angle
ρ_{gr}	Ground reflectivity coefficient
ΔG	Gibbs free energy
ΔH	Enthalpy

CHAPTER 1

1. INTRODUCTION

1.1. Energy Systems

Energy is an important element of our country's economy. World states and international organizations compete to obtain energy resources (oil, natural gas, coal etc.). Energy is the infrastructure of industrialization and an indispensable element of daily life. Therefore, the need for energy has a very important place on the national and international agenda. Due to the exhaustion of energy resources, the existence of external dependency and environmental effects; today, producing safe, sufficient, cheap, and clean energy for countries are among the main problems of economic and social life. In our country, which is growing rapidly with its industry, economy and population, the need for energy is constantly increasing. For this reason, it is of great importance to use the produced energy with high efficiency and to evaluate the potential of alternative and renewable energy sources as well as existing energy sources. The energy required for meeting the needs of people and healthily maintaining the development is especially used in sectors such as industry, housing and transportation. While energy sources indispensable benefits in our life, it also causes environmental pollution to a large extent during production, cycle, transportation and consumption [1].

This phenomenon forces scientific circles to reevaluate energy conversion tools and to develop new methods to benefit more from existing limited energy resources. Depending on the political developments in the world, the constant increase in energy prices and the fact that fossil fuels will run out after a certain period make it necessary to determine alternative energy sources. For this reason, it is advantageous in all respects to turn to renewable energy sources with less environmental impact.

1.2. Renewables Energy Systems

Renewable energy sources became important as global warming increased and fossil fuel resources are exhausted [2]. Clean energy sources such as sunlight, wind, geothermal energy, and hydro energy are renewable energy sources. The endless source of sun and wind make renewable energy more important day by day. In addition, the reduction in foreign dependency also increases the importance of renewable energy sources. Our country has a very efficient position in terms of both solar radiation and wind potential. This makes electricity production from solar energy and wind energy more important. However, the current high initial costs of renewable energy sources and low energy conversion efficiencies reduce the availability of renewable energy. Failure to produce electricity from solar energy in the evening also causes interruptions. Therefore, solar and wind energy systems integration are used as complementary systems. The combination of two or more renewable energy sources is called hybrid systems. Rather than using a single renewable energy source, the use of the hybrid system is both more advantageous in terms of cost and more advantageous in terms of efficiency. The intermittent electrical problem that may arise from the resources installed as a single system can solve the system established in solar-wind energy integration. The fact that the sun generates electricity during the day and the wind generates electricity during the evening provides complementary features [3]. Another problem that can be encountered in renewable energy sources is storage. As is known, the batteries used in solar energy do not make seasonal storage [4]. This indicates that over-produced electricity cannot be used. Therefore, hydrogen energy is activated as an alternative energy source. Storing energy in the form of hydrogen creates solutions for both daily and seasonal storage. With the help of the electrolyzer, water molecules are decomposed into H_2 and O_2 and stored in high-pressure tanks as hydrogen and oxygen. Fuel cells are also a source that converts the chemical energy generated by H_2 into electrical energy in this system. Fuel cells integrated into the solar-wind system are also an alternative solution to increase energy conversion. There are six types of fuel cells. Among them, proton exchange membrane fuel cell (PEM) is the most attractive due to its quiet operation and lower corrosion, high power density, low local emissions, low operating temperatures [5]. Therefore, in this thesis, PEMFC and PEM electrolyzer, which are integrated with hybrid systems, are

preferred.

1.3. Literature Survey

Ridha et al. investigated how the parameters and components of a stand-alone solar system affect the system. Depending on the system performance, hybrid systems have been developed. They also observed that factors such as temperature, dust, MPPT charge control significantly affect system performance [6]. Chandrika et al. analyzed the efficiency of the photovoltaic system installed in the building. The PV system of newly built buildings connected to the grid was installed and the performance of the system was optimized. PVsyst program was used to simulate the system. They found that the PV module would reduce the cost of the building while integrating the building structure [7]. Razmi et al. installed wind turbines at the Abhar and Kahah fields, two adjacent areas in Iran. It was aimed to produce uninterrupted electricity with clean energy sources without air pollution. When wind turbines are used alone, they may cause interruptions due to imbalances in power. This requires a storage system. At this point, they used the compressed air storage (CAES) system as a solution. CAES is an auxiliary storage system. Thus, they saw that the energy produced from the wind could be more efficient [8]. Diaf et al. analyzed the hybrid system consisting of PV and WT. First, they set up a system consisting of only PV and only WT. The cost analysis was calculated. Then the system was optimized and designed a hybrid system consisting of PV and WT. LCOE analysis was calculated according to the hybrid system. The PV and WT system was found as more costly than the hybrid system [9]. Samy et al. aimed to find solutions to power cuts in remote districts by making use of existing renewable energy sources. For this, they used a PV, WT hybrid system and fuel cell and electrolyzer for storage. The proposed system feeds the load of a tourism resort. The sale of excess electricity to the grid is also taken as a basis. Hybrid Firefly and Harmony Search optimization technique was used. The system has been optimized and 80 PV, 2 WT, 20 FC, 41 electrolyzer and 118 hydrogen tanks are used for the operation of the system. The results also showed that the volume of shopping with the grid reached 4 GW of purchases and 3 GW of sales. The LCOE analysis of the proposed system was found to be $0.0628/kWh and the grid selling price was set to be less than 0.1$/kWh [10]. Al-Bonsrulah et al. aimed to meet the electricity need with hybrid

systems by separating a grid-connected system from the grid. PV, WT, fuel cell and electrolyzer system was designed to meet the energy needs of the region, which needs 1.5 mW of energy. Fuel cell was designed with a requirement of 570.96 Watts at 0.61 volts and 1.04 A/Cm^2. LCOE analysis was found to be 0.169 USD/kWh [11]. Ishak et al. designed a PV, WT system for hydrogen, urea, and power generation. Aspen Plus and the EES software program was used. The power was provided to feed the PEM electrolyzer in the system from the wind turbine. Then it was converted it into ammonia and then synthesized urea by capturing CO_2. Thus, the power generation was increased. Solar PV was used to power the cryogenic air separation unit. The amount of electrical power produced by the system to be 2.14 MW was found. The designed system produced 518.4 kmol/d of hydrogen and synthesized 86.4 kmol/d of urea. The energy and exergy efficiencies of the designed system are 44.4% and 32.2%, respectively [12]. Al Riza aims to dimension and evaluates an independent photovoltaic system for the residential load. He wants to determine the photovoltaic panel and battery capacity, so he used to Peak Sun Hour method, and it did so via TRNSYS software. The results consist of a photovoltaic system requirement of 1.9 kW-p photovoltaic panels and a 2200 Ah battery capacity for a 24V system for a typical Malaysian terrace house with an electrical charge of approximately 6 kWh per day [13]. Also, Al Riza did light work in the rural areas via TRNSYS Software. He determined the number of photovoltaic panels for a typical Malaysian terrace house. Comparing simulation results and experimental results, he observed the results are the same [14]. Özcan and Günerhan examined the energy interaction of the system installed on the roof of Ege University and the photovoltaic-assisted energy system with experimental and simulation studies. The power produced and consumed by the panels through the TRNSYS Software was found. The simulation and experimental results were compatible with each other [15]. Yildirim aimed to operate the fuel cell by producing hydrogen from the water electrolyzer through the excessive power obtained from the wind turbines. It used the fuel cell as a supporting generator. In his future studies, he aims to carry out experimental studies to support these systems [16]. Shapiro worked to see if hybrid systems and PEM electrolyzer were compatible. He aims to test general system feasibility, characterization of the electrolyzer performance including 1.0 A/cm^2 at 2.0 V per cell, the performance of the electrolyzer as a compressor, and assessment of the system for direct-coupled use with a PV array. The

PEM electrolyzer and PV system can be compatible with each other was observed [17]. Kotowicz et al. aimed to establish a system integrated into the hybrid system with the hydrogen generator data obtained in the experimental environment. Presented the compatibility of a wind farm with a hydrogen generator characterized by different powers and different efficiencies [18].

Gorgun aims to develop a dynamic PEM electrolyzer model. He investigated with modeling subsystems via MATLAB/Simulink to measure the dynamic interactions of the PEM electrolyzer. Simulation studies have shown that the model can capture the transient dynamic behavior of the PEM electrolyzer [19]. Escobar et al. examined the effect of parameters such as temperature, voltage pressure on PEMFC and PEM electrolyzer. The simulation is made via the MATLAB/Simulink program. They tried the working temperature of the electrolyzer between 30°C and 70°C and the pressure between 1-10 atm. The aim is to find the efficiency of the electrolyzer according to different parameters. The temperature increase affected the yield by 10% more was found [20]. Gomez et al. examined the effects of currency fluctuations in a PEM electrolyzer on system performance. For this, the cell voltage was determined according to the static and dynamic processes in the experimental environment. The electricity needs with renewable resources was met. The current fluctuations negatively affect cell performance was observed [21]. Ipsakis and Voutetakis aim to test stand-alone system including photovoltaic array and wind generators and store excessive energy via water electrolysis for future use in PEMFC in Greece. The several modes of operation for the PEM electrolyzer and the fuel cell such as minimum capacity level, fixed or variable power level was examined. Efficient power management strategies (PMSs) have been developed for the system [22]. Panayiotou et al. aim to compare the PV system and the PV-wind hybrid system. The simulation results for both systems was compared by using TRNSYS Software. The PV system was more efficient due to the weather conditions in Cyprus compared to France was found [23].

CHAPTER 2

1. OVERVIEW OF HYBRID POWER SYSTEM

2.1. Hybrid Power System

The electricity production of photovoltaic solar panels and wind turbines varies according to climatic conditions. Therefore, they are not a very rich source of energy on their own. Combining systems is more effective in generating electricity. Hybrid systems are systems where more than one energy source is used. Solar energy provides half a day's energy. It is not suitable for production all day long. In summer, when the sun's rays are at their highest, the wind speed may be insufficient [24]. In this way, a system design that complements each other will provide more efficient and uninterrupted electricity production. Hybrid applications are especially applied in systems where there is a summer-winter energy requirement, and no interruption should be allowed or the installed solar or wind energy system should be supported. In hybrid applications, it is possible to use solar, wind and diesel energy sources, fuel cell as double or triple. The system is the same as the working system of Solar Energy or Wind Energy. It is only added as an additional component to the system [25].

2.1.2. Hydrogen Energy System Based Hybrid System

PEMFC needs H_2. H_2 is not a primary energy source. It is also not a directly offered fuel. H_2 can be obtained by many methods. H_2 can be obtained by methods such as fossil fuels, water electrolysis, biomass. Electrolysis is the separation of water into its components using electrical energy. Hybrid systems can be used as an electricity source. Thanks to the electricity produced from the sun or wind, the electrolyzer systems work and separate the water into its components. Thus, the hybrid system can work in harmony with the electrolyzer and fuel cell [26].

2.2.1.Solar Radiation Model

The solar radiation model is generally examined in two classes as a parametric model and a decomposition model [27]. The parametric model requires more detailed information than the other. Meteorological data are used by some parametric models as predictors. The decomposition model is used to predict the beam and sky components. The decomposition model uses only global solar radiation data. Both models provide information on the geometry of extraterrestrial radiation and solar radiation. Therefore, the geometry of extraterrestrial radiation and solar radiation will be explained in the following section [28].

2.2.1.1. Extraterrestrial Radiation and Solar Radiation Geometry

Radiation received from the Earth's atmosphere is extraterrestrial radiation. Extraterrestrial radiation changes due to earth-sun motion. The variation of extraterrestrial radiation due to the motion of the earth is shown in the equation below.

$$G_{0h} = G_{sc} r_s * sin(a) \quad (2.1)$$

Where G_{0h} is the total radiation falling on the atmosphere on a horizontal surface (extraterrestrial radiation), G_{sc} is the solar constant, which is equal to 1367 W/m^2, r_s is the vector of the solar radius, which is assumed as 1, a is altitude angle and which is calculated as below:

$$sin(a) = sin(\phi)\, sin(\boldsymbol{\delta}) + \boldsymbol{cos}(\boldsymbol{\phi})\, \boldsymbol{cos}(\boldsymbol{\delta})\, \boldsymbol{cos}(\boldsymbol{\omega}) \quad (2.2)$$

ϕ is the latitude of the location, $\boldsymbol{\delta}$ is the declination angle of the sun, $\boldsymbol{\omega}$ is the solar hour angle. **δ** and **ω** are calculated as follow:

$$sin(\boldsymbol{\delta}) = \mathbf{0.39795}\, \boldsymbol{cos}(\mathbf{0.98563}(\boldsymbol{N_d} - \mathbf{1})) \quad (2.3)$$

$$\boldsymbol{\omega} = \mathbf{15}(\boldsymbol{h_c} - \mathbf{12}) \quad (2.4)$$

Where $\boldsymbol{N_d}$ is day of year, $\boldsymbol{h_c}$ is current hour.

The total extraterrestrial radiation value is calculated as below:

$$G_{0h}{}_{w\prime\prime}^{w\prime} = \int_{w\prime}^{w\prime\prime} G_{sc}E(sin(\phi)sin(\delta) + cos(\phi)cos(\delta)cos(\omega))d\omega \quad (2.5)$$

2.2.1.2. Terrestrial Solar Radiation

Solar radiation reaching the earth is terrestrial radiation. Terrestrial radiation measured on the horizontal surface is also called global horizontal solar radiation. This radiation received from the earth's surface is divided into three as direct, scattered and reflected radiation. Beam radiation is radiation that comes directly from the sun to the earth's surface. Diffuse radiation is radiation that is scattered or absorbed after the sun enters the atmosphere. Reflected radiation is the radiation coming from the ground or in the world by hitting any object such as a tree or building [29]. Total solar radiation of a horizontal surface on the earth is calculated with Equation 2.6:

$$G_{th} = G_{Bh} + G_{Dh} + G_{Rh} \quad (2.6)$$

G_{th} is total radiation on a horizontal surface, G_{Bh} is beam radiation on a horizontal surface, G_{Dh} is diffuse radiation on horizontal surface and G_{Rh} is ground reflected on a horizontal surface.

2.2.1.3. Solar Radiation on the Tilted Surface

It is necessary to know the direct and diffuse radiation to calculate the solar radiation on the inclined surface. Hence if global horizontal solar radiation data is known, by using the decomposition model, the horizontal surface can be calculated. There are many methods in the literature for calculating solar radiation on an inclined surface. The TRNSYS software used the Perez model as it gave the most accurate result in terms of performance [30]. To calculate the total radiation on the tilted surface, direct, diffuse, and reflected radiation are considered. It is shown in Equation 2.7.

$$G_{Tt} = G_{Bt} + G_{Dt} + G_{Rt} \quad (2.7)$$

$$G_{Tt} = G_{Bh}r_b + G_{Dh}r_d + G_{Rh}r_r \quad (2.8)$$

r_b is calculated as below;

$$r_b = \frac{cos(\phi)}{cos(\theta_z)} \quad (2.9)$$

Where;

$$cos(\theta) = cos(\theta_z)cos(\beta) + sin(\theta_z)cos(\gamma_s - \gamma)sin(\beta) \quad (2.10)$$

$$cos(\theta_z) = sin(\phi)sin(\delta) + cos(\phi)cos(\delta)sin(\omega) \quad (2.11)$$

where γ_s and γ are solar azimuth angle and surface azimuth angle, respectively.

r_r is calculated as below ;

$$r_r = \frac{\rho_{gr}(1-cos(\beta))}{2} \quad (2.12)$$

ρ_{gr} is ground reflectivity coefficient. There are many methods for calculating r_d. The Perez model, which is among these methods, is the method preferred by TRNSYS in terms of its accuracy and reliability [28].

As a result, TRNSYS calculated the total radiation value on the inclined surface with the following equation:

$$G_{Tt} = G_{Bh}\frac{cos(\theta)}{cos(\theta_z)}\, r_d\, G_{Dh} + \frac{G_{Th}\,\rho(1-cos(\delta))}{2} \quad (2.13)$$

In this thesis study, the received radiation values are the total value of direct, diffuse and reflected radiation determined in the inclined plane. TRNSYS program supports weather data in various formats such as TMY, TMY2, TM2. In this thesis, data is provided with a TM2 format data file containing inclined plane radiations taken from the Meteonorm program. In addition, the weather station placed at Atilim University

has been integrated into TRNSYS, considering the temperature, humidity, pressure and solar radiation values.

2.2.2. Photovoltaic Model

Photovoltaic panels are devices that convert sunlight directly from the atmosphere into electricity without a heat engine or rotating equipment. Since it is not a movable part of PV equipment, it has a long life and low cost. It is a clean energy source as it generates electricity without emitting greenhouse or other gaseous emissions. The raw material of PV panels is based on the element Silicon obtained from quartz stone. The obtained silicon is heated in a quartz furnace at 1500 ºC to form ingots. Ingots are shaped into wafers [31]. When sunlight hits silicon, electrical charges are created and transmitted as direct current by these metal contacts. The electricity produced from a single cell is quite low so multiple cells are connected to form a module. These modules are called panels. The panels can be connected in series or parallel to produce electricity at the desired power.

In the lower section, the electrical power characteristics of photovoltaic panels will be introduced. The model will be able to predict the output parameters of PV panels. In addition, different commercial performances in electricity generation can be determined by changing the input data provided by the generators.

2.2.2.1. Electrical Model

A photovoltaic PV panel is essentially a combination of solar cells, connections, protective parts, and supports. As seen earlier, solar cells are made of semiconductor materials, usually silicon, and are specially processed to create an electric field that is positive on one side (backside) and negative on the other (front facing the sun). When solar energy (photons) hits the solar cell, electrons break away from atoms in the semiconductor material, forming electron-hole pairs. If electrical conductors are connected to the positive and negative sides, forming an electrical circuit, the electrons are captured in the form of an electric current called photocurrent, I_{ph} [32]. As can be seen from this explanation, in the dark the solar cell is not active and works like a

diode, that is, a p-n junction that does not produce any current or voltage. However, if it is connected to a large voltage source, it produces a current called a diode or dark current. This is also called I_d. The model is known as five parameters model [4].

As you have seen, to find the current (I) value, it is applied following equation ;

$$I = I_{ph} - I_D - I_{sh} \tag{2.14}$$

The model includes a current source $I_{ph,}$ which is called light current. Also called light current (I_L). The I_L current is produced by the photovoltaic effect.

It is the output current of the cell.

From Shockley's diode equation;

$$I_D = I_0[\exp\left(\frac{V+IR_S}{nV_t}\right) - 1] \tag{2.15}$$

Where;

$$V_t = \frac{kt}{q} \tag{2.16}$$

According to Ohm's Law;

$$I_{SH} = \frac{V+IR_S}{R_{SH}} \tag{2.17}$$

If the equations are arranged and substituted in equation 2.14, it becomes as follows;

$$I = I_{PH} - I_0\left[\exp\left(\frac{V+IR_S}{AV_t}\right) - 1\right] - \frac{V+IR_S}{R_{SH}} \tag{2.18}$$

Equation 2.18 is the general equation in the literature[3].

This equation can also be written in the form below;

$$I = I_{PH} - I_0 \left[\exp\left(\frac{eV}{kT_C}\right) - 1\right] \quad (2.19)$$

Where k is Boltzmann's gas constant, TC is the absolute temperature of the cell(K),e is the electronic charge, V is voltage imposed across the cell (V) and I_o is dark saturation current, which depends strongly on temperature (A).

Some parameters must be defined before the equation can be solved. R_{sh}, R_s, I_{ph}, I_o parameters are the parameters determined in the experimental environment specific to each PV. Measurements are made under Standard Test Conditions (STC). STC is the value taken in the AM 1.5 solar spectrum and 1000 W/m^2 are reference values at 25 ºC. In solar arrays supplied by manufacturers, the short-circuit current I_{SC} is the maximum current when the cell is short-circuited, and the voltage value is 0. The open-circuit voltage V_{oc} is the voltage measured when the current is 0 when the PV cell is not circuiting. In both cases, the power is 0 in an open circuit or short circuit. The current measured at the maximum power point is I_{mppt}, and the voltage value measured at the maximum power point is V_{mppt}. Equation 2.18 is the calculated value for a single PV cell. For a PV array consisting of n_s of cells connected in series, the following equation is applied.

$$I = I_{PH} - I_0 \left[\exp\left(\frac{V+IR_S}{n_S A V_t}\right) - 1\right] - \frac{V+IR_S}{R_{SH}} \quad (2.20)$$

Equation 2.20 has equations with 5 unknowns and the manufacturer's catalogs provide cell voltage and current at 3 key points.

At short-circuit current's equation is as follows;

$$I_{SC} = I_{PH} - I_0 \left[\exp\left(\frac{I_{SC}+R_S}{n_S A V_t}\right) - 1\right] - \frac{I_{SC}+R_S}{R_{SH}} \quad (2.21)$$

At Open-Circuit point's equation is as follows;

$$I_{OC} = I_{PH} - I_0 \left[\exp\left(\frac{V_{OC}}{n_S A V_t}\right) - 1\right] - \frac{V_{OC}}{R_{SC}} \quad (2.22)$$

At Maximum Power Point the characteristic equation;

$$I_{MPP} = I_{PH} - I_0 \left[\exp\left(\frac{V_{MPP}+I_{MPP}R_S}{n_S A V_t}\right) - 1\right] - \frac{V_{MPP}+I_{MPP}R_S}{R_{SC}} \quad (2.23)$$

If the derivative of the power with respect to the voltage at the maximum power point is taken;

$$\frac{\mathrm{dP}}{\mathrm{dV}} = \frac{\mathrm{d(IV)}}{\mathrm{dV}} = \frac{d\{I_{MPP}=I_{PH}-I_0\left[\exp\left(\frac{V_{MPP}+I_{MPP}R_S}{n_S A V_t}\right)-1\right]-\frac{V_{MPP}+I_{MPP}R_S}{R_{SC}}\ \}}{\mathrm{d}} = 0 \quad (2.24)$$

4 equations are written at 3 points. To solve the equation with 5 unknowns, 1 more equation must be written. Since the series resistance is relatively small compared to the shunt resistance, it is assumed to be equal according to Ulleberg [4].

$$I_L = I_{SC} \quad (2.25)$$

When Equation (2.25) is substituted in the previous equations, the number of unknown parameters is reduced to 4. Newton-Raphson method is used to solve the equation with 4 unknowns. In this method, derivatives of equations are taken, and nonlinear equations are linearized. These equations can also be solved using the Gaussian elimination method. It is reduced to the upper triangle matrix. The convergence process is performed until the best result is obtained. Parameters evaluated after these pre-emptive operations are valid for STC. Cell temperature also affects these parameters. The value read by the panel model from the meteorological data for a given location is the total solar radiation (Φ) on the PV surface.

$$I_0 = I_{0ref}\left(\frac{T_{cell}}{T_{cell,ref}}\right)^3 exp\left[\frac{qE_g}{kA}\left(\frac{1}{T_{cell,ref}} - \frac{1}{T_{cell}}\right)\right] \quad (2.26)$$

$$I_{PH} = \left[I_{SC,ref} + \mu_{Isc}(T_{cell} - T_{cell,ref}\right]\frac{\Phi}{1000} \quad (2.27)$$

R_{sh}, R_s and A are temperature dependent and are given in the equations below;

$$A = A_{ref} \frac{T_{pv}}{T_{pv,ref}} \tag{2.28}$$

$$R_{sh} = R_{sh,ref} \frac{\Phi_{pv,ref}}{\Phi_{pv}} \tag{2.29}$$

$$R_s = R_{s,ref} \tag{2.30}$$

2.2.2.2. Maximum Power Tracking System Model

Maximum power point tracking is the algorithm that finds the optimum output voltage for the PV panel to produce maximum power. Its main purpose is to increase the efficiency of the PV panel. In the previous section characteristic equation (equation 2.20) and is calculated unknown parameter.

The goal is to find the optimum voltage that reaches maximum power. For this, dP/dV=0 must be resolved. The cell temperature must be found for a specific weather parameter before and should be changed accordingly.

$$\frac{dP}{dV} = \frac{d(VI)}{dV} = I + V\frac{dI}{dV} = 0 \tag{2.31}$$

For the TRNSYS Software, this algorithm is set in the FORTRAN code in the PV panel. Its formulation is available in the component itself [30]. MPPT feature, which is optionally given in the PV panel settings in TRNSYS, has been kept optional as mode 0 (off), mode 1 (on).

2.2.3. Wind Turbine Model

Wind energy is a form of solar energy. The sun's rays create different temperatures, pressures, and humidity on the earth. Wind energy occurs due to this formation. Wind turbines are systems that first convert kinetic energy in the wind to mechanical energy and from mechanical energy to electrical energy. A wind turbine consists of a tower,

propeller, body, high and low-speed shafts, gearbox, braking system, rotor, anemometer, automatic steering gear, yaw mechanism, and generator parts. Wind turbines may consist of different elements according to design and construction. However, each turbine has similar components that perform the same task, although their properties are different. Wind turbine equipment is shown in Figure 2.1.

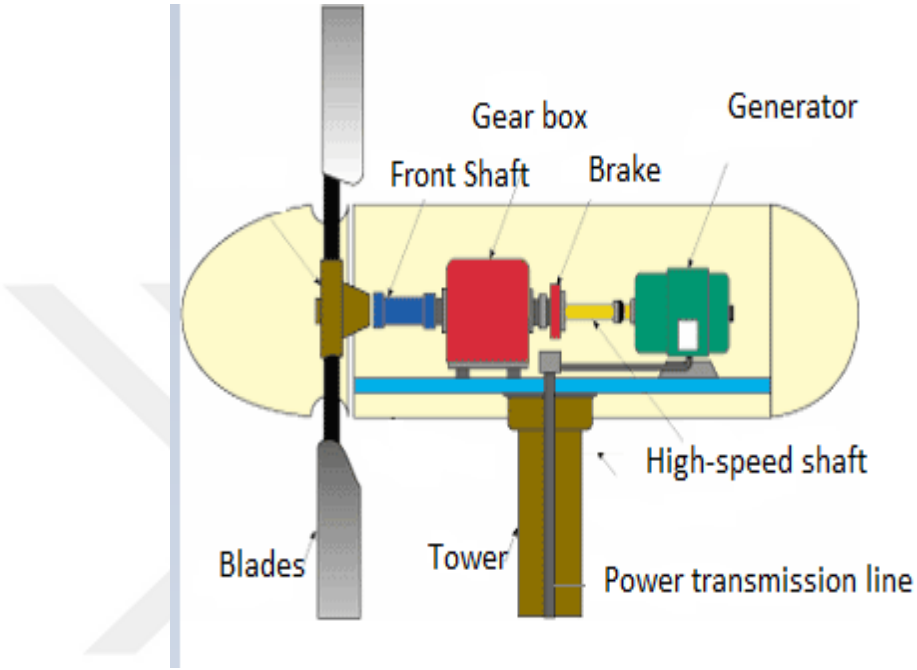

Figure 2. 1. Wind Turbine Equipment [33]

The blades catch the wind and transfer their power to the rotor. The rotor is the outermost unit that sends the power via the shaft to the gearbox and then to the generator. The kinetic energy contained in the wind is converted into useful energy with the help of wind turbines. Achieving maximum energy production from a wind turbine depends on several factors. These are factors such as the height of the wind turbine, the swept area and aerodynamic structure of the wind turbine blade, air density and wind speed. One of the most important of these factors is the aerodynamic structure of the wind turbine blade [34].

The energy obtained from the wind is directly proportional to the cube of the wind speed. Therefore, the forces that may occur at high wind speeds can be estimated. A braking system is used to control these forces. Especially in stormy weather, it is necessary to make a small surface against the wind, and even to stop it completely if

the plant will not be used. Various systems are applied to achieve these results [35]. The shaft is the equipment that connects the hydraulic systems that can operate the aerodynamic brakes to the pipes [36]. To the left of the gearbox is the low-speed shaft. The high-speed shaft, which rotates approximately 50 times faster than the low-speed shaft, is to its right. The power obtained by the rotation of the rotor (propeller) of the wind turbine is transferred to the generator by the power unit consisting of the main shaft, gearbox, and high-speed shaft. The slow rotation speed and high torque from the wind turbine rotor are converted into high speed, low torque power used for the generator by gearbox [37]. The generator is the part required to convert mechanical energy into electrical energy in wind turbines [33].

2.2.4. Controller

The controller regulates power imbalances in wind turbines or solar panels. It regulates fluctuations in current. It monitors the charge and discharge status of the system by constantly monitoring the battery bank. After the device input settings are made, it monitors the system voltage during operation and automatically activates the generator when the batteries go down to the set level. While the generator that is activated is feeding the load, it also charges the batteries [30].

2.2.5. Power Conditioner

Power conditioning units are devices that act as electrical converters. It converts the direct or alternating current produced by wind turbines or photovoltaic panels to the desired current level. That is, it provides DC/DC, DC/AC or AC/DC conversion.

2.2.6. Proton Exchange Membrane (PEM) Electrolyzer

The electrolyzer is a method of obtaining hydrogen from water. In the electrolysis method of water, water is decomposed into hydrogen coming out from the cathode side and oxygen coming out from the anode side with the help of electric current. Electrolyzers according to the type of electrolyte used divided into varieties. Electrolyzers are classified according to whether the electrolyte used is solid or liquid.

Liquid electrolyte is commonly used in alkaline electrolyzers, solid electrolyte is generally used in PEM electrolyzers and solid oxide electrolyzers. Since PEM electrolyzers can operate at more variable current densities, it is easier to integrate them into renewable energy sources whose energy production level is constantly variable. In addition, the PEM electrolysis method has many advantages over traditional hydrogen production techniques such as high efficiency, high purity and pressure hydrogen production, and environmental friendliness of the reaction products [38].

PEM water electrolyzer uses a polymer electrolyte membrane (or proton exchange membrane) as the ionic conductor. Water is oxidized at the anode and hydrogen and oxygen gases were produced anode and cathode, respectively [39]. The basic reactions for hydrogen and oxygen production in the water electrolyzer are given as follows;

Anode: $2H_2O \rightarrow O_2 + 4H^+ + 4e-$ (2.32)

Cathode: $4H^+ + 4e^- \rightarrow 2H_2$ (2.33)

Total cell reaction: $2\mathrm{H_2O\ (l)} + \text{electrical energy} \rightarrow 2\mathrm{H_2(g)} + \mathrm{O_2(g)}$ (2.34)

The working principle of the PEM Electrolyzer is shown in Fig. 2.7. Water is supplied to the PEM electrolyzer from the anode section. Water dissociates into oxygen gas, hydrogen ions and electrons of hydrogen in the anode catalyst layer. While the oxygen gas is taken out of the cell, hydrogen ions (H^+) pass through the electrolyte to the cathode. Electrons pass through the external circuit to the cathode and combine with hydrogen ions in the cathode catalyst layer to form hydrogen gas. Thus, the electrolysis process is completed [1].

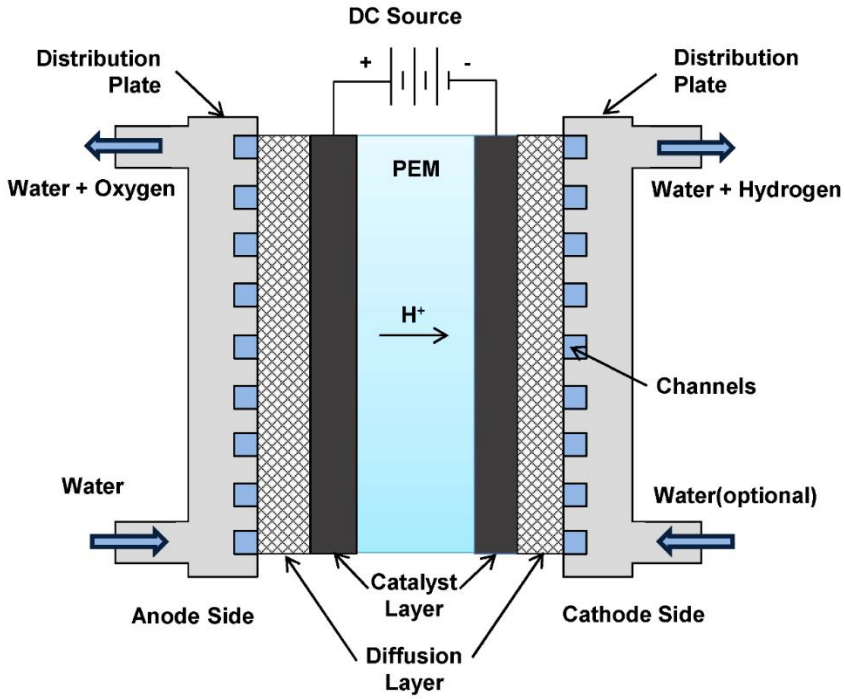

Figure 2. 2. Working principle of PEM electrolyzer [40]

In the electrolysis of water, the reversible cell potential V^0, which expresses the minimum potential difference that must be applied between the two electrodes for the theoretical decomposition reaction to occur, is calculated as follows:

$$V^0 = \frac{\Delta G}{nF} = 1.229\ V \tag{2.35}$$

In this equation, ΔG represents the Gibbs free energy, n represents the number of electrons, and F represents the Faraday constant. Gibbs free energy refers to the portion of the fuel that can be used (or converted to useful work) regarding ambient temperature and is calculated as follows:

$$\Delta G = \Delta H - T\Delta S \tag{2.36}$$

$$\Delta G = [(h_{H2} + \frac{1}{2}h_{O2}) - h_{H2O(s)}] - T[(s_{H2} + \frac{1}{2}s_{O2}) - s_{H2O(s)} \tag{2.37}$$

In this equation, h_{H2O}, h_{O2}, h_{H2} represent the enthalpies of water, oxygen and hydrogen,

s_{H2O}, s_{O2} and s_{H2} entropies, and T represents the temperature, respectively [41].

The value of 1.229 V is the minimum thermodynamic potential difference required for water to be separated into its components. However, due to irreversibility occurring in each system, electrolysis also starts at a higher potential [42]. In other words, since the system cannot receive heat from outside for the electrochemical process to take place, this energy is met by the extra potential difference applied to the cell. When irreversibility is considered, the minimum potential difference at which electrolysis occurs is called thermo-neutral voltage ($V_{thermo\text{-}neutral}$). Theoretical cell voltage under standard conditions:

$$V_{thermo-neutral} = \frac{\Delta H}{nF} = 1.48\ V \tag{2.38}$$

where ΔH is the minimum amount of energy (enthalpy) required to form or break molecular bonds.

2.2.7. Proton Exchange Membrane Fuel Cell (PEMFC)

The fuel cell is one of the most important renewable energy sources that does not emit carbon, that is, does not harm nature. The fuel cells are electrochemical converters. They convert chemical energy directly into electrical energy. They are clean energy sources because they do not have a combustion phase. PEMFC is one of the fuel cells types. Low operating temperature, high power density, fast operation and absence of noise pollution are among the advantages of PEMFC [43].

The main fuel of the PEMFC is hydrogen. Hydrogen reacts with air or O_2. As a result of the reaction, heat, electricity, and pure water are produced. Since pure water is produced as waste, it does not harm the environment. PEMFC works in the reverse of the electrolyzer. H_2 is supplied by the anode, while air or water is supplied by the cathode. H_2 is separated into positive and negative ions by the anode. Positive ions only allow positive ions to pass through and reach the cathode side with the aid of the electrolyte. Electrons remaining at the anode end tend to flow to the cathode side. This electron in the external circuit produces electricity [44]. Electrons that pass to the

cathode side combine with positive ions and air and form pure water [45]. The working principle of the PEMFC is given in Figure 2.3 [46]. Anode, cathode, and total cell reactions are given in Equations 2.39, 2.40 and 2.41, respectively.

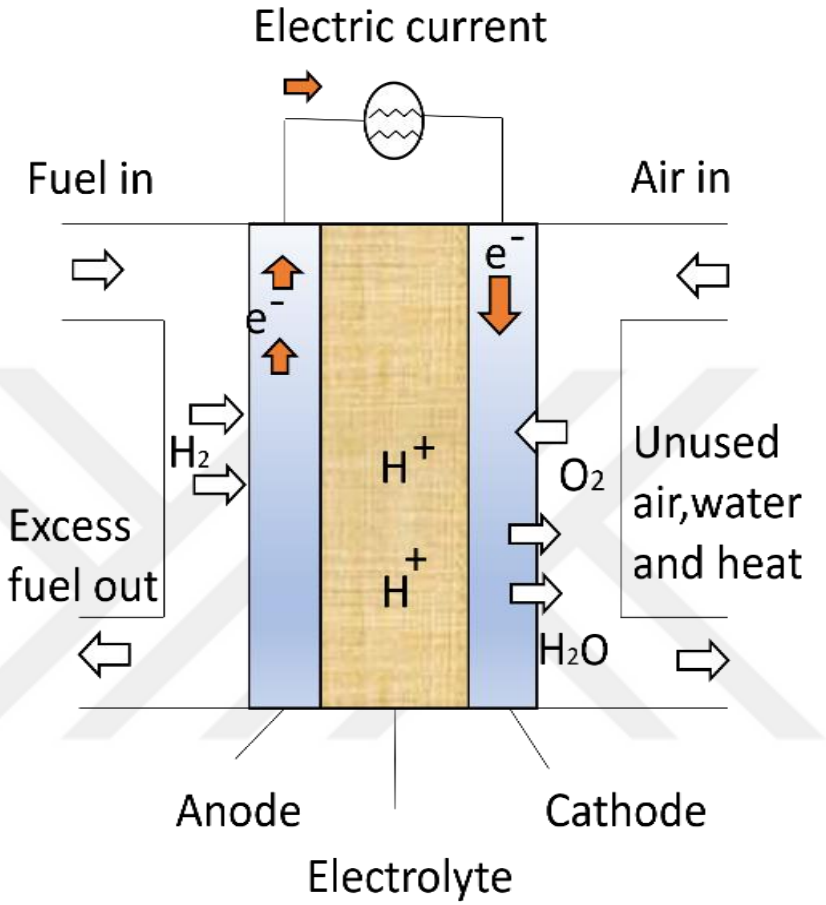

Figure 2. 3. Schematic Operation Diagram of PEMFC

Anode: $H_2 \rightarrow 2H^+ + 2e^-$ (2.39)

Cathode : $\frac{1}{2}O_2 + 2H^+ + 2e^- \rightarrow H_2O$ (2.40)

The total cell reaction: $H_2 + \frac{1}{2}O_2 \rightarrow H_2O + Energy$ (2.41)

The energy potential of PEMFC can be found with the Gibbs free energy;

$$E = \frac{-\Delta G}{nF} \tag{2.42}$$

At standard condition (T=25 ◦C, P=1 atm), the potential of PEMFC is theoretically equal to 1.23 V. However, due to some losses, this value is less than the theoretical potential.

Cell voltage (V_{cell}) can be found in any case using equation 2.43. When a cell powers the load, the no-load voltage (E); Activation (V_{act}), called voltage drop, is reduced by ohmic (V_{ohm}), and concentration (V_{conc}) over voltages [43].

$$V_{cell} = E - V_{act} - V_{ohm} - V_{conc} \tag{2.43}$$

2.3. Levelized Cost of Energy Analysis (LCOE)

When it comes to energy production, different energy sources require different financial models. Analyzing the economy of a project is essential and various calculation methods can be used accordingly. For renewable energy sources, using the leveled cost calculation method can be chosen as an important part of reaching the right feasibility about the cost. Electric level electricity cost, also known as LCOE, is the net present value of the cost in the electricity generation unit over the life of the generator asset. Energy unit price is calculated by considering initial investment cost, operating and maintenance costs and fuel costs [47]. There is no cost in these systems as no fuel is used in the sun and wind. Since H_2 and O_2 tanks will be included in the system as full, fuel prices are calculated separately. The initial investment cost, replacement cost and maintenance cost of each component in the hybrid system are calculated according to the power of the component [48]. Thus, the minimum price at which energy must be sold can be calculated in order to avoid loss [49].

LCOE is calculated according to Equation (2.44) as shown below [50];

$$LCOE = \frac{\sum_{i=0}^{N}\left[\frac{I_i + O_i + F_i - TC_i}{(1+r)^i}\right]}{\sum_{i=0}^{N}\left[\frac{E_i}{(1+r)^i}\right]} \tag{2.44}$$

where I_i, is the capital cost in year i, O_i, is the operation and maintenance costs (O&M) in year i, F_i is fuel cost in a year i, TC_i is total tax credits in a year i. In this study, the total tax credits were ignored. E_i has generated electricity in year i, N lifetime of the system (20 years), r is the real discount rate (3 %) [51]. When the component's lifetime is less than the lifetime of the designed systems, then the new component must be purchased by using the replacement cost for the year that the component lifetime ends [52].

2.4. Motivation of Study

In this thesis, a PV/wind/electrolyzer/PEMFC based hybrid energy system operating independently of the grid has been developed. The installation location of the proposed hybrid energy system has been determined as Atilim University Incek campus. Since meeting all the electricity needs of the university, independent of the network, requires a very large system, the design was based on a daily 25kWh fixed energy consumption.

The proposed hybrid energy system is illustrated in Figure 2.4. The system simulation was performed through the Transient System Simulation (TRNSYS) software program with real meteorology data obtained from the metarulogy station in Atilim University [30]. The electrolyzer and PEMFC system models are developed according to the experimental data in MATLAB and integrated into a TRNSYS [54]. Different design scenarios were investigated with different combinations to find the most economical system. The different scenarios also enable us to make the optimal decision about the composition of WTs and PVs that will be used by the PV/WT/electrolyzer/PEMFC hybrid system. The results highlight the important role of the H_2 chain in reducing the energy cost.

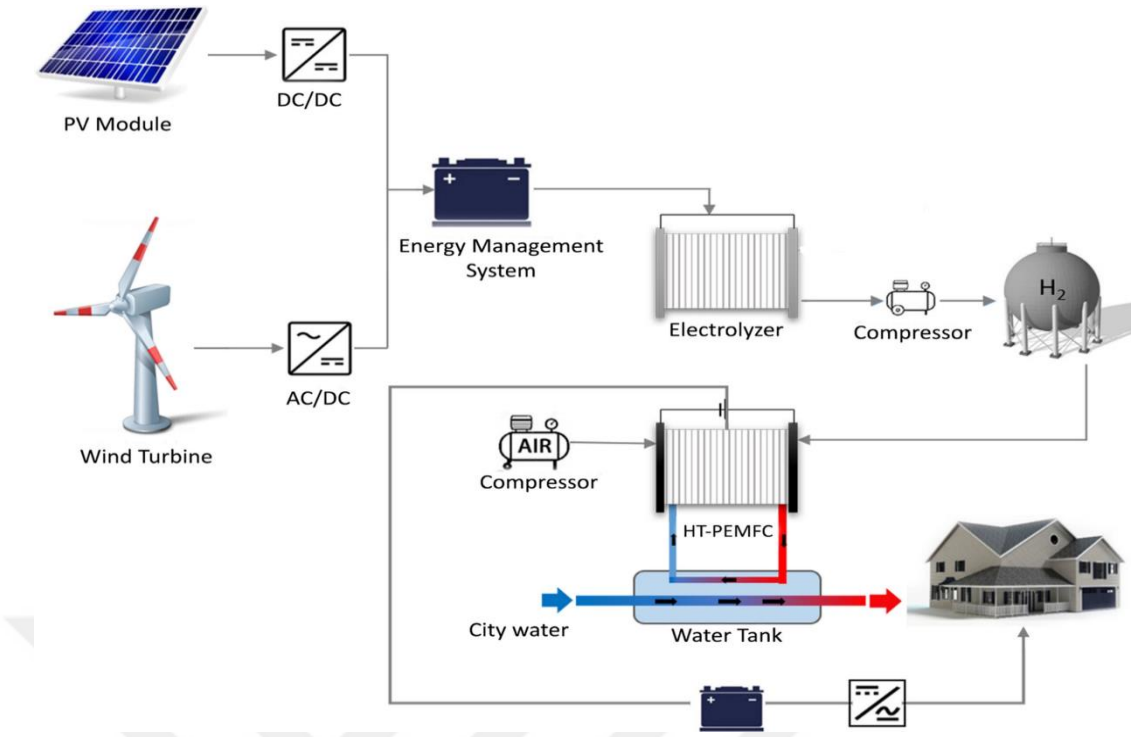

Figure 2. 4 Schematic diagram of the proposed hybrid energy system

CHAPTER 3

3. METHODOLOGY

3.1. Data Collection

The installation location of the PV/WT/electrolysis/PEMFC based hybrid energy system examined within the scope of the thesis has been determined as Atılım University, İncek campus. The Atilim University (39.813°N, 32.726 °E) located in Ankara, Turkey was selected as the location of the hybrid system installation (Figure 3.1).

Figure 3. 1. Location of Atilim University Incek Campus (Ankara, Turkey)

The daily energy need of Atilim University has been determined as 25 kWh and it is desired to provide from proposed hybrid systems. Additionally, the area where the hybrid system can be installed is determined as 250 m^2. The system design was carried out both by using real solar radiation, temperature, wind speed, etc. data measured

from the meteorology station installed in Atilim University Incek campus, as well as using data obtained from the Meteonorm estimation program, which can work integrated with the TRNSYS program.

3.1.1. Data Obtained from Meteonorm Program

Meteonorm is a reliable data tool program that gets representative weather data for any place in the world. It allows data access based on day, month, year. The database consists of more than 8,000 weather stations, five geostationary satellites and a globally calibrated aerosol climatologs [57]. In this thesis study, 2020 Meteorology data was taken from the Meteonorm program, which is one of the data acquisition methods, by choosing the IPCC AR4 B1 scenario, which is the most optimistic design [58]. The requested data were taken in TMY2 format following the Type 16.2 component in the subroutine of the TRNSYS program [59].

3.1.2. Data Obtained through Atilim University Meteorology Station Data

The Meteorology Station was installed in Atilim University Incek Campus (Figure 3.2). The meteorology data such as solar radiation, temperature, wind speed, humidity and atmospheric pressure were obtained meteorology station.

Figure 3. 2. Atilim University Meteorology Data Station

The collected data for 1 year is integrated into the TRNSYS Software with Type 16a component of the TRNSYS program. Type 16a component, which is in the subroutine of TRNSYS, provides the transfer of externally collected data to TRNSYS [60].

3.2.Design of Proposed Hybrid Energy System

The proposed hybrid system was designed to meet the uninterrupted daily 25 kWh energy requirement of the load completely independent of the grid. In the proposed off-grid system a battery bank is used for backup energy storage and the hydrogen tank with the associated PEM type electrolyzer and PEMFC is used for seasonal storage. Therefore, the design parameter of the PEMFC was determined to meet the H_2 and O_2 requirements of PEMFC throughout the year. The PEMFC was selected to supply load demand of 25 kWh. The system has a PEM-type electrolyzer to produce H_2 and O_2 that PEMFC needs [56]. The power requirement of the electrolyzer is supplied from PV and WT. The total power generated from WT and PV was delivered to the electrolyzer to produce H_2 and O_2 gas. Produced excess energy can be converted to H_2 using the PEM electrolyzer to obtain long-term interrupted energy storage [61].

The designed hybrid system was simulated in the TRNSYS Software [55]. PEMFC and PEM electrolyzer are not included in the subroutine of TRNSYS Software. Therefore, the codes of these components were designed in the MATLAB program [54].

PEMFCs can operate with both air and oxygen supply. Therefore the hybrid energy system was modeled using H_2/O_2 and H_2/air based PEMFCs and the effects of both designs on system performance and economic optimization were investigated. It was aimed to find out which of the two systems is more advantageous in terms of cost and performance. Figures 3.3 and 3.4 show hybrid systems design with H_2/O_2 and H_2/air based PEMFCs, respectively.

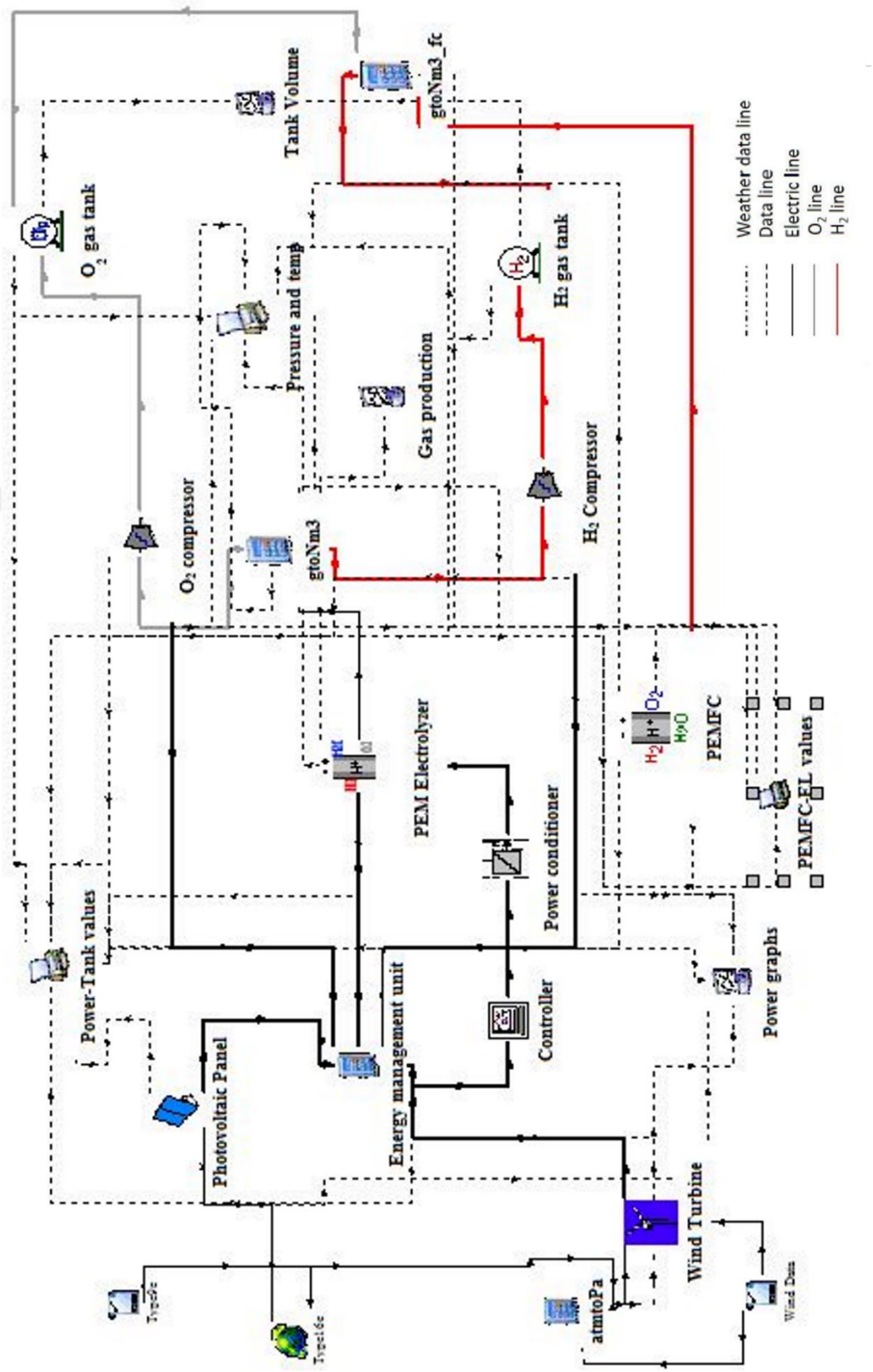

Figure 3.3. TRNSYS Model O_2 inlet hybrid system

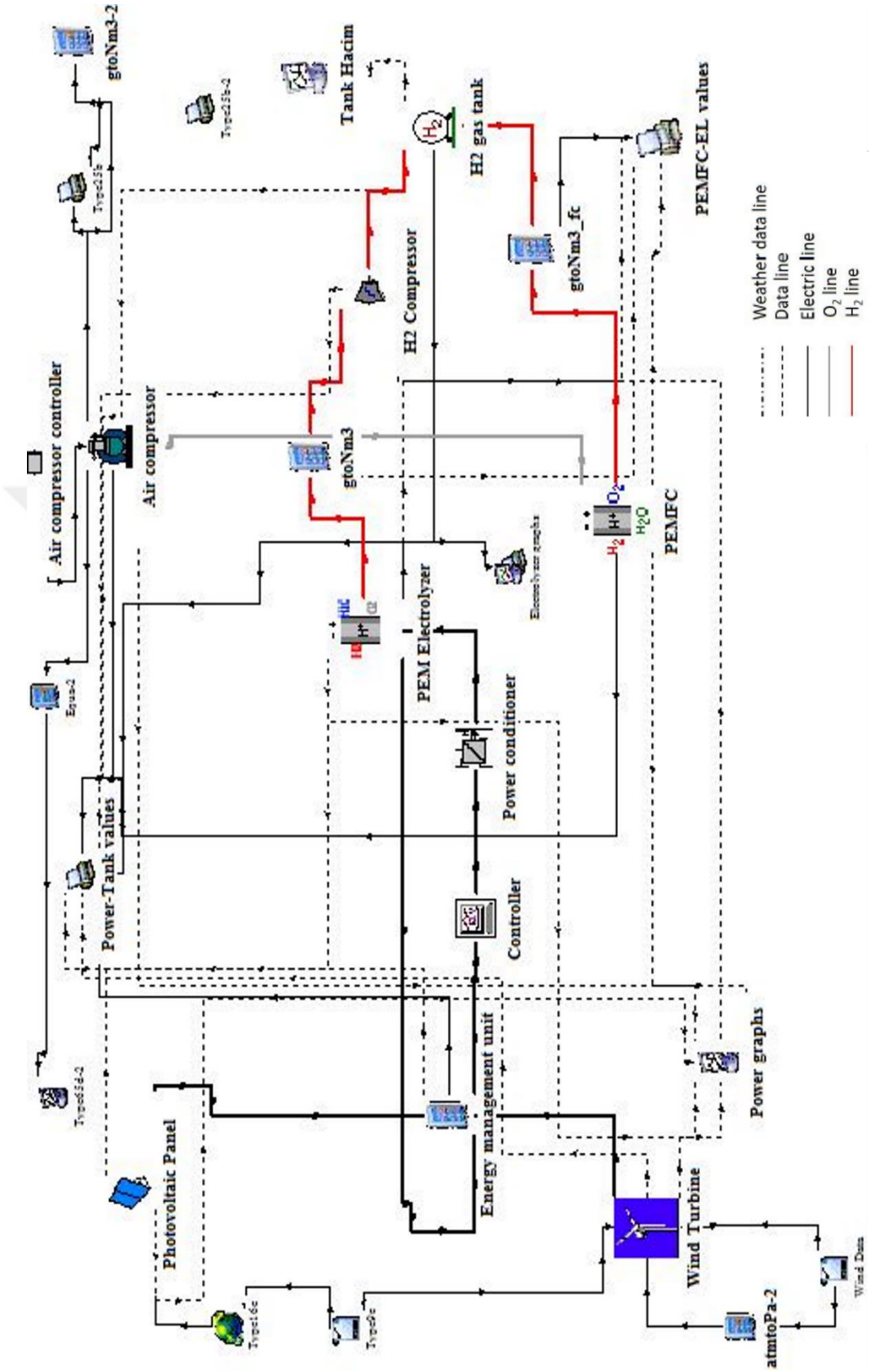

Figure 3.4. TRNSYS Model Air inlet hybrid system

3.2.1. Hybrid Energy System with H_2/O_2 PEMFC

In this system, O_2 separated from water with the help of an electrolyzer is stored in the O_2 tank. The stored O_2, which is under pressure, is used by the pressure regulator to reduce the pressure coming into the fuel cell. Since excess O_2 must carry products from the cell; 20-30% more O_2, should be provided stoichiometrically. Excess O_2 can be vented at the fuel cell outlet. However, most practical systems operate in a closed-loop configuration where excess O_2, is returned to the stack inlet. It is needed an active (pump) or passive (ejector) device to bring the low-pressure gas at the flue outlet to a higher pressure at the flue inlet. Through a simple water/gas separator, the liquid water in the exhaust can be separated and mixed with a dry gas from the tank to achieve the desired humidity [26].

3.2.2. Hybrid Energy System with H_2/Air PEMFC

In H_2/air systems, the air is provided via a fan or a blower (for low-pressure systems) or by an air compressor (for pressurized systems). In the first case, when exhaust exits PEMFC it opens directly to the environment, while in a pressurized system, the pressure is maintained by a pressure regulator. In all cases, a fan, blower, or compressor is driven by an electric motor, which requires electrical power. An electric motor is an equipment that represents power loss or parasitic load. Compression can be isothermal or adiabatic. The former allows for temperature equilibrium with the environment and implies an infinitely slow process. The second one expresses the opposite process. That is, it is such a fast process that there is no heat exchange with the environment during compression. This process is closer to real-life [26].

3.3. Modeling of the Hybrid System with TRNSYS

This thesis has been simulated with the TRNSYS program. TRNSYS is the preferred design of energy systems with many components. In addition, it allows importing the codes and files created in programs such as EXCEL and MATLAB. The data received from the Meteonorm program were transferred using the Type 15.6 component, which is a component of TRNSYS. The data collected by the station placed at Atilim

University was transferred to the hybrid system using Type 16a. Type 103b is used for photovoltaic panels which is using the 4 parameters model. Type 103 has to properties of Monocrystalline. Type 90 is used for wind turbines [62]. In the system, Type 100a which is called Controller is used for power imbalances caused by the panel and the turbine. The Type 175, power conditioning component, converts direct current to alternating current and vice versa. The PEM electrolyzer component used in the designed system was integrated into TRNSYS through the Type 155 component by creating a code in MATLAB. The H_2 and O_2 gases produced from the electrolyzer separating the water into its components are transmitted to the H_2 and O_2 tanks through the H_2 and O_2 compressors (Type 164b) [63]. Since the PEMFC is not included in the TRNSYS subroutine, it was designed in MATLAB and integrated into TRNSYS with Type 155. In H_2/air PEMFC system, an air compressor was used (Type 629) to provide an oxidant to PEMFC. The compressor controller was designed in MATLAB and integrated into TRNSYS [64]. TRNSYS contains a component that takes the function of the printer in its subroutine (Type 25). The printer component is used to output (or print) selected system variables at specified intervals of time [65].

3.4.Optimal Design Strategy of Proposed System

The power management strategies of the hybrid power system with H_2/O_2 PEMFC and H_2/Air PEMFC are illustrated in Figure 3.5 and Figure 3.6, respectively. The design parameter was determined to meet the H_2 and O_2 requirement of PEMFC for 5 h daily operation throughout the year. Therefore, the optimum numbers of PV and WT were determined for the uninterrupted operation of the proposed hybrid system throughout the year.

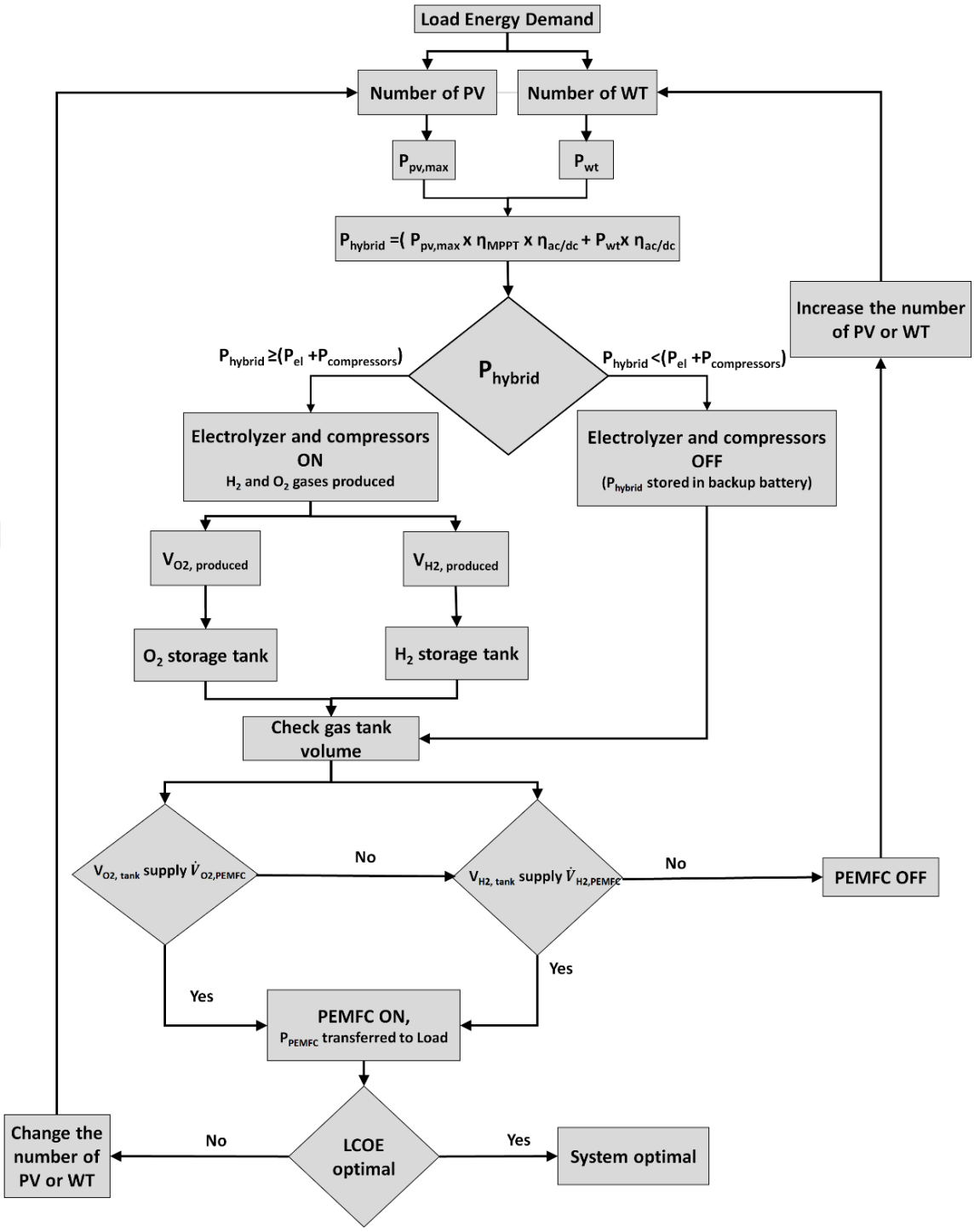

Figure 3.5. Power and gas management strategy of the hybrid power system with H_2/O_2 PEMFC

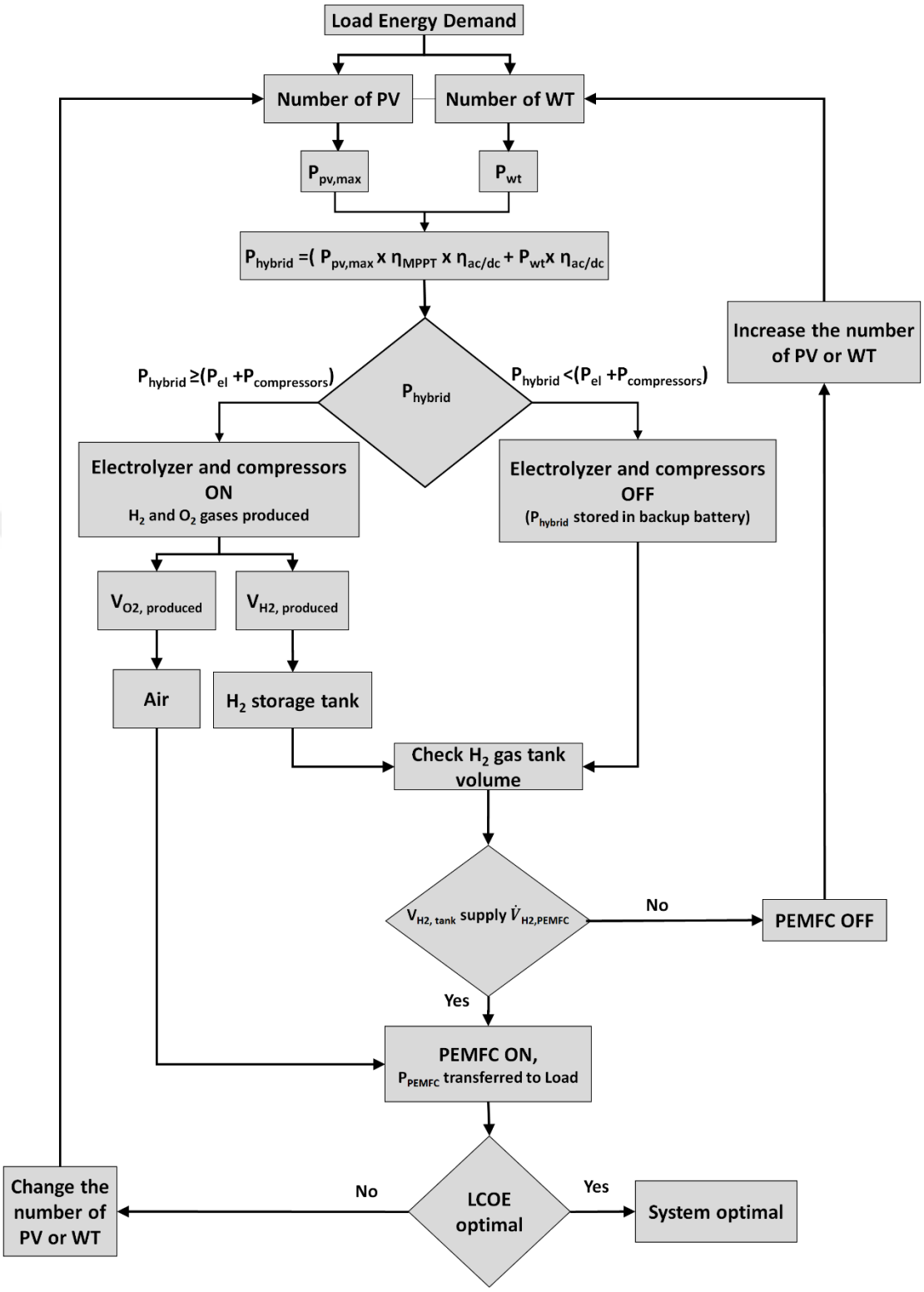

Figure 3.6. Power and gas management strategy of the hybrid power system with H_2/Air PEMFC

The control of the energy management is shown below.

If $(P_{hybrid}) > (P_{electrolyzer} + P_{compressors}), electrolyzer\ ON$

If $(P_{hybrid}) < (P_{electrolyzer} + P_{compressors}), electrolyzer\ off\ , excess\ \ power\ fed\ to\ the\ Backup\ Battery$

Where P_{hybrid} is the power produced by the hybrid system, $P_{compressor}$ is the power consumed by the compressor, $P_{electrolyzer}$ is the power consumed by the electrolyzer.

If the power generated by the hybrid system meets the needs of both the electrolyzer and the compressors, the electrolyzer works. For the O_2 system, the H_2 and O_2 gases produced via the electrolyzer are stored in the tanks. For the air system, the air is supplied through an air compressor. Moreover, the excess power is fed to the load and auxiliary components (BOP) of the PEMFC.

When the total power produced (P_{hybrid}) is adequate for the electrolyzer but not adequate for the power requirement of the compressors, the gases which are generated cannot be compressed and stored in tanks. Hence, if the generated power is not sufficient to start the compressors, the electrolyzer does not work and the power produced by PV and WT is fed to the load. In this case, the H_2 need of PEMFC was met from the storage tanks.

When there is not as much gas as PEMFC needs in the gas storage tanks, the simulation is repeated by changing the PV and WT numbers used in the design. A different number of scenarios are tried to find optimum system design. For both systems, LCOE values are also calculated.

3.5.Design Calculations

The design calculations of the proposed PV/WT/PEM Electrolyzer/PEMFC system are explained in the following sections.

3.5.1. Solar Calculation

Solar radiation measurements were taken according to the Atilim University Incek Campus (39.813 N, 32.726 E). The system installation area was selected as 250 m^2. The solar radiation data obtained from the Meteonorm program, and the Atilim University meteorology station are shown in Figure 3.7. The characteristics of the PV panel used are given in Table 3.1.

Table 3. 1. Properties of PV Panel

Name	**Value**	**Unit**
SunPower X-22 Series Nominal Power	370	W
MPPT Mode	0 or 1	
Modules short-circuit current at reference conditions (I_{sc})	6.66	A
Module open-circuit voltage at reference conditions (V_{oc})	69.5	V
Reference cell temperature	25	ºC
Reference insolation	1000	W/m^2
Rated voltage (V_{MPP})	59.1	V
Rated Current (I_{MPP})	6.26	A
Temperature coefficient of I_{sc} (ref. cond)	0.0029	A/K
Temperature coefficient of Voc (ref. cond)	-0.1674	V/K
Panel Efficiency	22.7	%
Module temperature at NOCT	40	ºC
Panel efficiency	22.7	%

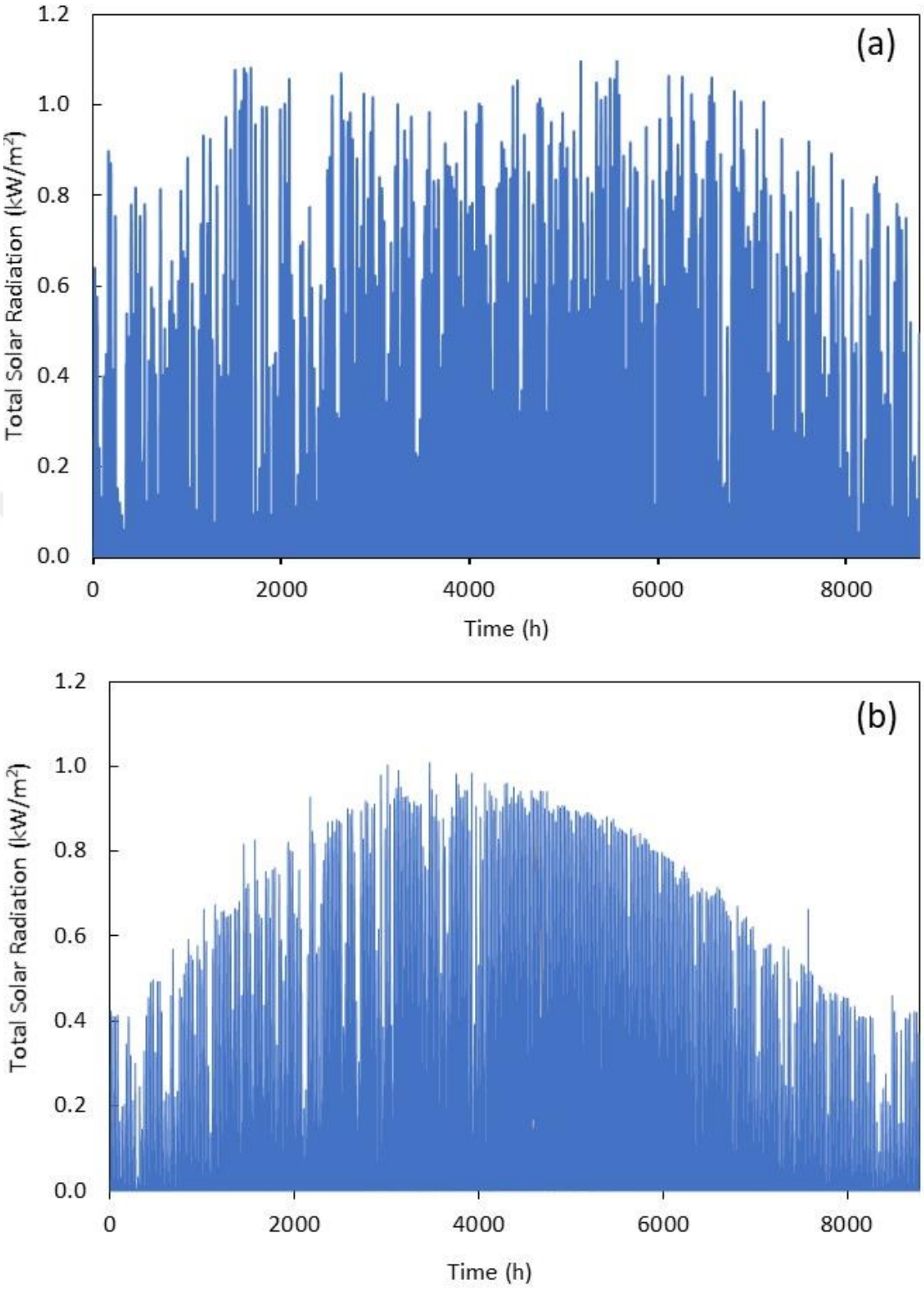

Figure 3. 7. Hourly Global Solar Radiation data received from a) Meteonorm program, b) Atilim University meteorology station

The maximum power of the photovoltaic panel can be found from the current and

voltage values.

The maximum power value is found as follows:

$$P_{max} = I_{mpp}V_{mpp} \tag{3.1}$$

Where I_{sc} is short circuit current, V_{oc} is open-circuit voltage and FF is filled factor.

The power of the PV array can be calculated according to Tebibel [66].

$$P_{PV} = N_{PV}\frac{G_I}{G_{I_{ref}}}[P_{PV,max} + \mu_P(T_{cell} - T_{c,ref})] \tag{3.2}$$

N_{PV} is the number of PV arrays, G_I and $G_{I_{ref}}$ are solar irradiance and the reference solar irradiation of PV, respectively, μ_P is the power thermal coefficient. $T_{c,ref}$ is the cell temperature at the reference temperature and it is 25 ºC. T_{cell} is cell temperature can be calculated as follows:

$$T_{cell} = T_a + G_I\frac{NOCT-20}{800} \tag{3.3}$$

T_a is ambient temperature, NOCT is nominal operating cell temperature which is equal to 45 ºC.

The panel layout is important in photovoltaic systems. Sun angles are required for this. The angle that the sun's rays make with the horizontal plane is the solar altitude angle, α. The angle between the longitude of the place under consideration and the line connecting the sun to the center of the earth is the hour angle, ω. These values may change according to the time of day or the number of days in the year [67]. The calculation of the sun elevation angle and the hour angle is shown in the previous section. The azimuth angle can be calculated as follows:

$$sin(\gamma_s) = \frac{\cos(\delta)\sin(\omega)}{\cos(\alpha)} \tag{3.4}$$

γ_s is solar azimuth angle, δ is declination angle, ω is hour angle and α is solar altitude angle. The declination angle can be found with the selected days for each month and the Cooper equation is used:

$$\delta = 23.45sin\left[\frac{360}{365}(N + 284)\right] \quad (3.5)$$

Time hour can be calculated as follows:

$$\omega = (ST - 12) \times 15 \quad (3.6)$$

ST is solar time. Solar time changes according to the angular movement of the sun in the sky. Solar time is calculated as follows:

$$ST = LT + ET - 4(SL - LL - DS) \quad (3.7)$$

Where LT is local standard time (14.00), ET is time correction, SL is the standard meridian (45), LL is the local meridian (32.44), and DS is the daylight-saving time application and varies between 0 and 60 minutes. In this thesis study, the hour with the highest radiation value (14.00) was used.

The orbital velocity of the earth changes throughout the year due to the variables caused by the earth's orbit around the sun. For this reason, the ST differs from the time measured by a clock used on earth, operating at a uniform speed. This difference is called the equation of time (ET) and can be calculated by Equation 3.8. Throughout the year, the average length of a day was assumed to be 24 hours; however, the length of a day depends on the earth's orbit and the tilt of the earth's axis [27].

$$ET = 9.87\sin(2B) - 7.53\cos(B) - 1.5\sin(B) \quad (3.8)$$

B can be calculated as follows:

$$B = (N - 1)\frac{360}{365} \quad (3.9)$$

The monthly angle values of the selected location are given in Table 3.2.

Table 3. 2. Monthly angle values of the selected location

Month	**Day of the year**	**The declination angle**	**Hour angle**	**Solar Altitude angle**	**Solar azimuth angle**
January	17	-20.92	15.00	47.85	22.68
February	48	-12.95	0.00	50.29	0.00
March	79	-2.42	15.00	48.18	22.84
April	105	9.41	15.00	48.35	22.92
May	135	18.79	15.00	48.51	23.00
June	162	23.09	15.00	48.58	23.03
July	198	21.18	15.00	48.55	23.02
August	228	13.45	15.00	48.42	22.95
September	258	2.22	15.00	48.23	22.87
October	288	-9.60	15.00	48.04	22.77
November	318	-18.91	15.00	47.88	22.70
December	344	-23.05	15.00	47.81	22.67

D_s is the shadow length, which can be measured as the difference between the bottom/front edge of a row and the maximum height using the module vertical projection in Figure 3.8, D_r is the spacing between the two rows in the south direction and can be calculated with Equation 3.12 and Equation 3.13 [1]. Primarily the lengths and heights of the panels were calculated with Equations 3.10 and 3.11, depending on the inclination angles (β) of the panels to calculate these dimensions. In this study, the optimum panel slope was determined by Koçer et al. selected from his work [68].

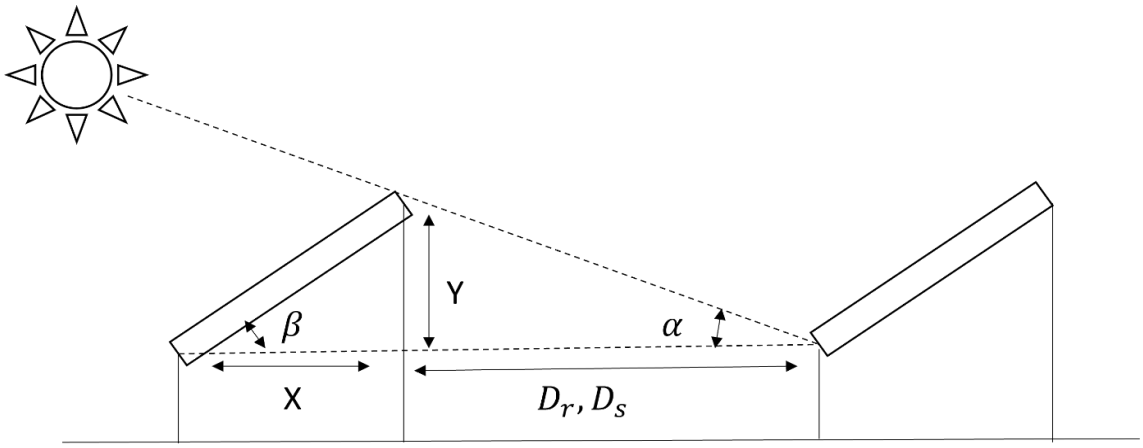

Figure 3. 8. Side view of PV arrays

$$X = L_m cos(\beta) \tag{3.10}$$

L_m is module length.

$$Y = L_m sin(\beta) \tag{3.11}$$

$$D_s = \frac{Y}{tan\propto} \tag{3.12}$$

$$D_r = D_s \times \cos(z) \tag{3.13}$$

The smallest azimuth angle value of 0 degrees was taken for the panel placement to be suitable for all months. The total length and width of the panels must be calculated to calculate the total area where the panels are installed with Equation 3.14 [67].

$$A_t = W_t \times L_t \tag{3.14}$$

W_t is total width and L_t is the total length. The total width is the number of PV panels connected in series and the width of one PV panel.

$$W_t = n_m \times W_m \tag{3.15}$$

Where n_m is the number of PV modules connected in series in a row, W_m is the width

of a PV module.

$$L_t = n_r \times X + (n_r - 1) \times D_r \quad (3.16)$$

Where n_r is the number of PV modules connected in parallel. Thus, the total area can be calculated as follows:

$$A_L = (n_m \times W_m) \times (n_r \times X + (n_r - 1) \times D_r) \quad (3.17)$$

3.5.2. Wind Calculation

In this thesis, E70 Pro wind turbine is used. Wind turbine properties are given in Table 3.3 [69]. The data were prepared in the form of data files by the TRNSYS Software and integrated into TRNSYS Software [70].

Table 3. 3. Properties of WT

Properties	**Value**	**Unit**
EnAir 70 Pro Power	5500	W
Rated Power	4000	W
Diameter	4.30	m
Swept Area	14.5	m^2
Wind to start	2	m/s
Rated Speed	11	m/s
Speed regulation of pitch	12	m/s
Survival Speed	60	V

The wind speed data obtained from the Meteonorm program and Atilim University meteorology station are shown in Figure 3.9 and Figure 3.10, respectively.

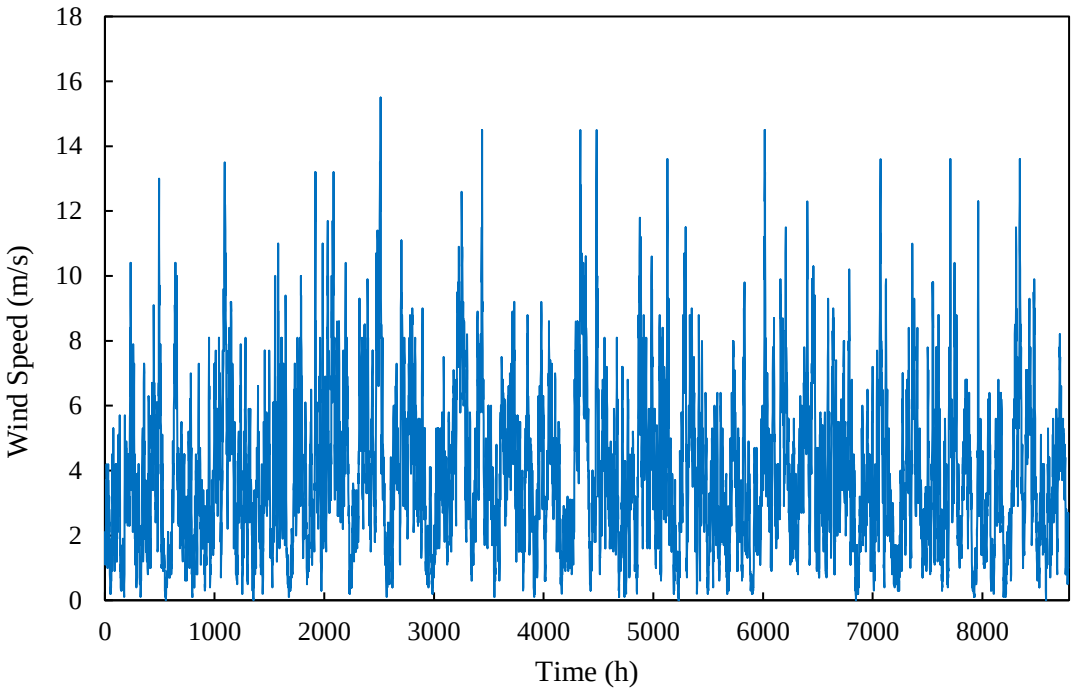

Figure 3. 9. Wind data obtained from the Meteonorm program

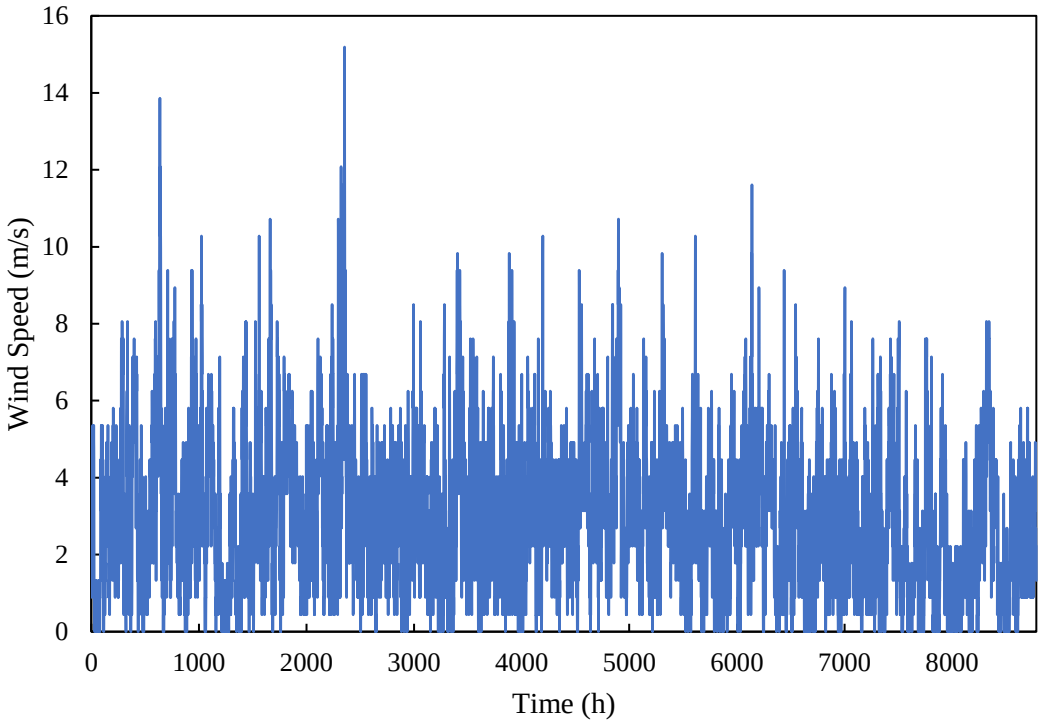

Figure 3. 10. Wind speed data obtained from Atilim University meteorology station

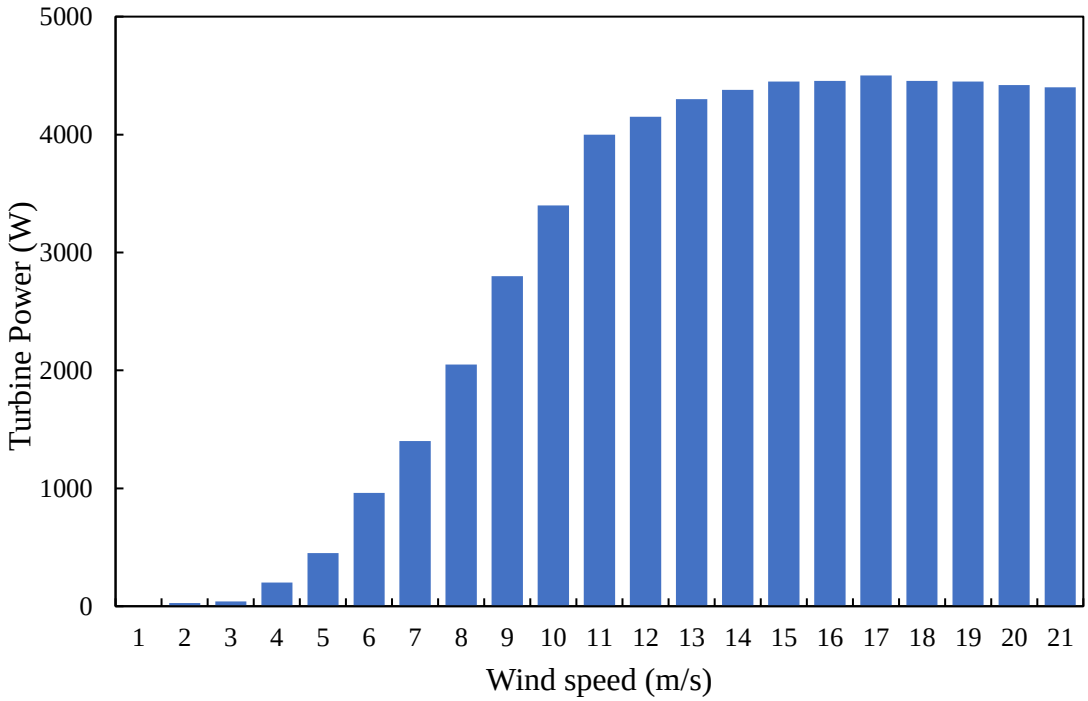

Figure 3. 11. Power & Wind Speed curve of WT

The power generation of the wind turbine can be determined from Equation 3.18.

$$P_{WT} = \frac{1}{2} \times \rho_{air} \times c_p \times A_r \times v^3 \tag{3.18}$$

c_p was taken as 0.14 to characterize ideal boundary layer conditions, the wind shear exponent. ρ_{air} is air density and it is taken 1.124 kg/m^3, v is the wind speed at turbine height and A_r is rotor swept area.

Backwater and wind shadow should be considered when placing wind turbines. The total WT installation area is obtained as in the equation below:

$$N_{TR} = \frac{L_R}{S_R} + 1 \rightarrow L_R = (N_{TR} - 1) \times S_R \tag{3.19}$$

where N_{TR} is the number of turbines in a row, L_R is row length and S_R is row spacing. The distance to the roadside of the turbines was not considered while calculating the area. Turbulence is formed by the rotation of more than one wind turbine installed in

a wind farm [71]. Distances should be maintained between wind turbines to minimize the effect of turbulence. While this distance is at least 4 rotor diameters in series connected turbines, it should be at least 10 rotor diameters in parallel connected wind turbines. WT placement is shown in Figure 3.12 [56].

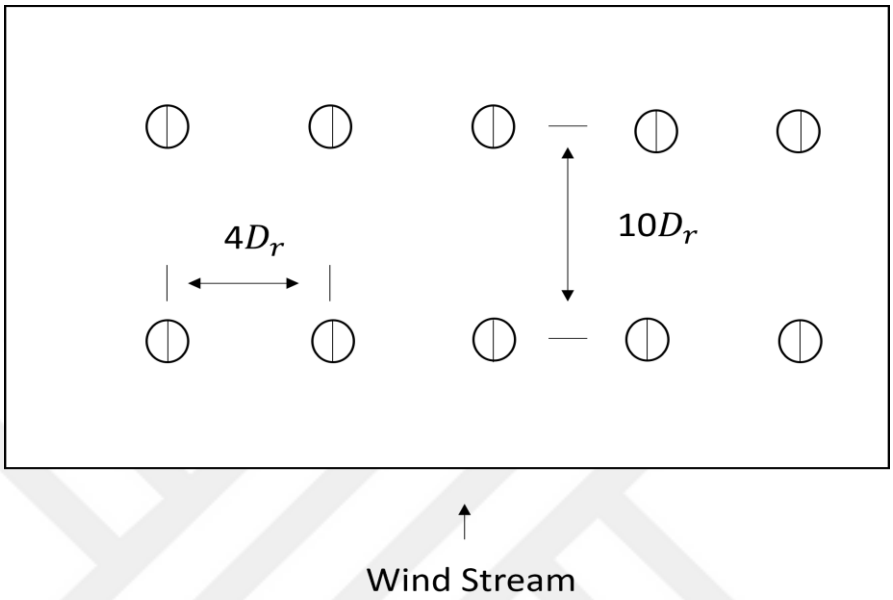

Figure 3. 12. Wind farm layout

3.5.3. PEM Electrolyzer Calculation

The electrolyzer is designed according to the PEMFC, which consumes 5 kW of power. For this, the minimum power required for the operation of the electrolyzer is calculated. This value is obtained according to the number of moles consumed by the PEMFC. The design was made by writing code in the MATLAB program and integrated into the TRNSYS Software [72].

Table 3. 4. Properties of Electrolyzer

Properties	**Value**	**Unit**
Electrolyzer current density	1.0	A/cm^2
Electrolyzer active area	625	cm^2
Electrolyzer cell voltage	1.55	V
Electrolyzer consumed power	18406.25	W
Faraday constant	96485	A.s/mol
The molecular weight of H_2	2.0158	g/mol
The molecular weight of O_2	31.998	g/mol
Operation temperature	80	ºC
Operation pressure	1	atm
Electrolyzer efficiency	0.88	-

The current of the PEM electrolyzer is found to calculate the performance of the electrolyzer:

$$I_{stack} = i_{cell} \times A \tag{3.20}$$

i_{cell} is electrolyzer current density, A is electrolyzer active area.

To find the number of moles produced by the PEM electrolyzer:

$$n_{\mathrm{H_{2,produced}}} = \frac{i_{cell} \times A_{ele} \times \eta_{\mathrm{ele}} \times \mathrm{n_{cell}}}{2\mathrm{F}} \tag{3.21}$$

The voltage of the stack is the product of the number of stacks and the cell voltage of the PEM electrolyzer:

$$V_{stack} = n_{cell} \times V_{cell} \tag{3.22}$$

The mass flow rate is found by the following equations and the unit is;

$$m_{H_2} = \frac{\mathrm{I_{stack}} \times \mathrm{n_{cell}} \times mw_{H_2} \times \eta}{2F} \tag{3.23}$$

η is electrolyzer efficiency and it is given in Table 3, F is Faraday constant, mw_{H_2} is molecular weight oh H_2, mw_{O_2} is the molecular weight of O_2.

If the same equation is applied for the mass flow rate of O_2:

$$m_{O_2} = \frac{I_{stack} \times n_{cell} \times mw_{O_2} \times \eta}{4F} \quad (3.24)$$

The volumetric flow rate can be passed from the ideal gas equation:

$$V_{H_2} = \frac{m_{H_2} \times R \times T_{ele}}{mw_{H_2} \times P} \quad (3.25)$$

$$V_{O_2} = \frac{m_{O_2} \times R \times T_{ele}}{mw_{O_2} \times P} \quad (3.26)$$

Where P is the operating pressure of the electrolyzer, R is the ideal gas constant, T is the operating temperature of the electrolyzer.

In this study, a PEM electrolyzer was designed. The parameters were selected in the value ranges where the PEM electrolyzer is more efficient. The design details of the electrolyzer, whose code is written in MATLAB, are given in Appendix A.

3.5.4. PEMFC Calculation

While designing PEMFC, the gas amounts on the anode and cathode sides are calculated. The flow rates of O_2 gas entering the cathode and hydrogen gas entering the anode are found [73]. PEMFC design was prepared in MATLAB according to the equations below and calculations were made in MATLAB according to the constants in Table 3.5.

Table 3. 5. Properties of PEMFC

Properties	**Value**	**Unit**
PEMFC density for O_2 inlet	1.0	A/cm^2
PEMFC density for air inlet	0.6	A/cm^2
PEMFC active area for O_2 inlet system	225	cm^2
PEMFC active area for air inlet system	375	cm^2
Stoichiometry of H_2 for O_2 inlet system	1.2	-
Stoichiometry of O_2 for O_2 inlet system	1.5	-
Stoichiometry of H_2 for air inlet system	1.2	-
Stoichiometry of O_2 for air inlet system	2.5	W/m^2
Working time	5	h
The inlet temperature of H_2	25	ºC
The inlet temperature of O_2	25	ºC
The inlet temperature of the air	25	ºC
Anode pressure	1	atm
Cathode pressure	1	atm
ΔP	0.2	atm
Parasitic loss	0	-
Humidity rate	0.8	-

The flow rate of reactants at the inlet of PEMFC must be equal to or greater than the rate at which these reactants are consumed in the cell [74].

The rates at which H_2 and O_2 are consumed and water is produced are determined by Faraday's law:

$$N_{H2} = \frac{I \times A \times \delta_{H2} \times N_{cell}}{2F} \quad (3.27)$$

$$N_{O2} = \frac{I \times A \times \delta_{O2} \times N_{cell}}{4F} \quad (3.28)$$

$$N_{H2O} = \frac{I}{2F} \quad (3.29)$$

Where N is consumption rate, I is current, F is the Faraday constant of PEMFC.

The current value is expressed as the product of the current density and the active area in PEMFC:

$$I = i \times A \tag{3.30}$$

The mass flow rate is found by the following equations and the unit is g/s.

$$m_{H_2} = N_{H2} \times mw_{H_2} \tag{3.31}$$

$$m_{O_2} = N_{O2} \times mw_{O_2} \tag{3.32}$$

$$m_{H_2O} = \frac{I}{2F} \times mw_{H_2O} \tag{3.33}$$

The volumetric transition of the reactants can be obtained from the ideal gas equation:

$$PV = NRT \tag{3.34}$$

Where P is pressure, N is the number of moles, R is the ideal gas constant and T is the temperature.

Volumetric flow rates:

$$V_{H_2} = \frac{\mathrm{N} \times R \times t_{fc} \times 3600}{P} \tag{3.35}$$

$$V_{O_2} = \frac{\mathrm{N} \times R \times t_{fc} \times 3600}{P} \tag{3.36}$$

$$V_{H_2O} = \frac{\mathrm{N} \times R \times t_{fc} \times 3600}{P} \tag{3.37}$$

Here, t_{fc} is working time of fuel cell.

The cell number of PEMFC can be found through the power of PEMFC:

$$N_{cell} = \frac{\text{W}}{I_{stack} \times V_{cell}} \tag{3.38}$$

W_{ele} is the power of the electrolyzer.

The relative humidity is the water vapor partial pressure, which is the maximum amount of water vapor that can be found in the gas under certain conditions.

Saturation pressure values can be found in thermodynamic tables. Saturation pressure for any given temperature between 0 ºC and 100 ºC.

$$Pvs = e^{a/T + b + cT + dT^2 + eT^3 + f\ln(T)} \tag{3.39}$$

a, b, c, d, e, and f values are -5800.2206, 1.3914993, -0.048640239, $0.417647680 \times 10^{-4}$, $-0.14452093 \times 10^{-7}$, and 6.5459673, respectively.

The dew point temperature at the anode outlet depends on the molar gas flow rates.

The molar flow of hydrogen leaving the cell;

$$N_{H2\_out} = (S_{H_2} - 1) \times N_{H_2\_consumption} \tag{3.40}$$

S_{H_2} is the stoichiometric ratio of H_2 and $N_{H_2\_consumption}$ is the number of moles of consumed H_2. The net drag coefficient, r_d, defined as the molar flow rate of the water leaving the cell is :

$$r_d = \frac{N_{H2O\_in\_H2\_in} - N_{H2O\_in\_H2\_out}}{I/F} \tag{3.41}$$

$N_{H2O\_in\_H2\_in}$ is the amount of water at the H_2 inlet, $N_{H2O\_in\_H2\_out}$ is the amount of water at the H_2 outlet.

For dry H_2 input:

$$N_{H_2O\_in\_H_2\_out} = -r_d \times {}^{I}/_{F} \quad (3.42)$$

The molar flow rate of depleted air at the cathode;

$$N_{air\_out} = N_{air\_in} - N_{O_2\_consumption} \quad (3.43)$$

N_{air_in} is the molar flow rate of the incoming air and $N_{O_2\_consumption}$ is the molar flow rate of consumed O_2.

In this equation, it is assumed that dry air contains 79% N_2 and 21% O_2. Assuming the air is dry at the inlet, the molar stream of water vapor exiting the cathode side;

$$N_{H_2O\_in\_air\_out} = N_{H_2O\_gen} - N_{H_2O\_in\_H_2\_out} \quad (3.44)$$

The consumption of reactants in PEMFC is proportional to the current and the number of cells. The stoichiometric ratio is the ratio of the actual reactant flow at the PEMFC inlet to its theoretical progenitor. Therefore, all flow rates of reactants and components at the inlet are also proportional to the current and the number of cells. Since cell power output is the consumption of reactants in PEMFC, it is proportional to the current and the number of cells [26]. Cell power output;

$$W_{el} = n_{cell} \times I \times V_{cell} \quad (3.45)$$

The mass flow rate of H_2 (g/s);

$$m_{H2\_in} = S_{H2} \times \ m_{H_{2,consumption}} = S_{H_2} \times \frac{m_{H2}}{2F} \times I \times n_{cell} \quad (3.46)$$

The mass flow rate of O_2 (g/s):

$$m_{O_2\_in} = S_{O_2} \times m_{O_{2_{consumption}}} = S_{O_2} \times \frac{m_{O2}}{4F} \times I \times n_{cell} \quad (3.47)$$

The mass flow rate of air (g/s) :

$$m_{Air\_in} = \frac{S_{O_2}}{r_{O_2}} \times \frac{m_{air}}{4F} \times I \times n_{cell} \quad (3.48)$$

The mass flow rate of nitrogen in the air:

$$m_{N_2\_in} = S_{O_2} \times \frac{m_{N2}}{4F} \times \frac{1-r_{O_{2\_in}}}{r_{O_{2\_in}}} \times I \times n_{cell} \quad (3.49)$$

Water vapor in the H_2 inlet with relative humidity (g/s):

$$m_{H_2O\_in\_H2\_in} = S_{H_2} \times \frac{m_{H2O}}{2F} \times \frac{Phi_{anot} \times P_{vs}(T_{an\_in})}{P_{an} - Phi_{anot} * P_{vs}(T_{an\_in})} \quad (3.50)$$

If air is used as the oxidant, the amount of water vapor in the air inlet;

$$m_{H2O\_in\_air\_in} = \frac{S_{O2}}{r_{O2}} \times \frac{m_{H2O}}{4F} \times \frac{Phi_{cat} \times P_{vs}(T_{cat\_in})}{P_{cat} - Phi_{cat} \times P_{vs}(T_{cat\_in})} \quad (3.51)$$

The equations for mass flow rates at the outlet must consider the consumption of reactants, water production, and net water transport through the membrane. The flow rate of H_2 at the outlet:

$$m_{H_2O\_out} = (S_{H_2} - 1) \frac{m_{H_2}}{2F} \times \mathrm{I} \times n_{cell} \quad (3.52)$$

Water balance on the cathode side;

$$m_{H_2O\_in\_H_2\_out} = m_{H_2O\_in\_H_2\_in} - m_{H_2O_{ED}} - m_{HH_2O_{BD}} \quad (3.53)$$

Water balance on the cathode side; Electroosmotic drag is proportional to current, just like any other flow entering or leaving the fuel cell. ED=1, called the electroosmotic resistance coefficient, refers to the number of water molecules per proton.

$$m_{H_2O_{ED}} = ED \times \frac{m_{H_2O}}{F} \times I \times n_{cell} \quad (3.54)$$

The back diffusion of water depends on the water concentration on both sides of the membrane, the water diffusion from the membrane, and the thickness of the membrane:

$$m_{H2O_{BD}} = BD \times m_{H2O_{ED}} \tag{3.55}$$

Depending on the hydrogen flow rate, i.e., stoichiometry, and the conditions at the outlet (T, P), the water in the H_2 exhaust may only exist as steam. The water vapor content at the anode outlet is the smaller of the total water flow at the anode outlet and the maximum amount the gas can carry:

$$m_{H_2O\_in\_H_2\_out\_v} = \min\left[(S_{H_2} - 1)\frac{m_{H2O}}{2F} \times \frac{Pvs(T_{out\_an})}{P_{an} - \Delta P_{an} - Pvs(T_{out\_an})}\ I \times n_{cell}, m_{H_2O\_in\_H_2\_out}\right. \tag{3.56}$$

ΔPan refers to the pressure drop across the anode. If liquid water vapor is present, it is the difference between the total amount of water present and the water vapor:

$$m_{H_2O\_in\_H_2\_out\_l} = m_{H_2O\_in\_H_2\_out} - m_{H_2O\_in\_H_2\_out\_v} \tag{3.57}$$

Similar equations can be applied to the cathode. The flow rate of O_2 at the outlet;

$$m_{O_{2_{out}}} = \left(S_{O_2} - 1\right)\frac{m_{O2}}{4F} \times I \times n_{hücre} \tag{3.58}$$

The air flow rate consumed is the sum of the flow rates of O_2 and N_2:

$$m_{air\_out} = [(S_{O_2} - 1)m_{O_2} + \frac{1 - r_{O2_{in}}}{r_{O2_{in}}} m_{N_2}]\frac{I \times n_{hücre}}{4F} \tag{3.59}$$

Water entering with air at the cathode:

$$m_{H_2O\_in\_air\_out} = m_{H_2O\_in\_H_2\_in} + m_{H_2O\_gen} + m_{H_2O\_ED} - m_{H_2O\_BD} \tag{3.60}$$

The water vapor output in the air at the cathode is the smaller of the total water flux at the cathode exit and the maximum amount that the exhaust gas can carry:

$$m_{H_2O\_in\_air\_out\_v} = \min\left[\frac{S_{O2}-r_{O2\_in)}}{r_{O2_{in}}}\frac{m_{H_2O}}{4F}\frac{Pvs(T_{out\_cat})}{P_{cat}-\Delta P_{cat}-Pvs(T_{out\_cat})} \times I \times n_{cell}, m_{H_2O\_in\_air\_out}\right] \quad (3.61)$$

ΔP_{cat} is the pressure drop on the cathode side. The amount of liquid water entering with air :

$$m_{H_2O\_in\_air\_out\_l} = m_{H_2O\_in\_air\_out} - m_{H_2O\_in\_air\_out\_v} \quad (3.62)$$

In this study, the PEMFC design was made using the MATLAB program. The designed PEMFC was integrated into the TRNSYS Software with the Type 155 component in the TRNSYS program [75]. Details of the design code are given in Appendix B and Appendix C.

3.5.5. H_2 Storage Calculation

H_2 and O_2 gases are stored in the compressed gas tank. The real gas model calculated the pressure in the tank according to the van der Waals equations. The pressure of the tank can be calculated as follows [76].

$$P = \frac{n \times R \times T}{V_{ST} - nb} - a \times \frac{n^2}{{V_{ST}}^2} \quad (3.63)$$

Where P is the pressure of the tank, n is mol number of gas, R is the ideal gas constant, V_{ST} is the volume of the compressed gas storage tank, T is the temperature of the gas, a is the constant value.

3.5.6. Economic Optimization and Levelized Cost of Energy (LCOE)

The capital recovery factor is used to account for the present value of equipment:

$$CRF = \frac{i\,(1+i)^N}{(1+i)^N - 1} \tag{3.64}$$

CRF is the capital recovery factor, I is the interest rate, N is the period [77]. LCOE is calculated according to Equation (3.64) as shown below [78];

$$LCOE = \frac{\sum_{i=0}^{N}\left[\frac{I_i + O_i + F_i - TC_i}{(1+r)^i}\right]}{\sum_{i=0}^{N}\left[\frac{E_i}{(1+r)^i}\right]} \tag{3.65}$$

where I_i, is the capital cost in year i, O_i, is the operation and maintenance costs (O&M) in year i, F_i is fuel cost in the year i, TC_i is total tax credits in the year i. In this study, the total tax credits were ignored. E_i is generated electricity in year i, N lifetime of the system, r is the real discount rate (3 %) [51]. When the component's lifetime is less than the lifetime of the designed system, then the new component must be purchased by using the replacement cost for the year that the component lifetime ends [79]. Economic parameters of hybrid system components are shown in Table 3.6.

Table 3. 6. Parameters to LCOE calculation

Component	Parameter	Price	Unit
PV[80][53]	Investment cost	3490.00	$/kW
	Replacement cost	0.00	$/kW
	O&M cost	104.70	$/kW year
	Lifetime	25.00	year
WT[70]	Investment cost	2978.25	$/kW
	Replacement cost	0.00	$/kW
	O&M cost	44.67	$/kW year
	Lifetime	20.00	year
MPPT and Inverter[53]	MPPT investment cost	347.08	$/kW
	Inverter investment cost	456.00	$/kW
	Inverter replacement cost	456.00	$/kW
	MPPT O&M cost	10.41	$/kW year
	Inverter O&M cost	13.68	$/kW year
	MPPT lifetime	20.00	year
	Inverter lifetime	12.00	year
Compressor[79]	Investment cost	798.00	$/kW
	Replacement cost	798.00	$/kW
	O&M cost	23.94	$/kW year
	H_2 compressor power	2.20	kW
	O_2 compressor power	1.08	kW
	Lifetime	10.00	year
Electrolyzer[53][81]	Investment cost	5700.00	$/kW
	Replacement cost	855.00	$/kW
	O&M cost	171.00	$/kW year
	Electrolyzer power	18.406	kW
	Lifetime	10.00	year
Compressed storage tank[79]	H_2 tank investment cost	51.30	$/$m^3$
	O_2 tank investment cost	3.51	$/$m^3$
	H_2 tank replacement cost	0.00	$/$m^3$
	O_2 tank replacement cost	0.00	$/$m^3$
	H_2 tank O&M cost	1.54	$/$m^3$ year
	O_2 tank O&M cost	0.11	$/$m^3$ year
	Lifetime	20.00	year
PEMFC system[79]	Investment cost	1699	$/kW
	Replacement cost	900.00	$/kW
	O&M cost	90.00	$/kW year
	Power	5.00	kW
	Lifetime	10.00	year

CHAPTER 4

4. RESULTS AND DISCUSSION

4.1. Hybrid System Design Results

The simulations were executed for the uninterrupted operation of the hybrid system throughout the year, and the system LCOE values were calculated by determining the required PV and WT numbers. The simulation results of the proposed hybrid energy system containing H_2/O_2 PEMFC with the data taken from Meteonorm and Atilim University meteorology station are compared in Table 4.1.

The uninterrupted operation of the hybrid system throughout the year was investigated using PV, WT and PV/WT based hybrid systems when the H_2 gas tank was initially empty. In the simulations, WT numbers were selected as 0, 1, 2, 5, 10 and the PV numbers required for the optimum hybrid energy system design were determined. When the results obtained by the TRNSYS simulation using the Meteonorm forecasting program are compared with the simulation results made with the data of Atilim University meteorology station, it has been determined that more PV is needed for Meteonorm forecasting program data simulation. This is because the solar radiation and wind speed data obtained with the Meteonorm forecast program are lower than the actual data obtained from the meteorological station. Due to the use of more PV, the initial investment cost of the hybrid system is higher. This means additional cost and is undesirable in the commercial area. In this context, it has been seen that the results obtained because of one-year observation are much more advantageous than the results obtained from the estimation program. For uninterrupted hybrid system operation, there must be sufficient H_2 supply for PEMFC. As a result of the analysis, it was determined that many PV and WT are required to ensure sufficient H_2 production from electrolyzer, especially in months when solar and wind data are low.

Table 4.1. Design results of the hybrid system with H_2/O_2 PEMFC for different operating scenarios

Data Source	**WT (n_1)**	**PV (n_2)**	**Installation cost ($1K)**	**E_{served} * (MWh)**	**LCOE ($/kWh)**
Meteonorm Program	0	295	585	131.40	0.4486
	1	286	584	130.50	0.4501
	2	279	586	130.56	0.4506
	5	244	540	123.50	0.4610
	10	194	561	113.57	0.4831
	52	0	830	179.27	0.4223
Meteorology Station	0	156	364	82.69	0.4464
	1	153	373	82.52	0.4566
	2	150	382	82.51	0.4660
	5	134	398	78.68	0.5054
	10	115	436	74.55	0.5754
	76	0	1160	123.34	0.8627

**Total Generated Energy*

To examine the effect of the initial H_2 tank level on simulation, the initial H_2 tank level was examined as approximately 5, 10 and 15 m^3. Table 4.2 illustrates the simulation results of the proposed hybrid system with different initial H_2 tank volumes using the Meteonorm program data.

Table 4.2. Design results of the hybrid system with Meteonorm program data according to different initial H_2 tank volume

Initial H_2 tank volume (m^3)	**WT (n_1)**	**PV (n_2)**	**Installation cost ($1K)**	**E_{served} (MWh)**	**LCOE ($/kWh)**
5	0	138	336	52.02	0.67313
	1	133	346	53.83	0.65857
	2	130	350	56.25	0.64356
	3	126	358	58.17	0.63253
	25	0	460	77.48	0.56368
	5	119	374	62.32	0.61180
	0	128	320	48.81	0.68727
	1	125	329	51.03	0.67183
	2	122	337	53.39	0.65612
	5	112	363	60.02	0.61848
	23	0	433	72.06	0.57444
10	0	108	289	42.82	0.71699
	1	107	300	45.68	0.69464
	1	106	299	45.54	0.69381
	1	105	298	45.36	0.69353
	1	104	297	45.24	0.69599
	2	102	306	47.93	0.67230
	5	93	333	55.89	0.61775
	20	0	391	64.65	0.58846
15	0	99	274	41.61	0.70985
	1	98	286	44.45	0.68764
	1	97	285	44.13	0.68932
	1	96	283	43.96	0.68901
	1	95	282	43.79	0.68844
	2	93	292	46.70	0.66505
	5	84	319	55.02	0.61686
	18	0	364	59.64	0.60064

When 5 m^3 of initial H_2 gas is used in the tank, a decrease has been observed in the number of PV and WT that should be used when the tank is empty to meet the electricity requirement of the load. Therefore, the initial setup cost of the system has decreased, but the LCOE value has increased due to the decrease in the total power produced. It has been determined that when more than 15 m^3 H_2 gas is filled in the tank at the beginning, the number of PV and WT used in the hybrid system decreases. However, it has been observed that the electrolyzer does not need to work too much throughout the year as the gas tank required for PEMFC is sufficiently full. In this case, LCOE increases as the number of PV and WT used is less. Therefore, further increasing the initial amount of the H_2 gas has not been studied.

4.2. Hybrid System Optimization Studies

In the studies carried out within the scope of the project, the optimization problem is to determine the optimal values of the number of WTs and PVs. Various constrained optimization problems can be created depending on the needs and goals of the decision-makers. In any setup of the optimization problem, the decision variables at hand are the number of WTs (n_1) and the number of PVs (n_2). For this hybrid system design, it is appropriate to minimize the LCOE, subject to a certain set of constraints. For example, if the aim is to minimize the LCOE according to a certain area of the facility planned to be established, a suitable optimization problem for a system that provides uninterrupted power to the load is formulated with the equation given in Equation 4.2. For the given A_0, optimum n_1, n_2 values that minimize the LCOE are determined.

$$\begin{cases} \min LCOE(n_1, n_2) \\ \text{Subject to} \\ \text{Area}(n_1, n_2) \leq A_o \\ n_1, n_2 > 0 \end{cases} \tag{4.2}$$

where Area (n_1, n_2) is the total area of the plant consisting of n_1 WT and n_2 PV and A_0 is the possible installation site area. We aim to find the optimum n_1, n_2 values that minimize the LCOE with given A_0. For this purpose, LCOE values were calculated for

different n_1, n_2 values. The pair (n_1*, n_2*) that minimizes LCOE and provides Area (n_1, n_2) $\leq A_0$ is chosen as the optimal solution.

In Table 4.3, when the area where the hybrid system can be installed is determined as A_0=250 m^2, all possible (n_1, n_2) values that provide Area (n_1, n_2) $\leq A_0$ are given as a result of the simulations. For all cases given in Table 4, when the system is supplied with uninterrupted power to the load, the pair (n_1*, n_2*) that minimizes the LCOE value is chosen as the optimum configuration. According to the results given in Table 5, the LCOE value is minimized when n_1*= 1 and n_2* = 95. This configuration needs an area of 210 m^2 and the corresponding LCOE is 0.6884.

Table 4.3. Satisfying the condition in Equation 4.1. (n_1, n_2) (when A_0=250 m^2)

WT (n_1)	**PV (n_2)**	**A_T (m^2)**	**LCOE ($/kWh)**
0	108	221	0.7170
1	107	163	0.6946
1	105	235	0.6935
1	104	235	0.6960
0	99	207	0.7099
1	98	221	0.6876
1	97	150	0.6893
1	96	218	0.6890
1	95	210	0.6884
2	93	270	0.6651

Using the data obtained from the Meteonorm program, it was determined that the most optimal design was the design using 1 wind turbine and 95 solar panels, with a 15 m^3 H_2 tank occupancy rate. In Table 4.4, the comparison of the results obtained from the data measured from the Atilim University meteorology station in the simulation of the hybrid energy system and the forecast data of the Meteonorm program is given.

According to the results obtained, in the design made with real wind and solar radiation data, both the produced energy was obtained more and the LCOE value of the system was calculated lower.

Table 4.4. Comparison of the results obtained with Atilim University meteorology station data and Meteonorm program data in hybrid energy system simulation

Data Source	**WT** **(n_1)**	**PV** **(n_2)**	**A_T** **(m^2)**	**A_{PV}** **(m^2)**	**E_{served}** **(MWh)**	**LCOE** **($/kWh)**
Meteonorm Program	1	95	210	192	43.80	0.6884
Meteorology Station	1	95	210	192	46.46	0.6342

In Figures 4.1 and 4.2, the time-dependent power generation determined from TRNSYS simulation using the Meteonorm program and Atilim University meteorology station data in optimum hybrid system design, respectively, is given. Since the actual solar and wind data are higher than the estimated values, 46.46 MW more energy is produced at the same number of solar panels and wind turbines and the same gas occupancy rates.

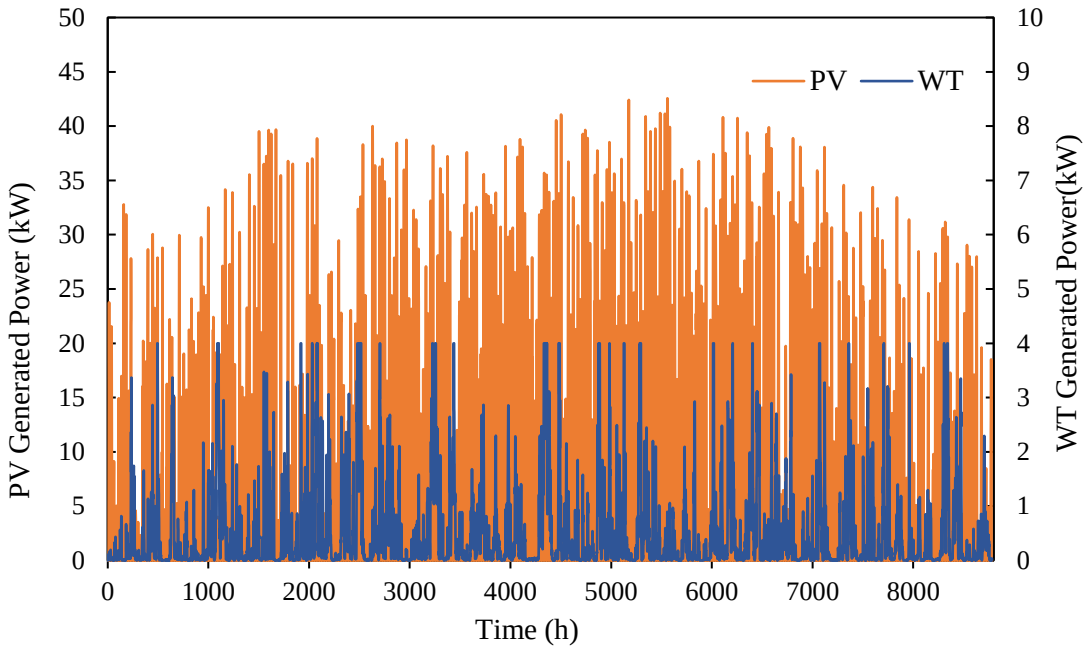

Figure 4.1. Time-dependent power generation of the hybrid system (PV=95 and WT=1) with Meteonorm program data

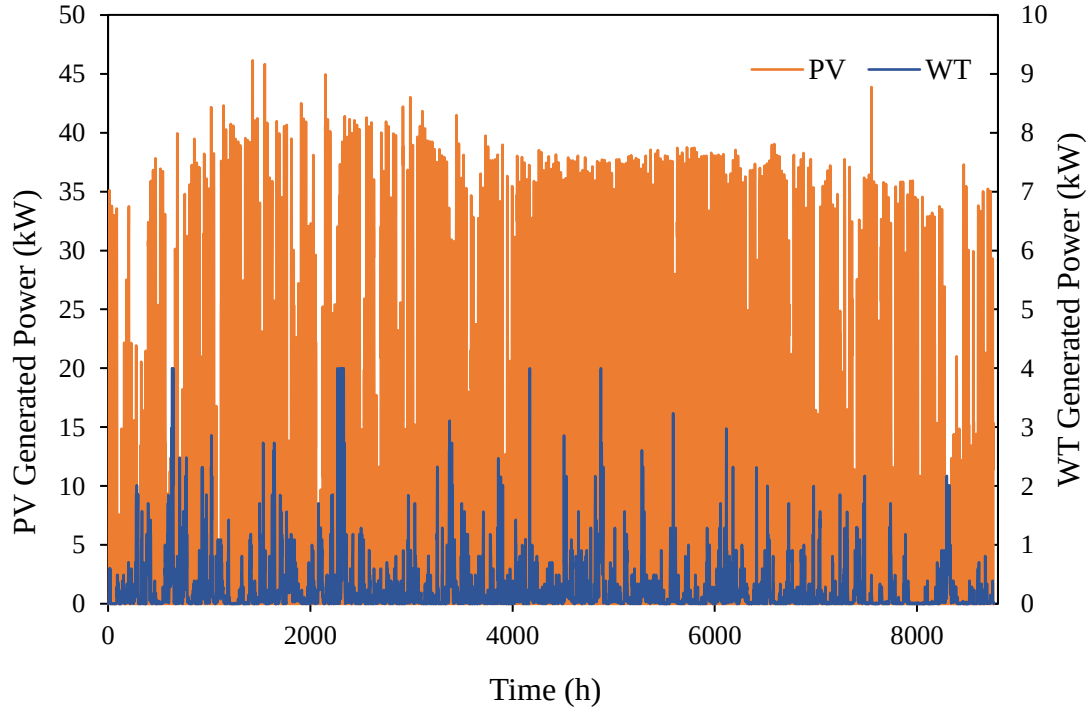

Figure 4.2. Time-dependent power generation of the hybrid system design (PV=95 and WT=1) using weather station data

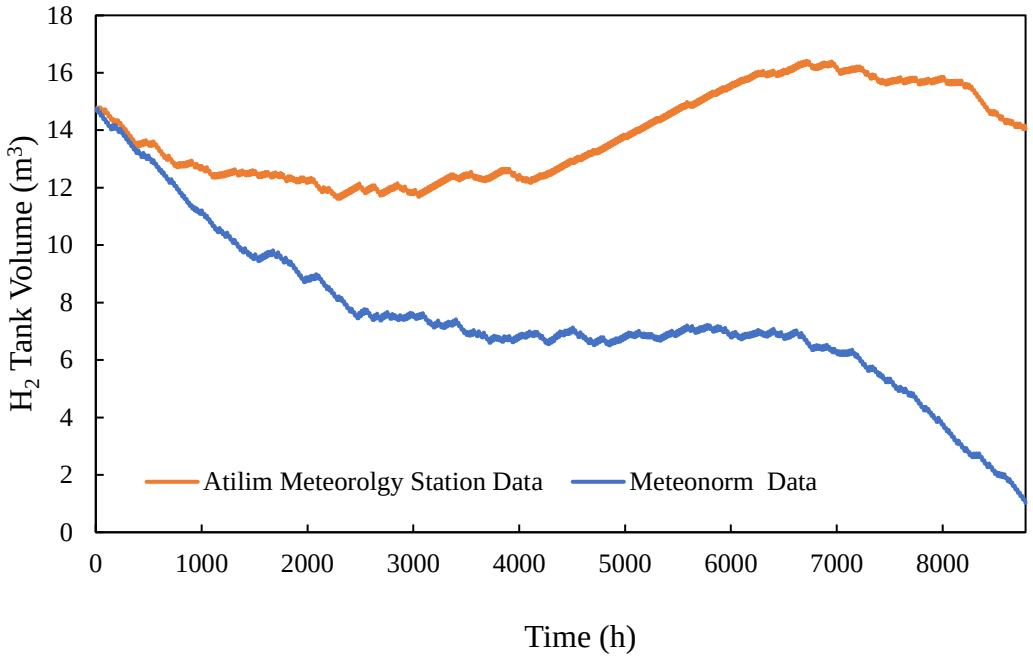

Figure 4.3. Comparison of the one-year H_2 gas storage of the hybrid system (PV=95 and WT=1) for meteorology station and Meteonorm program data

H_2 produced in the proposed hybrid energy system was stored at 200 bar in high-pressure cylinders, which is the most common storage method. Long-term storage increases system reliability on cloudy days without sunlight and when wind speed is not sufficient. Figure 4.3 shows the comparison of the stored H_2 gas in the storage tank during a one-year simulation for the optimum hybrid system design (PV=95 and WT=1) with the meteorology station and Meteonorm program data. According to the obtained results, there is more H_2 production depending on the power generation with the meteorology station. According to the forecast data of the Meteonorm program, the tanks in the hybrid energy system must be refilled every year for the system to operate uninterruptedly, while according to the data obtained with the meteorology station, the tanks need to be filled only during the first installation of the system.

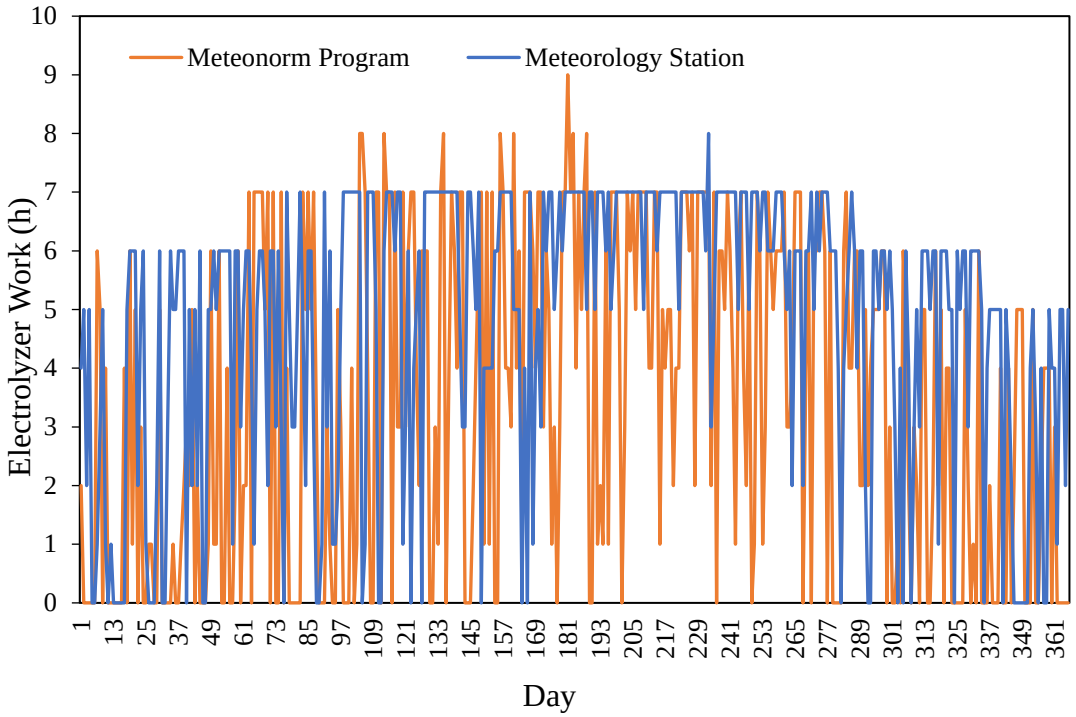

Figure 4.4. Comparison of the electrolyzer operating time of the hybrid system (PV=95 and WT=1) for meteorology station and Meteonorm program data

When the data obtained from the meteorology station were examined, while the optimum PV number was 95 with the Meteonorm program, 72 PV was sufficient in the meteorology station. According to the meteorology station, when 95 PV was used, more electricity was produced. For this reason, the design that will provide uninterrupted power generation and reduce the installation cost with the data obtained from the meteorology station has been examined.

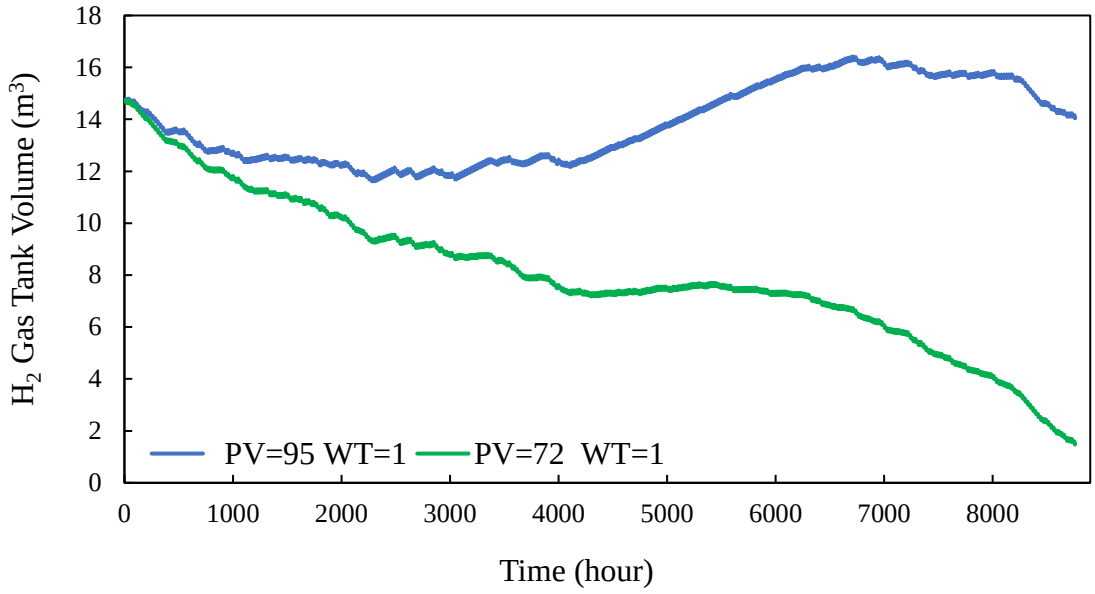

Figure 4.5. Comparison of the stored H_2 gas during one-year simulation for the hybrid system design for the meteorology station (PV=95, WT=1) and Meteonorm program (WT=1 PV=72) data

In Figure 4.5, the effect of using 95 PVs and 1 WT and 72 PVs and 1 WT on the amount of H_2 stored in the system is compared according to the data obtained with the Meteorology station. In the use of 72 PVs and 1 WT, the H_2 gas stored in the system runs out at the end of 1 year and the tanks in the hybrid energy system must be refilled at a certain level every year for the system to operate uninterruptedly. However, it has been determined that the hybrid energy system is a more suitable system due to its uninterrupted operation and lower initial installation cost.

In Table 4.5, the results of the hybrid energy system simulation using the data measured from the Atilim University meteorology station are given. In the study, it was determined that a minimum of 72 panels could be used for the uninterrupted operation of the hybrid energy system at the determined load. With the data measured from the Atilim University meteorology station, both the number of solar panels to be used and the initial installation cost are reduced.

Table 4.5. Comparison of the LCOE values of the hybrid system design for the meteorology station (PV=95, WT=1) and Meteonorm program data (WT=1 PV=72)

WT (n_1)	**PV (n_2)**	**A_T (m^2)**	**A_{PV} (m^2)**	**E_{served} (MWh)**	**LCOE ($/kWh)**
1	95	210	192	46.46	0.6342
1	72	161	142	39.82	0.6627

4.3. Comparison of Hybrid System with H_2/O_2 and H_2/Air supplied PEMFC Systems

For the O_2 inlet and air inlet system, the optimum value of the PV number was found by keeping the WT numbers constant in 1,5 and 15 m^3 initial H_2 tank volume. The hybrid system simulation with H_2/O_2 PEMFC and H_2/Air PEMFC for the data of Atilim University meteorology station are shown in Table 4.6 and Table 4.7, respectively. When the PV/Electrolyzer/PEMFC and the WT/Electrolyzer/PEMFC systems are compared using both H_2/O_2 and H_2/air PEMFC, it has been determined that the installation cost of the PV-based hybrid energy system is lower than the WT-based hybrid system. Since the wind speed is not sufficient in the studied region, more WT is needed to obtain uninterrupted power. Therefore, the installation cost of the WT-based hybrid system is higher. For this reason, the optimum hybrid system design has been examined for the case where only 1 WT can be used and the minimum required PV number has been determined. When the H_2/O_2 PEMFC based hybrid energy system is compared with the H_2/air PEMFC based hybrid energy system, it has been determined that the installation cost of the H_2/air PEMFC based system is lower. In the system where O_2 is used, it is necessary to ensure uninterrupted O_2 production together with H_2, and more PV should be used in the system. Additionally, it was mentioned in the previous sections that the gases are stored in the H_2 and O_2 tanks in the hybrid system with O_2-supplied PEMFC. When the H_2 and O_2 tanks of the hybrid system were initially filled, the fuel costs were added to the LCOE calculations. Therefore, the system installation cost is higher in the H_2/O_2 PEMFC based hybrid energy system. However, the LCOE value of the H_2/O_2 PEMFC based hybrid energy

system is still low due to more energy produced than needed.

Table 4.6. Design results of the hybrid system with H_2/O_2 PEMFC for Atilim University meteorology station data

Initial H_2 tank level (m^3)	**WT (n_1)**	**PV (n_2)**	**Installation cost ($1K)**	**E_{served} (MWh)**	**LCOE ($/kWh)**
1	0	156	364	82.69	0.4464
	1	153	373	82.52	0.4566
	2	150	382	82.51	0.4660
	5	134	398	78.68	0.5054
	10	115	436	74.55	0.5754
	76	0	1160	123.34	0.8627
5	0	101	276	47.46	0.6124
	1	100	288	48.78	0.6179
	2	99	301	50.04	0.6240
	5	93	332	51.58	0.6587
	10	85	388	55.63	0.6991
	63	0	981	96.87	0.9387
15	0	73	233	38.17	0.6625
	1	72	245	39.815	0.6629
	2	71	257	41.158	0.6677
	5	68	293	45.001	0.6827
	10	63	354	51.447	0.7023
	42	0	619	67.985	0.8583

Table 4.7. Design results of the hybrid system with H_2/air PEMFC for Atilim University meteorology station data

Initial H_2 tank level (m^3)	**WT (n_1)**	**PV (n_2)**	**Installation cost ($1K)**	**E_{served}, (MWh)**	**LCOE ($/kWh)**
1	0	143	343	73.61	0.4749
	1	138	348	72.26	0.4901
	2	134	357	71.78	0.5033
	5	126	385	73.94	0.5209
	10	109	426	70.84	0.5921
	62	0	855	100.85	0.7806
5	0	86	253	41.32	0.6491
	1	85	265	42.35	0.6588
	2	84	277	43.67	0.6638
	5	80	312	46.66	0.6873
	10	71	366	49.88	0.7381
	55	0	871	86.89	0.9343
15	0	70	227	37.43	0.6629
	1	69	240	38.43	0.6738
	2	68	252	39.71	0.6794
	5	66	290	43.46	0.6980
	10	61	350	49.87	0.7169
	40	0	595	64.78	0.8680

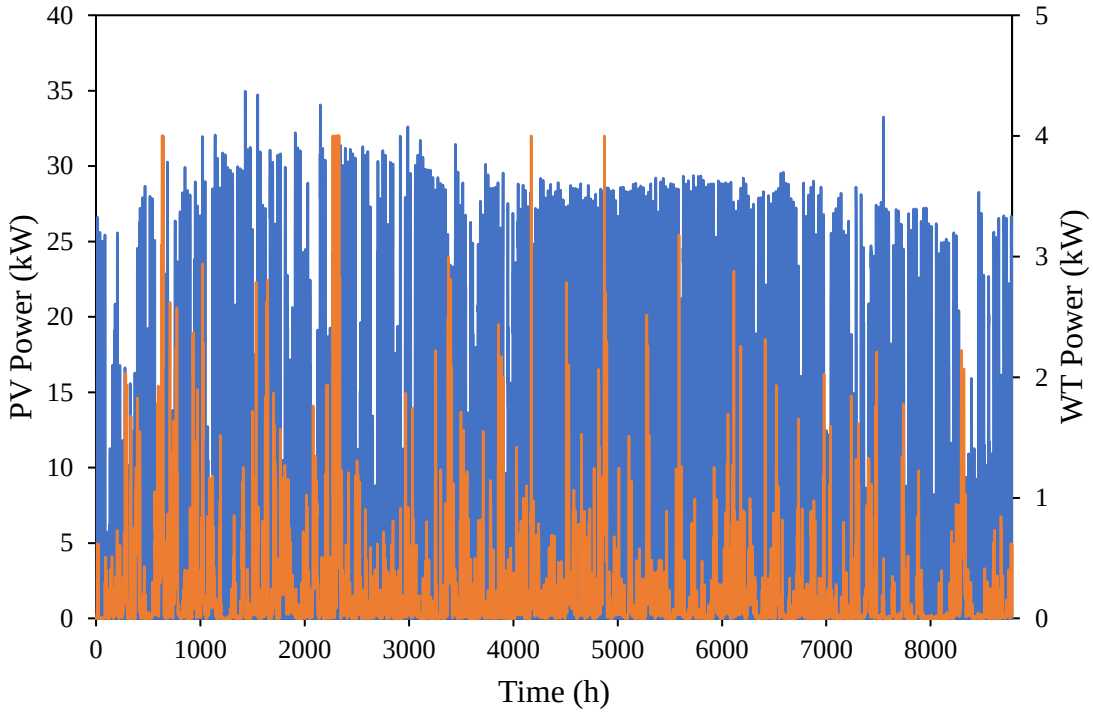

Figure 4.6. Time-dependent power generation of the hybrid system with H_2/O_2 PEMFC (PV= 72 and WT= 1) using meteorology station data

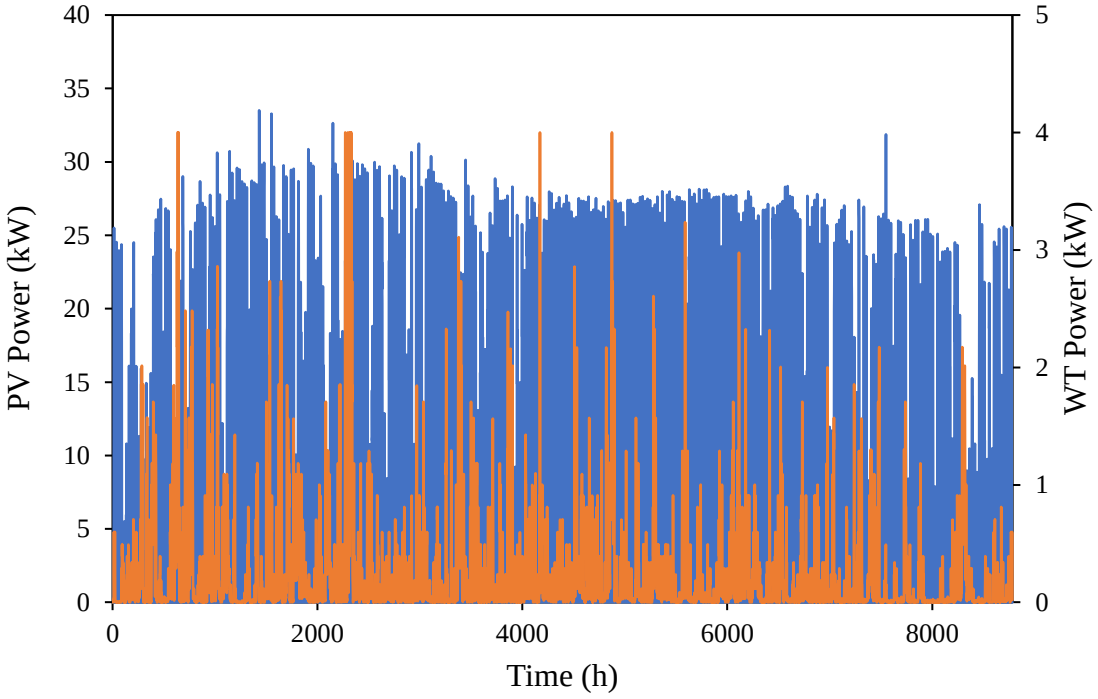

Figure 4.7. Time-dependent power generation of the hybrid system with H_2/air PEMFC (PV= 69 and WT= 1) using meteorology station data

In Figures 4.6 and 4.7, the annual power generation from the sun and wind of the optimum system design determined according to the data of Atilim University for the O_2 and air inlet system are given. TRNSYS analysis results are shown in APPENDIX E and APPENDIX F, respectively.

Figure 4.8 illustrates the change of the H_2 storage tank volume throughout the year. Since there is no energy production at the beginning, PEMFC uses H_2 in the tanks and the energy produced from the hybrid systems throughout the year provides uninterrupted electricity. In the air inlet system, the H_2 tank filling rate is lower compared to the O_2 inlet system.

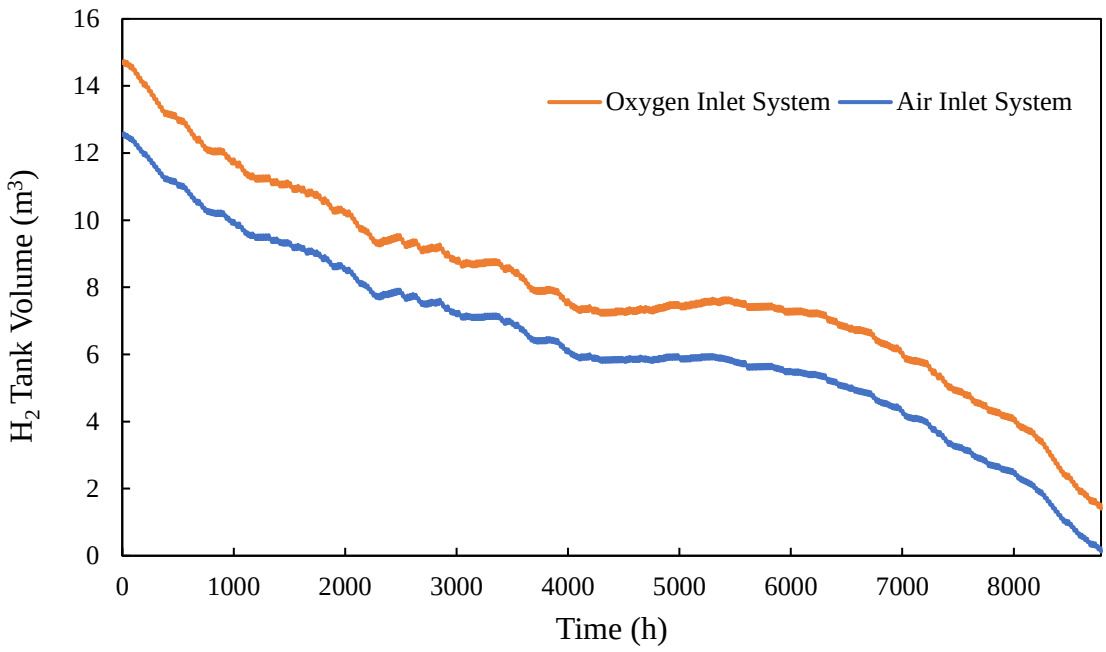

Figure 4.8. Comparison of the stored H_2 gas during one-year simulation for the hybrid system with H_2/O_2 PEMFC (PV= 72 and WT=1) and H_2/air PEMFC (PV= 69 and WT= 1) for the data of meteorology station

Figure 4.9 shows the electrolyzer operating times of the hybrid power system with the H_2/O_2 PEMFC (PV= 72 and WT= 1) and H_2/air PEMFC (PV= 69 and WT= 1) for the data of the meteorology station. It has been observed that the electrolyzer operating times are nearly the same in the two systems.

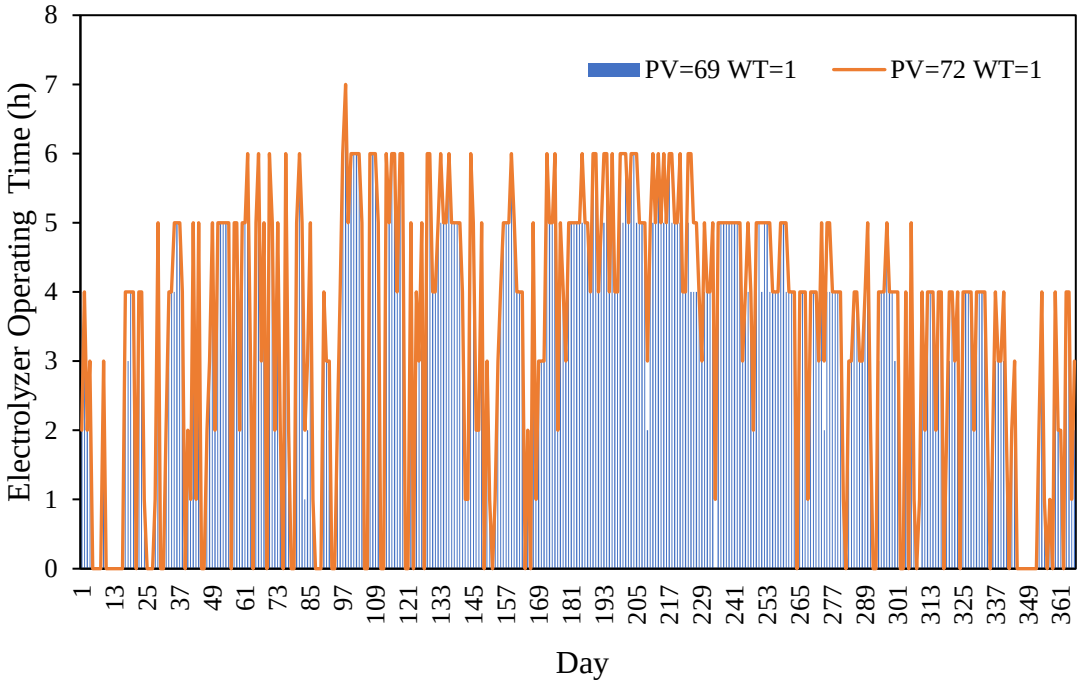

Figure 4.9. Comparison of electrolyzer operating times of hybrid system with H_2/O_2 PEMFC (PV= 72 and WT= 1) and H_2/air PEMFC (PV= 69 and WT=1) for the data of meteorology station

CHAPTER 5

5. CONCLUSION

Renewable energy sources are becoming more and more important every day in terms of the absence of greenhouse gas emissions and are a clean energy source. However, as it is known, the biggest problem in renewable energy sources is energy storage. With existing hybrid systems, only daily storage is possible, so long-term energy storage is not yet ready for use, even if hybrid sources produce more energy.

In this thesis, it is aimed to provide uninterrupted energy needs determined independently from the grid with the PV/WT/PEM electrolyzer/PEMFC hybrid energy system and to store the excess energy produced in the system as H_2. For this purpose, various hybrid system designs with different PV and WT were examined using TRNSYS software and MATLAB program and the systems were compared economically. In the system design, both the data obtained from the Meteonorm forecast program and the measured data from the Atilim University meteorology station were used and both systems were compared. Within the scope of the thesis, the economic evaluation of the hybrid energy system was also carried out and optimization was made according to this parameter. When the LCOE values of the proposed hybrid energy system based H_2/O_2 PEMFC are examined, the lowest LCOE values were obtained for 0.4501 (PV=286, WT=1) and 0.4566 (PV=153, WT=1) for the designs made using Meteonorm and weather station data, respectively.

In the hybrid system design, the energy required for H_2 production from the electrolyzer was provided from PV and WTs, and the continuous energy needed for the load was provided from PEMFC. For this purpose, both H_2/O_2 and H_2/air fed PEMFC were used and the effect of using H_2/O_2 and H_2/air fed PEMFC in the proposed hybrid energy system was investigated. When hybrid energy systems using H_2/O_2 and H_2/air based PEMFC are compared, it is determined that the system using H_2/O_2 based PEMFC is more costly due to the additional O_2 compressor and an O_2 tank used in the system. For H_2/O_2 based PEMFC, it is necessary to produce sufficient

O_2 as well as H_2. Therefore, extra power is spent to produce enough O_2 required for PEMFC operation, and accordingly, the number of PV panels used in the system increases. When evaluated in general, it has been observed that the system using H_2/air-based PEMFC is more advantageous than the H_2/O_2 system. Additionally, since the wind data of the location where the hybrid energy system is examined are not sufficient, the optimum number of turbines that can be used in the PV/WT/electrolyzer/PEMFC system was determined as one. When the PV/WT/electrolyzer/PEMFC system is compared with the PV/electrolyzer/PEMFC systems, it has been determined that the PV/electrolyzer/PEMFC system is more optimal.

Although renewable energy based green H_2 production technologies are not available today with reasonable efficiency and cost, they are of great importance for sustainable energy and clean environment in the future. This thesis will be an exemplary study for PV/WT/ electrolyzer/PEMFC based energy systems and green H_2 production, and it shows that the storage of excess energy produced in hybrid energy systems as H_2 can be considered as an alternative to energy storage in the future.

REFERENCES

[1] E. Ozden and I. Tari, "Energy-exergy and economic analyses of a hybrid solar-hydrogen renewable energy system in Ankara, Turkey," *Appl. Therm. Eng.*, vol. 99, pp. 169–178, 2016, doi: 10.1016/j.applthermaleng.2016.01.042.

[2] J. A. Fay and D. S. Golomb, (2002, June 15), *Energy and the Environment*. (2nd edition*)* [Online], Available: www.course.sdu.edu.cn [February 5, 2022].

[3] S. Karabanov, Y. Kukhmistrov, B. Miedzinski, and Z. Okraszewski, (2003, May 5),*Photovoltaic systems*.Available:www.researchergate.net/scientific [February 5, 2022].

[4] Arman Uluoğlu "Solar-Hydrogen Stand-Alone Power System Design and Simulations" M.A Thesis, University of Middle East Technical University, Turkey, 2010.

[5] Y. Devrim and L. Bilir, "Performance investigation of a wind turbine–solar photovoltaic panels–fuel cell hybrid system installed at İncek region – Ankara, Turkey," *Energy Convers. Manag.*, vol. 126, pp. 759–766.

[6] H. M. Ridha, C. Gomes, H. Hizam, M. Ahmadipour, A. A. Heidari, and H. Chen, "Multi-objective optimization and multi-criteria decision-making methods for optimal design of standalone photovoltaic system: A comprehensive review," *Renew. Sustain. Energy Rev.*, vol. 135, no. April 2020, p. 110202, 2021.

[7] V. S. Chandrika *et al.*, "Performance assessment of free standing and building integrated grid connected photovoltaic system for southern part of India," *Build. Serv. Eng. Res. Technol.*, vol. 42, no. 2, pp. 237–248.

[8] A. R. Razmi, M. Soltani, A. Ardehali, K. Gharali, M. B. Dusseault, and J. Nathwani, "Design, thermodynamic, and wind assessments of a compressed air energy storage (CAES) integrated with two adjacent wind farms: A case study at Abhar and Kahak sites, Iran," *Applied Energy*, vol. 221, p. 119902.

[9] S. Diaf, G. Notton, M. Belhamel, M. Haddadi, and A. Louche, "Design and techno-economical optimization for hybrid PV/wind system under various meteorological conditions," *Applied Energy*, vol. 85, no. 10, pp. 968–987, 2008.

[10] M. M. Samy, M. I. Mosaad, and S. Barakat, “Optimal economic study of hybrid PV-wind-fuel cell system integrated to unreliable electric utility using hybrid search optimization technique,” *International Journal of Hydrogen Energy*, vol. 46, no. 20, pp. 11217–11231, 2021.

[11] H. A. Z. AL-bonsrulah *et al.*, “Design and Simulation Studies of Hybrid Power Systems Based on Photovoltaic, Wind, Electrolyzer, and PEM Fuel Cells,” *Energies*, vol. 14, no. 9, p. 2643, 2021.

[12] H. Ishaq, O. Siddiqui, G. Chehade, and I. Dincer, “A solar and wind driven energy system for hydrogen and urea production with CO2 capturing,” *International Journal of Hydrogen Energy*, vol. 46, no. 6, pp. 4749–4760, 2021.

[13] D. F. Al Riza and S. I. U. H. Gilani, “Standalone photovoltaic system sizing using peak sun hour method and evaluation by TRNSYS simulation,” *International Journal of Renewable Energy Res.*, vol. 4, no. 1, pp. 109–114, 2014.

[14] D. F. AL RIZA, “Sizing Optimization of Standalone Photovoltaic System for Residential Lighting,” M.A thesis,University of Teknologi PETRONAS,Malezia, 2011.

[15] H.Ozcan and H.Gunerhan, “Fotovoltaik destekli iklimlendirme sisteminin deneysel ve simülasyon çalişmalari ile incelenmesi” *Bildiriler kitabı*, pp. 0–10,2010.

[16] B. Yildirim, “ScienceDirect Advanced controller design based on gain and phase margin for microgrid containing PV / WTG / Fuel cell / Electrolyzer / BESS,” *International Journal of Hydrogen Energy*, vol. 46, no. 30, pp. 16481–16493, 2020.

[17] D. Shapiro, J. Duffy, M. Kimble, and M. Pien, “Solar-powered regenerative PEM electrolyzer / fuel cell system,” *Solar Energy*,vol. 79, pp. 544–550, 2005.

[18] J. Kotowicz, M. Jurczyk, and D. We, “ScienceDirect The possibilities of cooperation between a hydrogen generator and a wind farm,” *International Journal of Hydrogen Energy*,vol. 6, 2020.

[19] H. Görgün, “Dynamic modelling of a proton exchange membrane (PEM)

electrolyzer," *International Journal of Hydrogen Energy*, vol. 31, no. 1, pp. 29–38, 2006.

[20] R. Escobar-Yonoff, D. Maestre-Cambronel, S. Charry, A. Rincón-Montenegro, and I. Portnoy, "Performance assessment and economic perspectives of integrated PEM fuel cell and PEM electrolyzer for electric power generation," *Heliyon*, vol. 7, no. 3, 2021.

[21] Á. Hernández-Gómez, V. Ramirez, D. Guilbert, and B. Saldivar, "Cell voltage static-dynamic modeling of a PEM electrolyzer based on adaptive parameters: Development and experimental validation," *Renewable Energy*, vol. 163, pp. 1508–1522, 2021.

[22] D. Ipsakis, S. Voutetakis, and P. Seferlis, "Power management strategies for a stand-alone power system using renewable energy sources and hydrogen storage," *International Journal of Hydrogen Energy*, vol. 34, no. 16, pp. 7081–7095, 2009.

[23] G. Panayiotou, S. Kalogirou, and S. Tassou, "Design and simulation of a PV and a PV-Wind standalone energy system to power a household application," *Renewable Energy*, vol. 37, no. 1, pp. 355–363, 2012.

[24] N. Naseri, S. El Hani, A. Aghmadi, H. Mediouni, I. Aboudrar, and M. Benbouzid, "Solar Photovoltaic Energy Storage as Hydrogen via PEM Fuel Cell for Later Conversion Back to Electricity," in *Proc. IEEE*, vol. 3805, no. 10, pp. 4549–4554, 2019.

[25] "Hibrit Sistemler," *Altern. Enerj. Kaynakları Arş. ve Uyg. Merk.*, 2014.

[26] F. Barbir, *PEM Fuel Cell Theory and Practice*, *Copyright*. Kaynak: https://books.google.com.tr/ [31 Ocak 2022].

[27] H. Zang, M. Guo, Z. Wei, and G. Sun, "Determination of the Optimal Tilt Angle of Solar Collectors for Different Climates of China,"*Sustaibility*,pp. 1–16, 2016.

[28] Dimas Firmanda Al Riza "SIZING OPTIMIZATION OF STANDALONE PHOTOVOLTAIC SYSTEM FOR RESIDENTIAL LIGHTING," *International Journal of Renewable Energy Research*,vol. 13, no. 128, p. 234, 2011.

[29] “Solar Radiation, Internet:www. nrel.gov. [31 January 2022].

[30] S. C. Library, “TRNSYS 18 a TRa N s i e n t About This Manual,” vol. 3, pp. 315–319, 1962.

[31] Zeynep Deniz Eygi, N. G. Gözeleri, “Güneş Hücreleri Çeşitleri Günümüzdeki Göze Çeşitleri.”Mühendislik Fakültesi, 30 Mayıs 2019.

[32] Zeynep Deniz Eygi, Fotovoltaik Sistemler “Güneş Hücresi ve Çalı sma Prensibi Güneş Gözeleri avantajları.” Mühendislik Fakültesi, 30 Mayıs 2019.

[33] Berkcan Çakır "K. Tasarimi and V. E. Anal" M.A Thesis, University of Karabük, Karabük, 2016.

[34] Ayşe Bektaş “Binalarda Rüzgar Enerjisi Kullanımının farklı bölgeler açısından değerlendirilmesine yönelik bir çalışma : TOKİ TARIMKÖY PROJESİ ÖRNEĞİ,” M.A Thesis, University of Istanbul, Istanbul 2013.

[35] W. Gao, V. Zheglov, G. Wang, and S. M. Mahajan, “PV - Wind - Fuel Cell - Electrolyzer Micro-grid Modeling and Control in Real Time Digital Simulator.” International Conference on Clean Electrical Power,Italy 2009

[36] “Wind Energy.” www.wind-watch.org, [4 February, 2021]

[37] Ersin Şekerci, “RÜZGÂR TÜRBİNİ TAHMİNİ YILLIK ENERJİ ÜRETİM HESAPLAMA YÖNTEMLERİ ve ARAZİYE UYGUN RÜZGÂR, Havacılık ve Uzay Mühendisliği Bölümü,” O. Doğu, T. Üniversitesi, and İ. Bulvarı, pp. 1–5.

[38] M. Said. Ergöktaş, “Kontak Direnci ve Sıkıştırma Kuvvetinin proton geçirgen membranlı Elektrölizör Performansı üzerindeki etkileri ve hızlandırılmış ömür testleri ile performans düşüşlerinin incelenmesi" M.A.thesis, University of Nigde, Nigde, 2015.

[39] B. A. Mccormick, “Modellind and Transient Simulation of Solar-Powered”M.A thesis,University of Queens,Canada, 2018.

[40] S. Sood et al., Generic dynamical model of PEM electrolyser under intermittent sources,*Energies,* vol. 13, no. 24. 2020.

[41] Ö. GENÇ and M. A. KALLİOĞLU, "ProtonElektrolit Membranli (Pem)Elektrolizörün SayisaİncelenmesiVe Deneysel Doğrulanmasi," *Ömer Halisdemir Üniversitesi Mühendislik Bilim. Derg.*, vol. 7, no. 1, pp. 370–380, 2018.

[42] C. Wang and A, "MODELING AND CONTROL OF HYBRID WIND/PHOTOVOLTAIC/FUEL CELL DISTRIBUTED GENERATION SYSTEMS," *International Journal of Advanced Science and Engineering Research*, vol. 40, no. 11, pp. 1210–1214, 1951.

[43] Gürsel Şefkat, M. Ali Özel, "PEM YAKIT PİLİNİN SİMULİNK MODELİ ve ANALİZİ," *Uludağ Universitesi Mühendislik Fakç Dergisi*, vol. 23, no. 2, pp. 351–366, 2018.

[44] Oğuz Kağan Özdemir, P.-N. E. Hazırlanması, "Elektrik İle Biriktirme Yöntemiyle PEM Tipi Yakıt Hücreleri İçin Etkin," *Fırat Üniversitesi Mühendislik Bilim dergisi* vol. 29, no. 1, pp. 355–362, 2017.

[45] Yılser Devrim, Yakıt Hücreleri "yakıt_hucreleri[1818]." Mühendislik Fakültesi 2020 .

[46] E. Ozden and I. Tari, "ScienceDirect PEM fuel cell degradation effects on the performance of a stand-alone solar energy system," *International Journal of Hydrogen Energy*, vol. 42, no. 18, pp. 13217–13225, 2017,

[47] Levelized cost analysis,"LCOE" www.elektrikport.com, [4 February,2022].

[48] H. Kord and A. Rohani, "An integrated hybrid power supply for off-grid applications fed by wind/photovoltaic/fuel cell energy systems," 2009, [Online].Available:https://www.researchgate.net/profile/Ahmad_Rouhani/publication/237594025_An_Integrated_Hybrid_Power_Supply_for_OffGrid_Applications_Fed_by_WindPhotovoltaicFuel_Cell_Energy_Systems/links/54c01ccd0cf28eae4a67a01c.pdf.

[49] V. Papadopoulos, J. Desmet, J. Knockaert, and C. Develder, “Improving the utilization factor of a PEM electrolyzer powered by a 15 MW PV park by combining wind power and battery storage – Feasibility study,” *International Journal of Hydrogen Energy*, vol. 43, no. 34, pp. 16468–16478, 2018.

[50] I. Dincer and A. Abu-Rayash, “Sustainability modeling,” *Energy Sustainability, Elsevier*, 2020, pp. 119–164.

[51] A. C. Duman and Ö. Güler, “Techno-economic analysis of o ff -grid PV / wind / fuel cell hybrid system combinations with a comparison of regularly and seasonally occupied households,” *Sustainability Cities Society.*, vol. 42, no. May, pp. 107–126, 2018.

[52] Y. Budak and Y. Devrim, “Comparative study of PV/PEM fuel cell hybrid energy system based on methanol and water electrolysis,” *Energy Conversation Management.*, vol. 179, pp. 46–57, 2019.

[53] L. Gracia, P. Casero, C. Bourasseau, and A. Chabert, “Use of hydrogen in off-grid locations, a techno-economic assessment,” *Energies*, vol. 11, no. 11, Nov. 2018.

[54] Yrd.Doç.Mehmet Uzunoğlu, (01 October, 2002) *HerYonuIleMATLAB* (1nd edition), [Çevrimiçi], 27(3), Available: https://web.itu.edu.tr/kents/matlab.pdf [February 4,2022].

[55] A. B. Tarasenko, S. V Kiseleva, V. P. Shakun, F. M. Markos, and J. Sentian, “Performance simulation of a grid connected photovoltaic power system using TRNSYS 17 Performance simulation of a grid connected photovoltaic power system using TRNSYS 17,” 2017.

[56] D. Mazzeo, G. Oliveti, C. Baglivo, and P. M. Congedo, “Energy reliability-constrained method for the multi-objective optimization of a photovoltaic-wind hybrid system with battery storage,” *Energy*, vol. 156, pp. 688–708, 2018.

[57] Program“Weather Programmer”www.meteonorm.com, [4 February,2022].

[58] M. Demircan, "Senaryolarına Göre Türkiye İçin Sıcaklık ve Yağış Projeksiyonları," *Coğrafi Bilimler Dergisi*,vol. 14, no. 2, pp. 77–88, 2016.

[59] A. Remlaoui, D. Nehari, A. Elmeriah, and M. Laissaoui, "A TRNSYS model of a direct contact membrane distillation (DCMD) system coupled to a flat plate solar collector (FPC)," no. Dcmd, pp. 335–360, 2017.

[60] TRNSYS Users information platform.Trnsys-users@lists.onebuilding.org, [4 February,2022].

[61] E. Özgirgin, Y. Devrim, and A. Albostan, "Modeling and simulation of a hybrid photovoltaic (PV) module-electrolyzer-PEM fuel cell system for micro-cogeneration applications," *International Journal of Hydrogen Energy*, 2015, vol. 40, no. 44, pp. 15336–15342.

[62] K. Anoune, A. Laknizi, M. Bouya, A. Astito, and A. Ben Abdellah, "Sizing a PV-Wind based hybrid system using deterministic approach," *Energy Conversation Management*, vol. 169, pp. 137–148, 2018.

[63] B. Karacavus and K. Aydın, "Hydrogen production and storage analysis of a system by using TRNSYS," *International Journal of Hydrogen Energy*, Mar. 2020.

[64] Yavuz Selim İşler,"Şebekeden Bağımsız PV Sistemin TRNSYS ile Gerçek Zamanlı Modellenmesi," *KSÜ Mühendislik Bilimleri Dergisi*,vol. 20, no. 2, pp. 97–104, 2017.

[65] B. L. Gupta, M. Bhatnagar, and J. Mathur, "Optimum sizing of PV panel, battery capacity and insulation thickness for a photovoltaic operated domestic refrigerator," *Sustainanle Energy Technology Assessments*, vol. 7, pp. 55–67, 2014.

[66] H. Tebibel, S. Menia, and A. Khellaf, "Off grid PV system for hydrogen production using methanol electrolysis and an optimal management strategy," *Proc. 2016 Int. Renew. Sustain. Energy Conf. IRSEC 2016*, pp. 999–1004, 2017.

[67] Akram Abdulameer Abbood Al-Khazar"The Required Land Area for Installing a Photovoltaic Power Plant," *Iran. J. Energy Environ.*, 2017.

[68] A. KOÇER, S. Şevik, and A. GÜNGÖR, "Determination of Solar Collector Optimum Tilt Angle for Ankara and Districts," *Uludağ University Journal of The Faculty of Engineering*, 2016.

[69] Enair Energy, "Small Wind Turbine E70PRO - The latest technology." 2019.

[70] Enair, "O Wi n d T u r b i n e," 2020.

[71] S. Mathew,(2007, February 1,) *Wind energy: Fundamentals, resource analysis and economics*(2nd edition) [Online]Available: https://link.springer.com/book/10.1007/3-540-30906-3?noAccess=true[4 February 2022]

[72] B. Caglar, M. Araz, H. G. Ozcan, A. Calisan, and A. Hepbasli, "Energy and exergy analysis of a PV-T integrated ethanol PEM electrolyzer," *International Journal of Hydrogen Energy*, vol. 46, no. 24, pp. 12615–12638, 2021.

[73] C. Ceylan and Y. Devrim, "Design and simulation of the PV/PEM fuel cell based hybrid energy system using MATLAB/Simulink for greenhouse application," *International Journal of Hydrogen Energy*, vol. 46, no. 42, pp. 22092–22106, 2021.

[74] M. M. Mench, *Fuel Cell Engines*. 2008.

[75] TRNSYS-MATLAB MANUAL. https://sel.me.wisc.edu/trnsys/trnlib/trnsys-matlab/type155-manual.html, [4 February,2022].

[76] PennState, "Pricing and Lead-Time | General Stores & Central Distribution." [4 February,2022].

[77] N. City, "An Optimal Sizing of Stand-Alone Hybrid PV-Fuel Cell-Battery to Desalinate Seawater at Saudi,"*Processes*, 2020.

[78] X. T. Chadee and R. M. Clarke, "Wind resources and the levelized cost of wind generated electricity in the Caribbean islands of Trinidad and Tobago," *Renew. Sustain. Energy Rev.*, vol. 81, no. December 2016, pp. 2526–2540, 2018.

[79] C. van Leeuwen and A. Zauner, “Deliverable 8.3 - Report on the costs involved with PtG technologies and their potentials across the EU,”*Store and Go Project*, vol. April, no. 691797, p. 51, 2018.

[80] “SunPower® Residential DC Panel: X22-370.” [4 February,2022].

[81] B. Dubin-Thaler, “Analysis Summary,” *Hydrogen and Fuel Cells Program* pp. 1–15, 2007.

APPENDIX A

FORTRAN CODE OF PEM ELECTROLYZER MODEL

```
% --- Process Inputs
Ppv= trnInputs(1);
Pelmin=trnInputs(2);
icell= trnInputs(3);
Vcell= trnInputs(4);
A_elec=trnInputs(5);
eff=trnInputs(6);
Pres_el=trnInputs(7);
Temp_el=trnInputs(8);

% --- Calculate electrolyzer performance ---
Istack= icell*A_elec; %Electrolyzer current
ncell_eqn= Pelmin/(icell*Vcell*A_elec);
ncell=ceil(ncell_eqn);
Vstack= ncell*Vcell;
Pres_el_Pa=Pres_el*101325;
Temp_el_K= Temp_el+273.15
if (Ppv < Pelmin)
Pelmin=0;
mH2= 0;
VH2=0;
mO2=0;
VO2=0;
CS_H2_comp=0;
CS_O2_comp=0;
else
   twel= Ppv/Pelmin;
if  twel>=1
```

twel=1;

Pelmin=Pelmin;

mH_2= (Istack*ncell*twel*MWH_2*eff*3600)/(2*F);

VH_2= (mH_2*R*Temp_el_K)/(MWH_2*Pres_el_Pa);

mO2= (Istack*ncell*twel*MWO2*eff*3600)/(4*F);

VO_2= (mO_2*8.314*Temp_el_K)/(MWO_2*Pres_el_Pa);

CS_H_2_comp=1;

CS_O_2_comp=1;

else

Pelmin=0;

mH_2= 0;

VH_2=0;

mO_2=0;

VO_2=0;

CS_H_2_comp=0;

CS_O_2_comp=0;

end

end

% --- Set outputs ---

trnOutputs(1) = twel;

trnOutputs(2) = mH_2;

trnOutputs(3) = mO_2;

trnOutputs(4) = Vstack;

trnOutputs(5) = Pelmin;

trnOutputs(6) = VH_2;

trnOutputs(7) = VO_2;

trnOutputs(8) = CS_H_2_comp;

trnOutputs(9) = CS_O_2_comp;

trnOutputs(10) = Pres_el;

trnOutputs(11) = Temp_el;

APPENDIX B

FORTRAN CODE OF PEMFC MODEL FOR O_2 INLET SYSTEM

```
% --- Process Inputs
Pfc=trnInputs(1);
Ploss=trnInputs(2); %
Vcell_fc=trnInputs(3); %V
icell_fc=trnInputs(4); % A/cm^2
A_act=trnInputs(5); %15x15 cm
T_opt=trnInputs(6); %C
T_H2= trnInputs(7); %C
T_O2= trnInputs(8); %C
Panode= trnInputs(9); %atm
Pcathode=trnInputs(10); %atm
S_H2= trnInputs(11);
S_O2=trnInputs(12);
phi_cat=trnInputs(13);

%CALCULATION
daynumber=fix(trnTime/24);
x=daynumber*24
z=19+x;
z1=20+x;
z2=21+x;
z3=22+x;
z4=23+x;
if  trnTime==z
   CS=1;
elseif trnTime==z1
   CS=1;
elseif trnTime==z2
```

```
CS=1;
elseif trnTime==z3
    CS=1;
elseif trnTime==z4
    CS=1;
else
   CS=0;
end
   % Calculate the required stack current
T_opt_k = T_opt + 273.15; %Operation temperature
T_H2_ink = T_H2 + 273.15; % Hydrogen inlet temperature
T_air_ink = T_O2 + 273.15; % Air inlet temperature
Panode_kPa= Panode * 101.325;        %Unit Conversions
Pcathode_kPa = Pcathode * 101.325;     %Unit Conversions
t_fc= 60; % fuel cell working time (min)
Pdesign=((Pfc+(Pfc*(Ploss/100)))*CS);
I_stack_fc = icell_fc*A_act; %Fuelcell stack current
V_stack_fc2= Pdesign/I_stack_fc;
ncell_fc=ceil(V_stack_fc2/Vcell_fc); %
V_stack_fc=ncell_fc*Vcell_fc;
Pdesign=V_stack_fc*I_stack_fc;
Pdensity=icell_fc*Vcell_fc;
t_fc_s = t_fc*60;
% The total number of moles of hydrogen
N_H2_cons = (I_stack_fc *ncell_fc*CS)/(n_anode * F);
N_H2_act= S_H2*N_H2_cons;
N_H2_act_tot= N_H2_act* t_fc_s; % Total amount of electricity produced
m_H2_in = MW_H2 * N_H2_act_tot;
VH2_fc = (R * T_H2_ink * N_H2_act_tot)/(Panode*101325);   % Convert molar flow
rate to volumetric flow rate
VH2_sl= VH2_fc*1000;
% Water vapor in the hydrogen inlet
Pvs_amb = Pvs(T_H2_ink);    % Saturation pressure of air
```

m_H_2O_H2_in= N_H_2_act_tot*MW_H2O* phi_an * Pvs_amb/(Panode_kPa - phi_an * Pvs_amb);

N_H_2_out= (S_H_2-1)*N_H_2_cons;

N_H_2_totout= N_H_2_out*t_fc_s;

m_H_2_out= N_H_2_totout* MW_H2;

VH_2_out = (R * T_opt_k * N_H2_totout)/(Panode*101325);

VH_2_sl_out= VH2_out*1000;

DeltaP = 28.028;

Pvs_op = Pvs(T_opt_k);

m_H_2O_eo= (C_eo*I_stack_fc*ncell_fc*MW_H2O*t_fc_s*CS)/F;

m_H_2O_bd= m_H2O_eo;

m_H_2O_H2_out=m_H_2O_H_2_in+m_H_2O_bd-m_H_2O_eo;

m_H_2O_H_2_out_v2= ((S_H2-1)*MW_H_2O* phi_an * Pvs_amb*t_fc_s*CS)/(Panode_kPa - DeltaP - Pvs_amb);

m_H_2O_H_2_out_vpr= min(m_H_2O_H_2_out,m_H_2O_H_2_out_v2);

m_H_2O_H_2_out_lqd=m_H_2O_H_2_out-m_H_2O_H_2_out_vpr;

% Calculate the higher heating value of hydrogen

h_HHV_0 = HHV_25 - (cp_H2 + 0.5 * cp_O2 * MW_O2 / MW_H_2 - MW_H_2O * cp_H_2O_l/ MW_H_2) * T_H2;

h_H_2_in = (m_H_2_in/t_fc_s) * (cp_H2 * T_H2 + h_HHV_0);

h_H_2_out = (m_H_2_out/t_fc_s) * (cp_H2 * T_opt + h_HHV_0);

% Energy flow for water in O2 in

h_H_2O_H_2_in_v = (m_H2O_H2_in/t_fc_s) * (cp_H_2O_v * T_H2 + h_fg);

%Water vapor in O2 out

h_H_2O_H_2_out_v = (m_H_2O_H_2_out_vpr/t_fc_s) * (cp_H_2O_v * T_opt + h_fg);

% Energy flow for water in O_2 out

h_H_2O_H_2_out_l = (m_H_2O_H_2_out_lqd/t_fc_s) * cp_H_2O_l * T_opt;

% The oxygen flow rate at the cell inlet

% The oxygen flow rate at the cell inlet

N_O_2_cons = (I_stack_fc*ncell_fc*CS) /(n_cathode * F);

N_O_2_act= S_O_2 * N_O_2_cons;

N_O_2_act_tot=N_O_2_act*t_fc_s;

m_O_2_in=N_O_2_act*t_fc_s*MW_O_2;

VO2_in_fc= (R * T_air_ink * N_O2_act_tot)/(Pcathode*101325); % Convert molar flow rate to volumetric flow rate

VO2_sl= VO2_in_fc*1000;

N_O2_totout= (S_O2-1)*N_O2_cons*t_fc_s;

m_O2_out= N_O2_totout*MW_O2;

VO2_out_fc = (R * T_opt_k * N_O2_totout)/(Pcathode*101325);

VO2_out_sl= VO2_out_fc*1000;

% The saturation pressure at the operating temperature

Pvs_op = Pvs(T_opt_k);

% Mole fraction of water in air

x_s_op = (MW_H2O/MW_O2) * Pvs_op*phi_cat/(Pcathode_kPa - phi_cat * Pvs_op);

% Amount of water needed for the humidification of air

m_h2o_in_O2 = x_s_op * m_O2_in* t_fc_s;

% Saturation pressure of air

Pvs_amb = Pvs(T_air_ink);

% Mole fraction of water in ambient O2

x_s_amb = (MW_H2O/MW_O2) * phi_air * Pvs_amb/(Pcathode_kPa - phi_air * Pvs_amb);

% Mass of water in ambient O2

m_h2o_in_amb_O2 = x_s_amb * m_O2_in* t_fc_s;

% Amount of water needed for humidification of air

m_h2o_needed = m_h2o_in_O2 - m_h2o_in_amb_O2;

Pvs_in = Pvs(T_air_ink); % Calculate the saturation pressure at T_H2_in

% Calculate the amount of water in O2

m_h2o_O2_in = (S_O2 * MW_H2O* phi_cat * Pvs_in * I_stack_fc * ncell_fc*t_fc_s*CS)/ (n_cathode* F * (Pcathode_kPa - (phi_cat * Pvs_in)));

% Calculate the water generated

m_h2o_gen = (I_stack_fc *ncell_fc* MW_H2O*t_fc_s*CS)/(n_anode * F);

% Calculate the saturation pressure at T_air_out

Pvs_out = Pvs(T_opt_k);

% Calculate the water vapor in the O2 outlet

m_H2O_O2_out = m_h2o_O2_in + m_h2o_gen - m_H2O_bd + m_H2O_eo;

m_H2O_O2_out_v2= ((S_O2-1)* MW_H2O* I_stack_fc *ncell_fc*

```
Pvs_out*t_fc_s*CS) /((n_cathode * F) *(Pcathode_kPa - DeltaP - Pvs_out));
m_H2O_O2_out_vpr= min(m_H2O_O2_out,m_H2O_O2_out_v2);
m_H2O_O2_out_lqd= m_H2O_O2_out - m_H2O_O2_out_vpr;
% Energy flow for O2 in
h_O2_in = (m_O2_in/t_fc_s)* cp_O2 * T_O2;
% Energy flow for O2 out
h_O2_out =  (m_O2_out/t_fc_s)* cp_O2 * T_opt;
% Energy flow for water in O2 in
h_H2O_O2_in_v = (m_h2o_O2_in/t_fc_s) * (cp_H2O_v * T_O2 + h_fg);
%Water vapor in O2 out
h_H2O_O2_out_v = (m_H2O_O2_out_vpr/t_fc_s) * (cp_H2O_v * T_opt + h_fg);
% Energy flow for water in O2 out
h_H2O_O2_out_l = (m_H2O_O2_out_lqd/t_fc_s) * cp_H2O_l * T_opt;
% From the energy balance, energy flow for air in
Q = h_H2_in+ h_H2O_H2_in_v+ h_O2_in + h_H2O_O2_in_v - h_H2_out -
h_H2O_H2_out_v -h_H2O_H2_out_l- h_O2_out - h_H2O_O2_out_v -
h_H2O_O2_out_l - Pdesign;

% --- Set outputs ---
trnOutputs(1) = (Pfc*CS);
trnOutputs(2) = Pdesign;
trnOutputs(3) = V_stack_fc;
trnOutputs(4) = I_stack_fc;
trnOutputs(5) = N_H2_act;
trnOutputs(6) = N_O2_act;
trnOutputs(7) = Q;
trnOutputs(8) = VH2_fc;
trnOutputs(9) = VO2_in_fc;
trnOutputs(10) =m_H2_in;
trnOutputs(11) = m_O2_in;
trnOutputs(12) =Panode;
trnOutputs(13) = T_H2;
trnOutputs(14) = T_opt;
```

```
mFileErrorCode = 0; % Tell TRNSYS that we reached the end of the m-file without errors
function result = Pvs(T)
a = -5800.2206;
b = 1.3914993;
c = -0.048640239;
d = 0.000041764768;
e = -0.000000014452093;
f = 6.5459673;
result = exp(a/T + b + c * T + d * T * T + e * T * T * T + f * log(T))/1000;
end
```

APPENDIX C

FORTRAN CODE OF PEMFC MODEL FOR AIR INLET SYSTEM

```
% --- Process Inputs
Pfc=trnInputs(1)
Ploss=trnInputs(2); %
Vcell_fc=trnInputs(3); %V
icell_fc=trnInputs(4); % A/cm^2
A_act=trnInputs(5); %15x15 cm
T_opt=trnInputs(6); %C
T_H2= trnInputs(7); %C
T_O2= trnInputs(8); %C
Panode= trnInputs(9); %atm
Pcathode=trnInputs(10); %atm
S_H2= trnInputs(11);
S_O2=trnInputs(12);
phi_cat=trnInputs(13);
m_air_in_kg= trnInputs(14);

daynumber=fix(trnTime/24);
x=daynumber*24
z=19+x;
z1=20+x;
z2=21+x;
z3=22+x;
z4=23+x;

if  trnTime==z
   CS=1;
elseif trnTime==z1
   CS=1;
```

```
elseif trnTime==z2
    CS=1;
elseif trnTime==z3
    CS=1;
elseif trnTime==z4
    CS=1;
else
   CS=0;
end

% Calculate the required stack current
T_opt_k = T_opt + 273.15; %Operation temperature
T_H2_ink = T_H2 + 273.15; % Hydrogen inlet temperature
T_air_ink = T_O2 + 273.15; % Air inlet temperature
Panode_kPa= Panode * 101.325;         %Unit Conversions
Pcathode_kPa = Pcathode * 101.325;     %Unit Conversions
t_fc= 60; % fuel cell working time (min)
Pdesign=((Pfc+(Pfc*(Ploss/100)))*CS);
I_stack_fc = icell_fc*A_act; %Fuelcell stack current
V_stack_fc2= Pdesign/I_stack_fc;
ncell_fc=ceil(V_stack_fc2/Vcell_fc); %
V_stack_fc=ncell_fc*Vcell_fc;
Pdesign=V_stack_fc*I_stack_fc;
Pdensity=icell_fc*Vcell_fc;
t_fc_s = t_fc*60;

%  The total number of moles of hydrogen
N_H2_cons = (I_stack_fc *ncell_fc*CS)/(n_anode * F);
N_H2_act= S_H2*N_H2_cons;
N_H2_act_tot= N_H2_act* t_fc_s; % Total amount of electricity produced
m_H2_in = MW_H2 * N_H2_act_tot;
VH2_fc = (R * T_H2_ink * N_H2_act_tot)/(Panode*101325);   % Convert molar flow
rate to volumetric flow rate
```

```
VH2_sl= VH2_fc*1000;
% Water vapor in the hydrogen inlet
Pvs_amb = Pvs(T_H2_ink);    % Saturation pressure of air
m_H2O_H2_in=  N_H2_act_tot*MW_H2O*  phi_an  *  Pvs_amb/(Panode_kPa  -
phi_an * Pvs_amb);
N_H2_out= (S_H2-1)*N_H2_cons;
N_H2_totout= N_H2_out*t_fc_s;
m_H2_out= N_H2_totout* MW_H2;
VH2_out = (R * T_opt_k * N_H2_totout)/(Panode*101325);
VH2_sl_out= VH2_out*1000;
DeltaP = 28.028;
Pvs_op = Pvs(T_opt_k);
m_H2O_eo= (C_eo*I_stack_fc*ncell_fc*MW_H2O*t_fc_s*CS)/F;
m_H2O_bd= m_H2O_eo;
m_H2O_H2_out=m_H2O_H2_in+m_H2O_bd-m_H2O_eo;
m_H2O_H2_out_v2=          ((S_H2-1)*MW_H2O*          phi_an          *
Pvs_amb*t_fc_s*CS)/(Panode_kPa - DeltaP - Pvs_amb);
m_H2O_H2_out_vpr= min(m_H2O_H2_out,m_H2O_H2_out_v2);
m_H2O_H2_out_lqd=m_H2O_H2_out-m_H2O_H2_out_vpr;
% Calculate the higher heating value of hydrogen
h_HHV_0 = HHV_25 - (cp_H2 + 0.5 * cp_O2 * MW_O2 / MW_H2 - MW_H2O *
cp_H2O_l/ MW_H2 ) * T_H2;
h_H2_in = (m_H2_in/t_fc_s) * (cp_H2 * T_H2 + h_HHV_0);
h_H2_out = (m_H2_out/t_fc_s) * (cp_H2 * T_opt + h_HHV_0);
% Energy flow for water in O2 in
h_H2O_H2_in_v = (m_H2O_H2_in/t_fc_s) * (cp_H2O_v * T_H2 + h_fg);
%Water vapor in O2 out
h_H2O_H2_out_v = ( m_H2O_H2_out_vpr/t_fc_s) * (cp_H2O_v * T_opt + h_fg);
% Energy flow for water in O2 out
h_H2O_H2_out_l = (m_H2O_H2_out_lqd/t_fc_s) * cp_H2O_l * T_opt;
 % The oxygen flow rate at the cell inlet
   m_air_in = m_air_in_kg*1000*CS;
   N_air_tot= m_air_in/ MW_Air;
```

```
    N_air= N_air_tot/t_fc_s;
    N_O2_act= N_air*r_O2in;
    N_O2_cons= N_O2_act/S_O2;
    m_O2_in=N_O2_act*t_fc_s*MW_O2
    N_N2_cons = (N_O2_act* (1-r_O2in)*CS)/r_O2in;
    N_N2_tot= N_N2_cons*t_fc_s;
    m_N2_in= MW_N2*N_N2_tot;
    Vair = (R * T_air_ink * N_air_tot*CS)/(Pcathode*101325);
    Vair_sl= Vair*1000;
    N_O2_totout= (S_O2-1)*N_O2_cons*t_fc_s;
    m_O2_out=N_O2_totout*MW_O2;
    N_N2_out=N_N2_tot;
    N_air_out= N_N2_out+ N_O2_totout;
    m_N2_out=N_N2_out*MW_N2;
    Vair_out = (R * T_opt_k * N_air_out)/(Pcathode*101325);
    Vair_out_sl=Vair_out*1000;
% The saturation pressure at the operating temperature
Pvs_op = Pvs(T_opt_k);
% Mole fraction of water in air
x_s_op = (MW_H2O/MW_Air) *phi_cat * Pvs_op/(Pcathode_kPa - phi_cat
*Pvs_op);
% Amount of water needed for the humidification of air
m_h2o_in_air = x_s_op * m_air_in *t_fc_s;
% Saturation pressure of air
Pvs_amb = Pvs(T_air_ink);
% Mole fraction of water in ambient air
x_s_amb = (MW_H2O/MW_Air) * phi_air * Pvs_amb/(Pcathode_kPa - phi_air *
Pvs_amb);
% Mass of water in ambient air
m_h2o_in_amb_air = x_s_amb * m_air_in*t_fc_s;
% Amount of water needed for humidification of air
m_h2o_needed = m_h2o_in_air - m_h2o_in_amb_air;
%Water Injection Flow Rate
```

```
Pvs_in = Pvs(T_air_ink); % Calculate the saturation pressure at T_H2_in
% Calculate the amount of water in air
m_h2o_air_in = (S_O2 * phi_cat * MW_H2O * Pvs_in * I_stack_fc * ncell_fc*t_fc_s*CS)/ (r_O2in * n_cathode * F * (Pcathode_kPa -phi_cat * Pvs_in));
n_anode = 2;
% Calculate the water generated
m_h2o_gen = I_stack_fc *ncell_fc* MW_H2O*t_fc_s/(n_anode * F);
% Calculate the saturation pressure at T_air_out
Pvs_out = Pvs(T_opt_k);
% Calculate the water vapor in the O2 outlet
m_h2o_in_air_out = m_h2o_air_in + m_h2o_gen - m_H2O_bd + m_H2O_eo;
m_h2o_in_air_out_v2= (S_O2-r_O2in)* MW_H2O* I_stack_fc * ncell_fc* Pvs_out*t_fc_s /r_O2in*(4 * F) *(Pcathode_kPa - DeltaP - Pvs_out) ;
m_H2O_air_out_vpr=min(m_h2o_in_air_out_v2, m_h2o_in_air_out);

m_H2O_air_out_lqd=m_h2o_in_air_out-m_H2O_air_out_vpr;

%Water vapor in O2 out
h_H2O_air_out_v = (m_H2O_air_out_vpr/t_fc_s) * (cp_H2O_v * T_opt + h_fg)
% Energy flow for water in O2 out
h_H2O_air_out_l = (m_H2O_air_out_lqd/t_fc_s) * cp_H2O_l * T_opt
% From the energy balance, energy flow for air in
Q = h_H2_in +  h_H2O_H2_in_v+ h_H2O_air_in_v + h_Air_in - h_H2_out - h_H2O_H2_out_v -h_H2O_H2_out_l- h_Air_out - h_H2O_air_out_v - h_H2O_air_out_l - Pdesign
% --- Set outputs ---
trnOutputs(1) = (Pfc*CS);
trnOutputs(2) = Pdesign;
trnOutputs(3) = V_stack_fc;
trnOutputs(4) = I_stack_fc;
trnOutputs(5) = N_H2_act;
trnOutputs(6) = N_air;
trnOutputs(7) = Q;
```

```
trnOutputs(8) = VH2_fc;
trnOutputs(9) = Vair;
trnOutputs(10) = VH2_sl;
trnOutputs(11) = Vair_sl;
trnOutputs(12) = m_H2_in;
trnOutputs(13) = m_air_in;
trnOutputs(14) = CS;
        function result = Pvs(T)
a = -5800.2206;
b = 1.3914993;
c = -0.048640239;
d = 0.000041764768;
e = -0.000000014452093;
f = 6.5459673;
result = exp(a/T + b + c * T + d * T * T + e * T * T * T + f * log(T))/1000;
end
```

APPENDIX D

FORTRAN CODE OF AIR COMPRESSOR CONTROLLER FOR AIR INLET SYSTEM

```
daynumber_comp=fix(trnTime/24);
x_comp=daynumber*24
z_comp=19+x_comp;
z1_comp=20+x_comp;
z2_comp=21+x_comp;
z3_comp=22+x_comp;
z4_comp=23+x_comp;
if  trnTime==z_comp
   CS=1;
elseif trnTime==z1_comp
   CS=1;
elseif trnTime==z2_comp
    CS=1;
elseif trnTime==z3_comp
    CS=1;
elseif trnTime==z4_comp
    CS=1;
else
   CS=0;
End
```

APPENDIX E

TRNSYS SCREENSHOT OF O_2 INLET OPTIMUM SYSTEM RESULTS

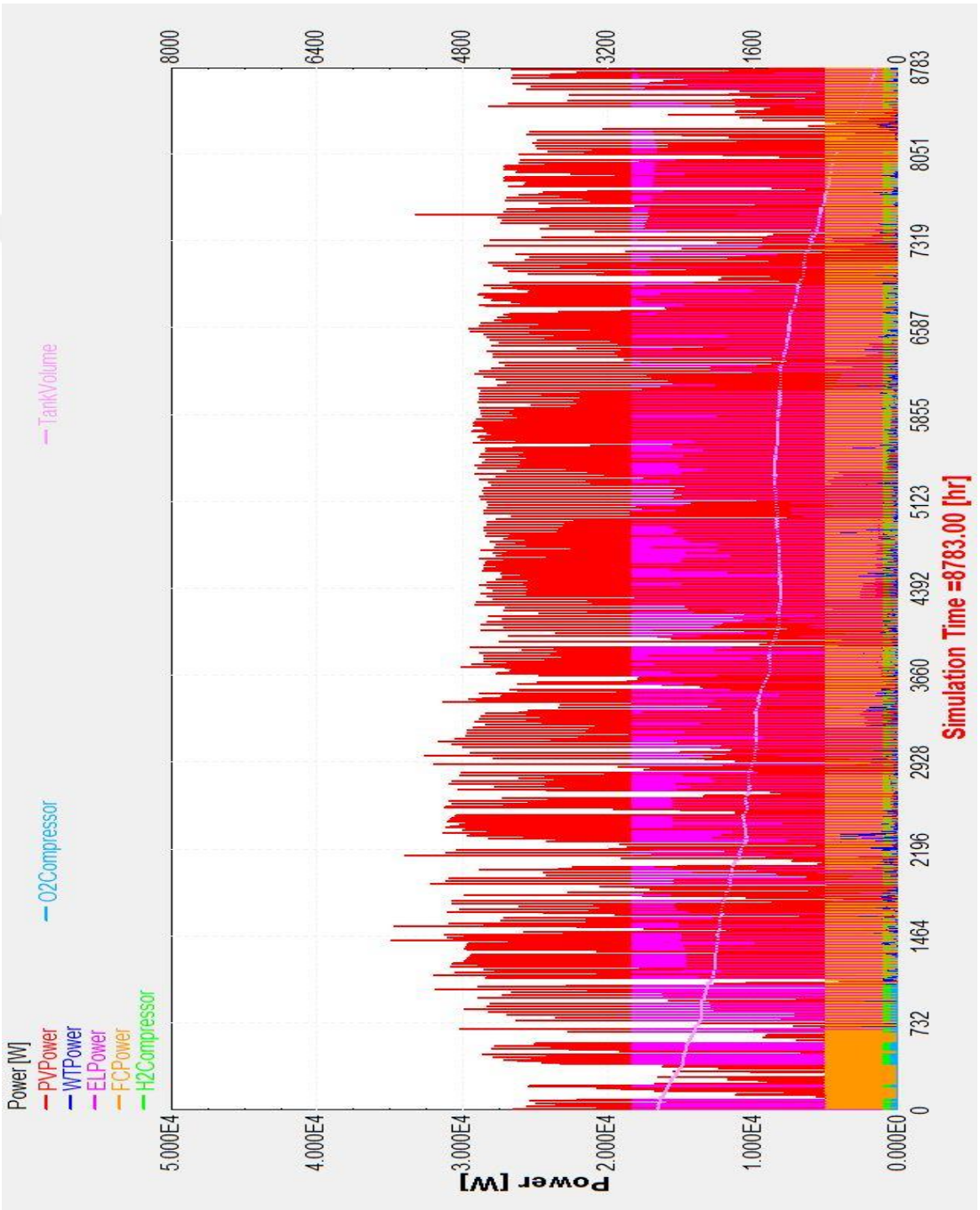

APPENDIX F

TRNSYS SCREENSHOT OF AIR INLET OPTIMUM SYSTEM RESULTS